

QUASARS PROBING QUASARS III: NEW CLUES TO FEEDBACK, QUENCHING, AND THE PHYSICS OF MASSIVE GALAXY FORMATION

J. XAVIER PROCHASKA^{1,2} & JOSEPH F. HENNAWI^{3,4}

Accepted to ApJ, September 10 2008

ABSTRACT

Galaxies hosting $z \sim 2$ quasars are the high- z progenitors of today's massive 'red-and-dead' galaxies. With close pairs of quasars at different redshifts, a background quasar can be used to study a foreground quasar's halo gas in *absorption*, providing a wealth of information about feedback, quenching, and the physics of massive galaxy formation. We present a Keck/HIRES spectrum of the bright background quasar in a projected pair with angular separation $\theta = 13.3''$ corresponding to $R_{\perp} = 108$ kpc at the redshift of the foreground quasar $z_{\text{fg}} = 2.4360 \pm 0.0005$, precisely determined from Gemini/GNIRS near-IR spectroscopy. Our echelle spectrum reveals optically thick gas ($N_{\text{HI}} \approx 10^{19.7} \text{ cm}^{-2}$) coincident with the foreground quasar redshift. The ionic transitions of associated metal-lines reveal the following properties of the foreground quasar's halo: (1) the kinematics are extreme with absorption extending to $+780 \text{ km s}^{-1}$ relative to z_{fg} ; (2) the metallicity is nearly solar; (3) the temperature of the predominantly ionized gas is $T \lesssim 20,000 \text{ K}$; (4) the electron density is $n_e \sim 1 \text{ cm}^{-3}$ indicating a characteristic size $\sim 10 - 100 \text{ pc}$ for the absorbing 'clouds'; (7) there is little (if any) warm gas $10^5 \text{ K} \lesssim T \lesssim 10^6 \text{ K}$; (8) the gas is unlikely illuminated by the foreground quasar, implying anisotropic or intermittent emission. The mass of cold $T \sim 10^4 \text{ K}$ gas implied by our observations is significant, amounting to a few percent of the total expected baryonic mass density of the foreground quasar's dark halo at $r \sim 100 \text{ kpc}$. The origin of this material is still unclear, and we discuss several possibilities in the context of current models of feedback and massive galaxy formation.

Subject headings: quasars: general – intergalactic medium – quasars: absorption lines – cosmology: general – surveys: observations

1. INTRODUCTION

Over the course of a quasar's lifetime, the accretion of material onto its $\sim 10^9 M_{\odot}$ supermassive black hole will liberate an enormous energy $E = \epsilon M_{\text{BH}} c^2 \simeq 2 \times 10^{62} \text{ ergs}^5$ affecting its environment from pc to Gpc scales. On cosmological scales, the collective emission from quasars dominates the ultraviolet background radiation field (Haardt & Madau 1996) that maintains roughly 90% of the universe as a highly ionized plasma (Gunn & Peterson 1965), while the harder photons produce the cosmic X-ray background (Fabian & Iwasawa 1999; Elvis et al. 2002; Ueda et al. 2003; Cao 2005). On Mpc scales, the ultraviolet flux photoionizes the nearby IGM resulting in the proximity effect, or the lower optical depth for Ly α absorption at the quasar redshift (Bajtlik et al. 1988; Scott et al. 2000). On the smallest scales of 1-100 pc, the interplay between black hole accretion, radiation, and the surrounding gas, produce the characteristic emission from the well-studied broad and narrow emission line regions (see Osterbrock & Ferland 2006).

But the degree to which a quasar can influence its host galaxy on scales $\sim \text{kpc} - \text{Mpc}$ is much less clear. Indeed, just a few percent of the energy $\sim 10^{62} \text{ ergs}$ emitted by a quasar is comparable to the binding energy of a massive galaxy $\sim 10^{60} \text{ erg}$, and thus capable of ejecting its interstellar medium (ISM) or shock-heating it to temperatures $T \sim 10^7 \text{ K}$. The bulges of all local galaxies harbor supermassive black holes (Kormendy & Richstone 1995), the masses of which are tightly correlated with the properties of their host spheroids, measured on scales $\sim \text{kpc}$ (Magorrian et al. 1998; Ferrarese & Merritt 2000; Gebhardt et al. 2000). This has led many to speculate that some "feedback" mechanism couples the quasar phase of rapid supermassive black hole growth with the evolution of its host galaxy (e.g. Silk & Rees 1998; Kauffmann & Haehnelt 2000; Wyithe & Loeb 2003; Granato et al. 2004; Scannapieco & Oh 2004; Springel et al. 2005a; Scannapieco et al. 2005; Kawata & Gibson 2005; Menci et al. 2006; Cox et al. 2006; Lu & Mo 2007; Sijacki et al. 2007; Hopkins et al. 2008).

Besides explaining the correlation between black holes and bulges, feedback from an AGN has also been invoked on even larger scales, as the energy source which "quenches" star-formation in massive galaxies, leaving them "red and dead". The observed bimodality in the galaxy color-magnitude diagram (Strateva et al. 2001; Baldry et al. 2004; Bell et al. 2004; Blanton et al. 2005; Faber et al. 2007) and the sharp cutoff at the bright end of the galaxy

¹ Department of Astronomy and Astrophysics, UCO/Lick Observatory; University of California, 1156 High Street, Santa Cruz, CA 95064; xavier@ucolick.org

² Visiting Astronomer, W.M. Keck Telescope. The Keck Observatory is a joint facility of the University of California and the California Institute of Technology.

³ Department of Astronomy, University of California Berkeley, Berkeley, CA 94720; joeh@berkeley.edu

⁴ NSF Astronomy and Astrophysics Postdoctoral Fellow

⁵ This energy is appropriate for a typical quasar near the peak of activity at $z \sim 2.5$, a radiative efficiency $\epsilon \sim 0.1$, and an Eddington ratio of 0.1.

luminosity function (Benson et al. 2003) both point to some physical mechanism which shuts off star-formation in massive galaxies. Otherwise, large quantities of gas should have accreted onto the progenitors of ellipticals resulting in an unseen population of very massive blue galaxies. It is generally believed that the coupling between the quasar and the galaxy is “kinetic” in nature, involving galactic-scale outflows which suppress gas accretion and inject heat, ultimately shutting off star-formation (e.g. Kauffmann & Haehnelt 2000; Scannapieco & Oh 2004; Springel et al. 2005a; Cox et al. 2006; Hopkins et al. 2007b).

An important laboratory for studying the astrophysics of quasar feedback and quenching are luminous high redshift radio galaxies (HzRGs; for a review see McCarthy 1993; Miley & De Breuck 2008). In these sources outflowing collimated relativistic plasma, or “radio jets”, can extend to several tens of kpc from the optical host galaxies, providing the most compelling evidence that an AGN can impact its galactic scale surroundings. It is unclear, however, whether this jet energy $\gtrsim 10^{60}$ erg (e.g. Miley 1980) couples strongly to the ambient ISM (Begelman & Cioffi 1989). In addition to the tremendous radio power, $z \gtrsim 2$ HzRGs are often associated with giant Ly α recombination nebulae, with sizes of up to ~ 200 kpc, sometimes extending well beyond the radio emission (see Villar-Martín et al. 2007, for a review). Ionizing radiation from the central AGN, thought to be obscured from our vantage point, is likely to play a significant role in exciting this emission. But the extreme kinematics of these nebulae (FWHM $\gtrsim 1000$ km s $^{-1}$ Nesvadba et al. 2006; Reuland et al. 2007; Villar-Martín et al. 2007), their complex irregular morphology, the tendency for the line emission to be aligned with the axis of the radio jets, and their near solar metallicities (Vernet et al. 2001; Humphrey et al. 2008), strongly suggest that jet-gas interactions or feedback from the AGN are giving rise to a large-scale outflow, and shocks from these motions could also be triggering the emission. But the comoving number density of HzRGs and giant Ly α nebulae, $n \sim 10^{-8}$ Mpc $^{-3}$ (Miley & De Breuck 2008), is about three orders of magnitude smaller than the number density of luminous quasars. Thus only about one in a thousand of the supermassive black holes in the Universe exhibit such dramatic evidence for feedback during their active phase⁶, which would do little to quench star-formation in the entire population of local massive galaxies. Is feedback occurring in the typical quasar in the Universe?

While it has been argued that heating from a quasar is responsible for quenching massive galaxies (Springel et al. 2005b; Hopkins et al. 2007a), an alternative scenario is related to the physics of structure formation in a hierarchical Universe. This idea goes back to a classic argument first made by Rees & Ostriker (1977) that the ability to cool on a dynamical timescale is what sets the upper bound for the mass of luminous galaxies. At low halo masses the cooling time of gas is shorter than the dynamical time resulting in a “cold accretion” mode, limited only by the supply of infalling material. For halos with $M \gtrsim 10^{12} M_{\odot}$, the cooling time exceeds the dynamical time, which is the criterion for the formation of a stable accretion shock (Dekel & Birnboim 2006). In these more massive halos, subsequent infalling gas is shock heated and pressure supported by a hot halo in quasi-hydrostatic equilibrium. However, cosmological hydrodynamical simulations have shown that although the majority of gas is shock-heated to the virial temperature, some level of “cold mode” accretion still takes place in even the most massive halos (Kereš et al. 2005; Ocvirk et al. 2008). It is unknown whether the formation of a hot-halo alone can quench future star-formation and explain the red and dead galaxy population. Dekel & Birnboim (2008) recently proposed a quenching scenario whereby the gravitational energy of cosmological accretion can serve as a heat source to quenching star formation, provided that a cold ($T \sim 10^4$ K) phase of pressure-confined (and thus long lived) gas clumps ($M \sim 10^5 - 10^8 M_{\odot}$) form, which can penetrate the halo and deliver the necessary heat.

Understanding the role that quasar feedback, hot halos, cold accretion, and pressure confined clumps play in quenching star-formation, requires studying the physical state of the gas on scales 10 kpc-1 Mpc in the high redshift progenitors of local massive red galaxies. Conroy et al. (2007, see also Wechsler et al. 1998) model the clustering and number density of $z \sim 2-3$ star-forming galaxies and deduced host dark halo masses $M \lesssim 10^{12} M_{\odot}$. These low masses allowed them to convincingly argue that $z \sim 2-3$ star-forming galaxies *do not* evolve into the quenched red and dead galaxies that we see today, but rather evolve into blue $\sim L_*$ galaxies similar to the Milky Way. But the strong clustering of luminous quasars at $z \sim 2$ implies larger dark halo masses $\gtrsim 10^{13} M_{\odot}$ (Croom et al. 2001; Porciani et al. 2004; Croom et al. 2005), indicating that they *are indeed the progenitors of local red and dead galaxies*. Of course, we are only observing a small fraction $\sim 10^{-2} - 10^{-3}$ of these progenitors as quasars at any given time because the quasar lifetime is much shorter than the age of the Universe.

However quasar spectra have thus far provided little insight into the state of gas in their galactic environments for two reasons. First, the large ionizing flux from the quasar typically photoionizes the hydrogen in and around the galactic host (Hennawi & Prochaska 2007; Prochaska et al. 2008b; Chelouche et al. 2007), which would otherwise be detected as strong H I absorption at the quasar redshift. Second, the interpretation of material that is detected in absorption along the line-of-sight to a quasar is limited by the unknown distance between the material and the quasar. A systematic search for the signatures of photoionized gas near quasars (e.g. via N V, O VI absorption) is only now being carried out on statistical datasets (Tripp et al. 2007; Fox et al. 2008). Observers do frequently identify narrow associated absorption lines (NAALs) or so-called “associated absorbers” which are believed to arise in the quasar environment. Some of these are attributed to gas on sub-pc scales (e.g. Elvis 2000), but other examples exhibit ionization states that suggest the gas lies at several tens of kpc (D’Odorico et al. 2004; Rix et al. 2007). Note that these associated absorbers are distinct from the broad absorption line (BAL) features which arise from dense clumps of material that have been ionized and accelerated by the quasar, and are generally believed to be confined to sub-kpc

⁶ Because the implied lifetime of the jets and nebulae are $\sim 10^8$ years, they cannot represent a short lived phase of evolution in every quasar.

scales (but see de Kool et al. 2001).

In a series of papers, we have introduced a novel technique to study the physical state of gas in the ISM and halo of luminous quasars, which has the potential to provide powerful constraints on feedback, quenching and the physics of massive galaxy formation. Namely, we use a background quasar (b/g quasar) sightline to probe the state of gas in absorption in the vicinity of a foreground quasar (f/g quasar; see also Bowen et al. 2006). Although such projected quasar pair sightlines are extremely rare, Hennawi et al. (2006b, see also Hennawi 2004) showed that it is straightforward to select $z \gtrsim 2$ projected quasar pairs from the imaging and spectroscopy provided by the Sloan Digital Sky Survey (SDSS; York et al. 2000). To date about 90 pairs of quasars have been uncovered with impact parameter $R < 300$ kpc and $z_{\text{fg}} > 1.6^7$. Spectroscopic observations of the b/g quasar in each pair reveals the nature of the IGM transverse to the f/g quasar on scales of a few 10 kpc to several Mpc. This approach has the advantage of tracing diffuse gas over a wide range of density and temperature, ranging from cold neutral material $T \sim 100$ K to collisionally ionized plasma $T \approx 10^6$ K, and with column densities in the range $N \sim 10^{12} - 10^{22} \text{ cm}^{-2}$. In Paper I (Hennawi et al. 2006a), we searched 149 b/g quasar spectra for optically thick absorption in the vicinity of $1.8 < z_{\text{fg}} < 4.0$ luminous f/g quasars, and uncovered a sample of 27 new quasar-absorber pairs with impact parameters ranging from 30 kpc – 2.5 Mpc. In Paper II (Hennawi & Prochaska 2007), we analyzed the clustering of these transverse absorbers with the foreground quasar and measured a large clustering signal on galactic scales. We also refer the reader to the manuscript by Tytler et al. (2007) who consider several applications of quasar pair spectroscopy.

In this paper, we present the first high resolution spectrum of the b/g quasar in the close projected quasar pair SDSSJ1204+0221. By mining the sky for very rare close associations of quasars (Hennawi 2004; Hennawi et al. 2006b,a), we previously discovered this rare system with angular separation $\theta = 13.3''$ corresponding to impact parameter $R_{\perp} = 108$ kpc at the redshift of the foreground quasar $z_{\text{fg}} = 2.4360 \pm 0.0005$, precisely determined from Gemini/GNIRS near-IR spectroscopy. The spectral and photometric properties of SDSSJ1204+0221FG make it an unremarkable quasar at $z \sim 2.4$. We estimate a bolometric luminosity of $L_{\text{QSO}} \simeq 1.4 \times 10^{46} \text{ erg s}^{-1}$ placing it near the ‘knee’ of the $z \sim 2.5$ quasar luminosity function (Croom et al. 2004; Richards et al. 2006), and corresponding to a supermassive black hole $M_{\text{BH}} \simeq 1.1 \times 10^9 \left(\frac{f_{\text{Edd}}}{0.1} \right)^{-1} M_{\odot}$, if it accretes at one tenth of the Eddington limit. The impact parameter of our background sightline $R_{\perp} = 108$ kpc, easily resolves the expected virial radius $r_{\text{vir}} = 250 \text{ kpc} (M/10^{13.3} M_{\odot})^{1/3}$ of the f/g quasar host, and pierces its halo at about the ‘cooling radius’, where gas shock-heated to the virial temperature should take about a Hubble time to cool. The only remarkable thing about SDSSJ1204+0221 is that it has a $z_{\text{bg}} = 2.53$ b/g quasar in close projection which is bright enough ($r = 19.0$) for high resolution spectroscopy. Our Keck HIRES Echelle spectrum of SDSSJ1204+0221BG, the first ever to probe the halo gas of a f/g quasar, resolves the velocity fields of the absorbing gas and allows us to measure precise column densities for H I and the ionic transitions of metals like Si, C, N, O, and Fe. These measurements allow us to place constraints on the physical state of the gas near the f/g quasar, such as its kinematics, temperature, ionization structure, chemical enrichment patterns, volume density, the size of the absorbers, the intensity of the impinging radiation field, as well as test for the presence of hot collisionally ionized gas. In § 2 we present the observations and provide column density measurements. We constrain the ionization state, estimate relative chemical abundances, and constrain the electron density of the gas in § 3. In § 4 we further discuss our results and how they relate to other observations of quasars, absorption line systems, and high redshift galaxies. The implications of our results for models of feedback, quenching, and massive galaxy formation are presented in § 5, and we conclude with a summary in § 6. The reader who is not concerned with the details of the observations and absorption line modeling can read Table 4 summarizing those results and then skip to § 4. Throughout the manuscript, we use the cosmological parameters $\Omega_m = 0.30$, $\Omega_{\Lambda} = 0.70$, $h = 0.70$, consistent to within $1 - \sigma$ with the parameters measured by the WMAP experiment (Dunkley et al. 2008) and we adopt the solar chemical composition compiled by Grevesse et al. (2007).

2. OBSERVATIONS AND ANALYSIS

The principal goal of our analysis is to search for and characterize gas associated with the foreground quasar SDSSJ1204+0221FG in the high resolution spectrum of a background quasar SDSSJ1204+0221BG identified in close projection. To establish a physical association, we demand that the absorption and SDSSJ1204+0221FG have nearly identical velocity. To this end, we must obtain a precise measurements for the quasar systemic redshift. But it is well known that the primary rest-frame ultraviolet emission lines which are redshifted into the optical for $z \gtrsim 2$ quasars can differ by up to $\sim 3000 \text{ km s}^{-1}$ from systemic, due to outflowing/inflowing material in the broad line regions of quasars (Gaskell 1982; Tytler & Fan 1992; Vanden Berk et al. 2001; Richards et al. 2002), with a more typical error being $\sim 1000 \text{ km s}^{-1}$. An accurate redshift can be determined from narrow ($\sigma \lesssim 200 \text{ km s}^{-1}$) forbidden emission lines, such as [O II] $\lambda 3727$ or [O III] $\lambda 5007$ which arise from the narrow line region, but at $z \gtrsim 2$, measurements of these lines require spectra covering the near infrared.

To this end we observed SDSSJ1204+0221FG using the the Gemini Near Infra-Red Spectrograph (GNIRS; Elias et al. 2006) on the Gemini-South telescope on March 27, 2006. We used the $0.15''/\text{pixel}$ camera and the 32 lines mm^{-1} grating in cross dispersed mode, giving complete coverage over the wavelength range $0.9\text{--}2.4 \mu\text{m}$. The slit width was $0.45''$ (~ 3 pixels) giving a resolving power of $R \simeq 1100$ or a FWHM $\simeq 270 \text{ km s}^{-1}$. The total exposure time was 5440s, which was broken up into $16 \times 340\text{s}$ exposures to prevent the brightest sky lines from saturating the detector. The GNIRS spectra were reduced using standard techniques with a custom data reduction pipeline written

⁷ The lower limit on redshift is motivated by the ability to detect redshifted Ly α absorption above the atmospheric cutoff $\lambda > 3200 \text{ \AA}$

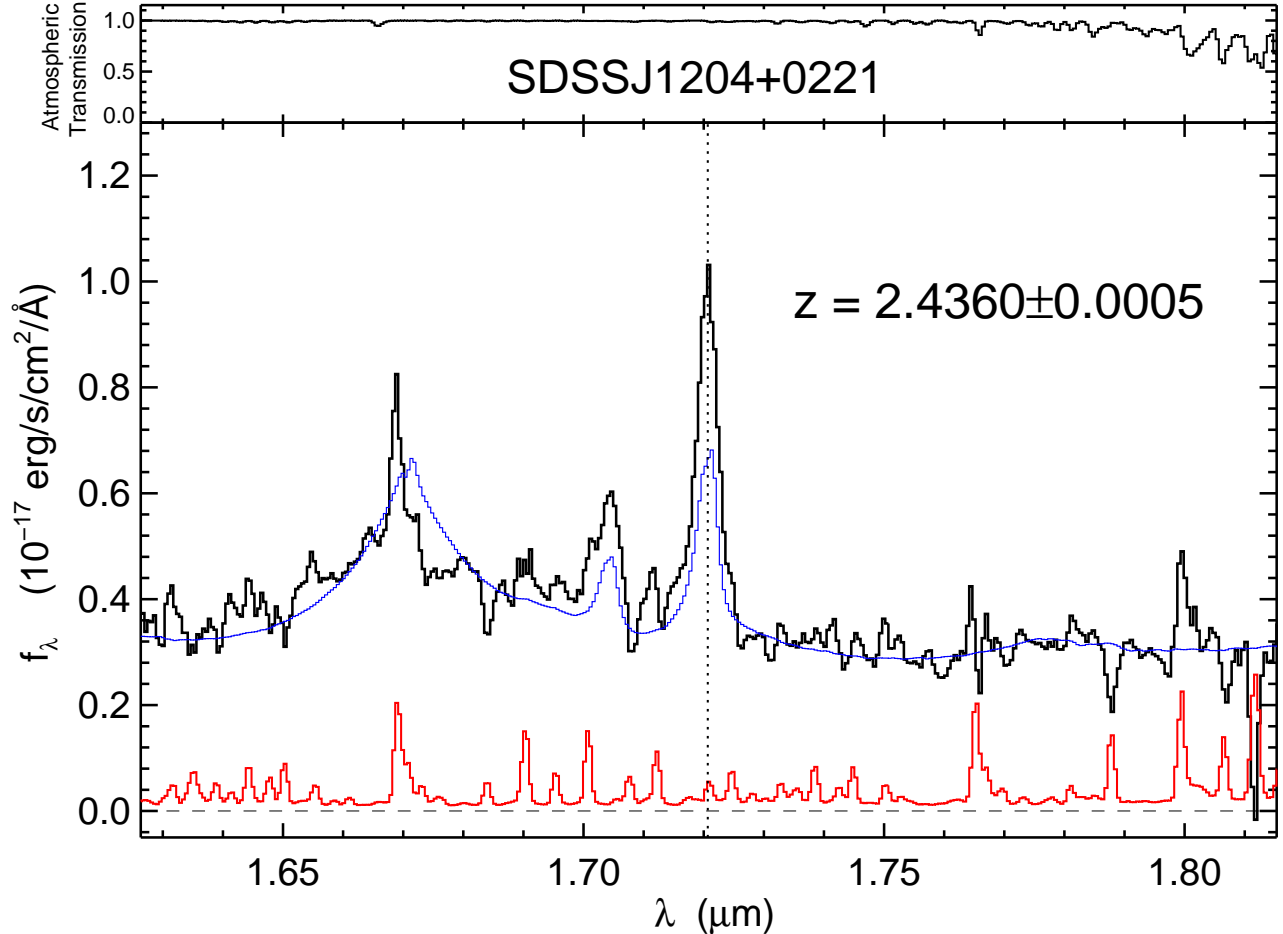


FIG. 1.— GNIRS spectrum of SDSSJ1204+0221FG centered on the $H\beta$ -[O III] emission line complex ($H\beta$ $\lambda 4861$, [O III] $\lambda 4959$, and [O III] $\lambda 5007$) which is redshifted into the H -band. This spectrum was used to determine the systemic redshift of the quasar, $z_{\text{fg}} = 2.4360 \pm 0.0005$, from the strong [O III] $\lambda 5007$ emission line. The lower red histogram is the $1\text{-}\sigma$ noise and the smooth blue curve overlaid on the data is the composite quasar template of Vanden Berk et al. (2001) redshifted to z_{fg} . The upper panel shows the atmospheric transmission for the corresponding wavelengths.

in the Interactive Data Language (IDL) and described in Hennawi & Prochaska (in prep.). Wavelength solutions were determined by comparing extracted spectra of the night sky to an atlas of OH sky emission lines, and heliocentric corrections were applied to the spectra. The RMS deviation in our wavelength fits were typically 1-1.5 Å (or about 0.2-0.3 pixels). In the H -band, this corresponds to a velocity uncertainty of 20–30 km s^{−1}, but since our fits typically use 50 lines, we believe that our wavelength solutions are accurate to better than $\lesssim 5$ km s^{−1}.

We computed a systemic redshift from the strong [O III] $\lambda 5007$ emission line⁸ which is redshifted to ~ 1.7 μm in the H -band for $z \sim 2.4$ (see Figure 1). We found that the most effective line-centering algorithm was to iterate a flux-weighted line-centering scheme until the line-center converged to within a specified tolerance. We achieved more stable results when the pixel values were weighted by a Gaussian kernel (true flux-weighting would correspond to a box-car kernel) with dispersion set to $\sigma_{[\text{O III}]} = 6.04$ Å, which is the average dispersion of the [O III] emission line measured by Vanden Berk et al. (2001). We do not estimate formal errors for the line centering, as they are smaller than the intrinsic error incurred by using [O III] as a proxy for the systemic frame. Boroson (2005) measured the distribution of velocity shifts of the [O III] line center about the systemic frame defined by low-ionization forbidden lines. He found that [O III] has an average blueshift of $\Delta v = 27$ km s^{−1} from systemic and a dispersion of $\sigma = 44$ km s^{−1} about this value. To account for the average shift, we add $\Delta v = 27$ km s^{−1} to the vacuum rest wavelength of 5008.24 Å when computing the redshift of the line. For the 1σ error on our [O III] near-IR redshifts we adopt $\sigma = 44$ km s^{−1}. We thus determine the systemic redshift of SDSSJ1204+0221FG to be $z_{\text{fg}} = 2.4360 \pm 0.0005$. All velocities are reported relative to this redshift value for the remainder of this paper. Figure 1 shows part of the H -band region of our GNIRS spectrum of SDSSJ1204+0221FG centered on the $H\beta$ -[O III] emission line complex ($H\beta$ $\lambda 4861$, [O III] $\lambda 4959$, and [O III] $\lambda 5007$) and our determination of the systemic redshift.

High resolution optical spectroscopy of the b/g quasar SDSSJ1204+0221BG was obtained on the nights of UT 13

⁸ The [O III] 4959 line is plagued by sky emission lines and the $H\beta$ lines are not as reliable a diagnostic as [O III] for QSO redshifts.

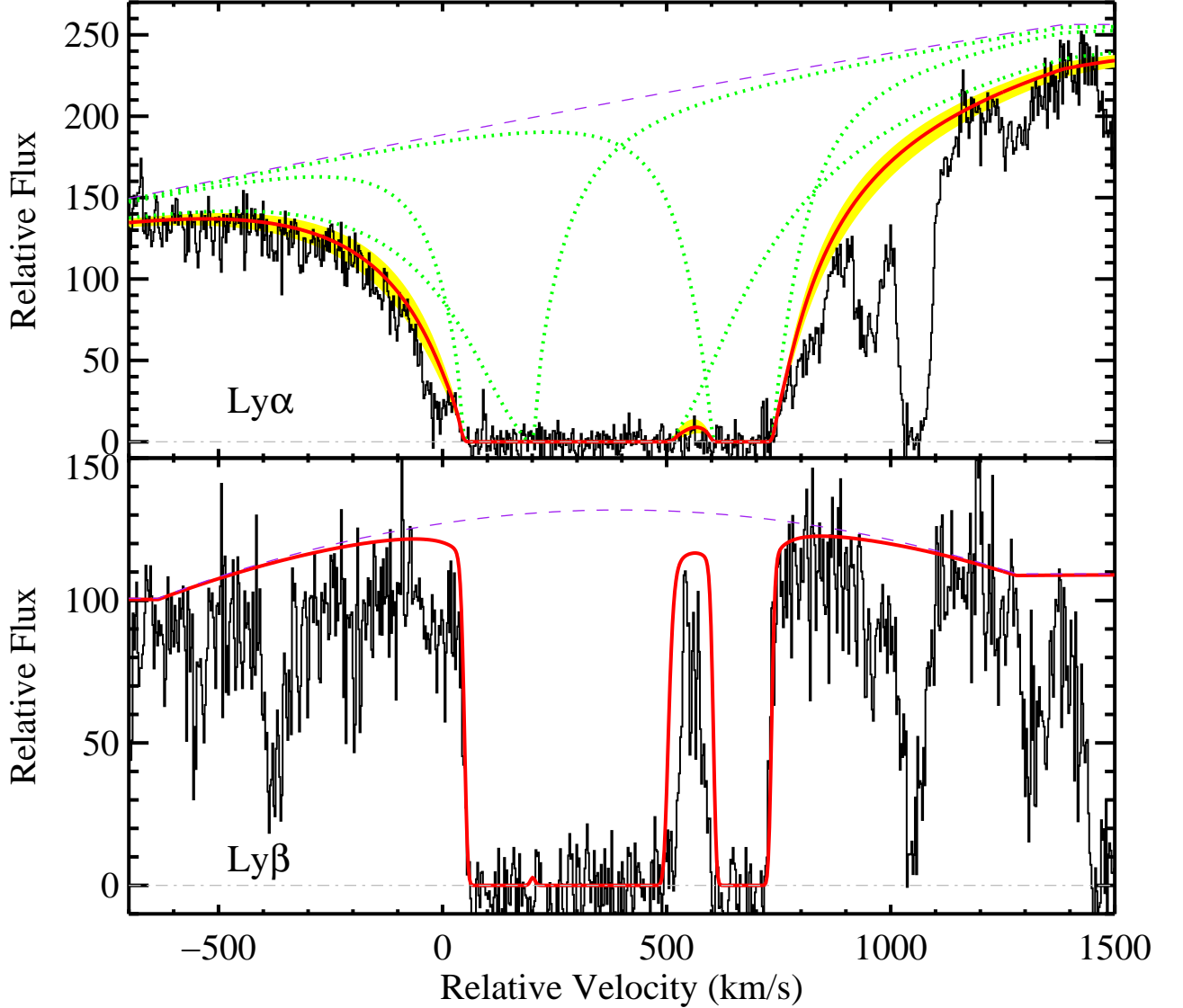


FIG. 2.— $\text{Ly}\alpha$ and $\text{Ly}\beta$ profiles for the super Lyman limit system identified in the spectrum of the background quasar SDSSJ1204+0221BG at a velocity consistent with the foreground quasar SDSSJ1204+0221FG. The relative velocity $v = 0 \text{ km s}^{-1}$ corresponds to the best-fit value for the redshift of SDSSJ1204+0221FG, $z_{\text{fg}} = 2.4360$. The purple dashed line indicates our estimate of the quasar continuum in these relative flux units. We have fitted these line-profiles with three H I components, each centered at the peak optical depth of low-ion absorption associated with this H I gas. The green dotted lines show the $\text{Ly}\alpha$ profiles for each component, and the solid red curve is the convolved fit. The $\text{Ly}\beta$ profile constrains the Doppler parameters of the outer two components to have $b < 25 \text{ km s}^{-1}$, while the $\text{Ly}\alpha$ profile requires these components have $N_{\text{HI}} < 10^{19} \text{ cm}^{-2}$. With these constraints on the outer components, we derive $N_{\text{HI}} = 10^{19.60 \pm 0.15} \text{ cm}^{-2}$ for the central component and note a mild degeneracy between this value and that for the outer components which is reflected in our error estimate.

April 2005 and 3 May 2005 (one 5400s exposure per night), using the HIRESb spectrometer (Vogt et al. 1994) on the KeckI telescope. The data were acquired through the C5 decker affording a $\text{FWHM} \approx 8 \text{ km s}^{-1}$ resolution and processed with the HIRedux⁹ pipeline (Bernstein et al. 2008). The signal-to-noise (S/N) ratio per 2.6 km s^{-1} pixel is approximately 15 at 4000 \AA and the combined spectrum offers nearly continuous wavelength coverage from $\lambda \approx 3450 \text{ \AA}$ to 6400 \AA . A search for gas in the spectrum of SDSSJ1204+0221BG at $z \approx z_{\text{fg}}$ revealed a strong $\text{Ly}\alpha$ profile and a series of metal-line transitions. In Figure 2, we present the $\text{Ly}\alpha$ and $\text{Ly}\beta$ profiles for this absorption system. One readily observes the damping wings of the $\text{Ly}\alpha$ profile which require a total H I column density $N_{\text{HI}} \gtrsim 10^{19} \text{ cm}^{-2}$ marking this absorber as a ‘super’ Lyman limit system (SLLS; also referred to as sub-damped $\text{Ly}\alpha$ systems Péroux et al. 2002). For the remainder of the paper, we refer to this absorption system as SLLS/SDSSJ1204+0221BG.

We have modeled the $\text{Ly}\alpha$ and $\text{Ly}\beta$ profiles by introducing three H I components at the velocities corresponding to the peak optical depths of three sets of metal-line complexes (defined below as subsystems A, B, and C). Having fixed the redshifts of the Lyman series, we then varied the N_{HI} values and Doppler parameters (b -values) of these three components. For subsystems A and C, the $\text{Ly}\alpha$ profile restricts the H I column densities to be $N_{\text{HI}}^{A,C} < 10^{19} \text{ cm}^{-2}$;

⁹ <http://www.ucolick.org/~xavier/HIRedux/index.html>

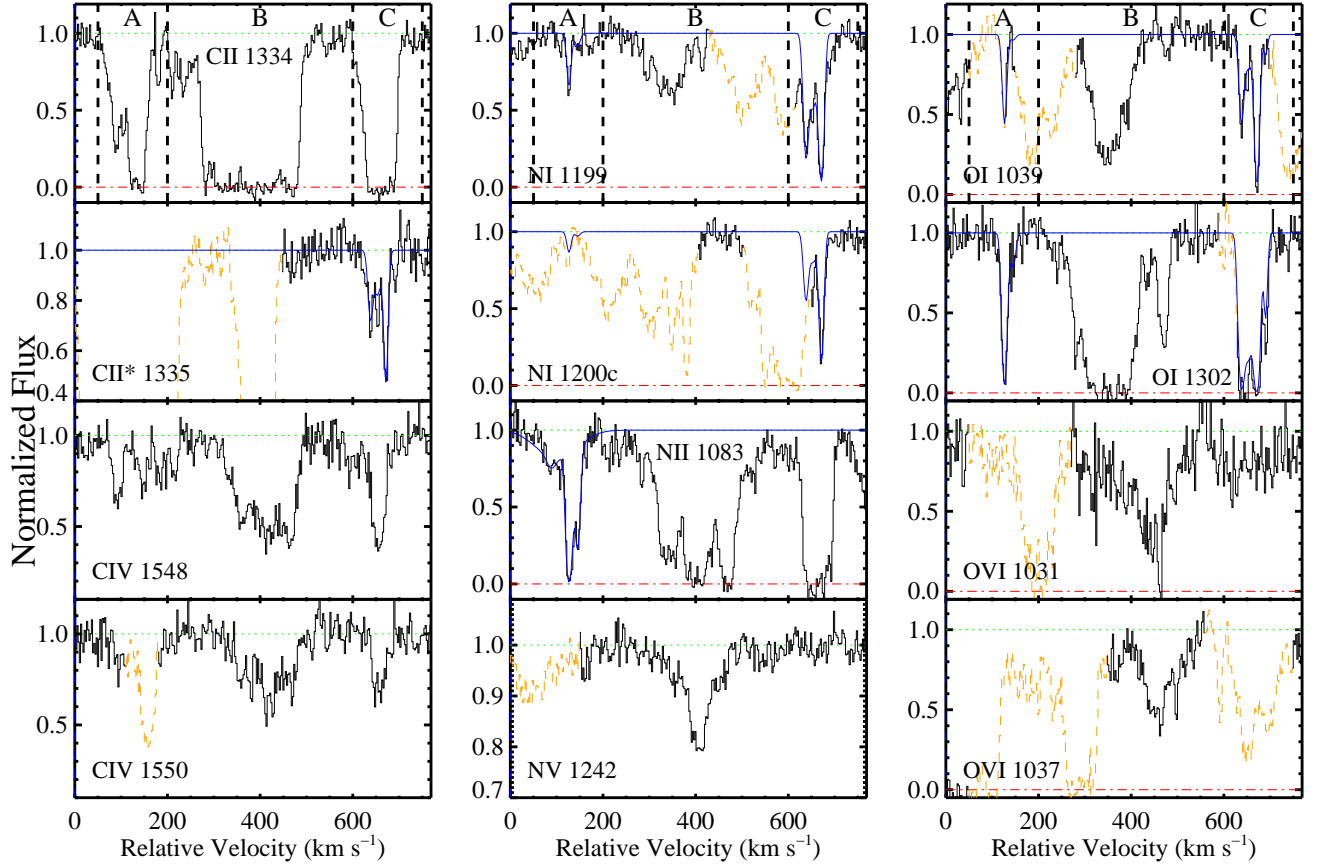


FIG. 3.— Metal-line transitions from the super Lyman limit system identified at the redshift of SDSSJ1204+0221FG. The velocities are relative to the measured redshift of SDSSJ1204+0221FG, $z_{\text{fg}} = 2.4360$. The absorption occurs in three velocity intervals which we designate as subsystems A,B,C as denoted by the vertical dashed lines in the upper panel of each subplot. Note the strong low-ion and N II absorption, the absence of Si II* 1264, the relatively weak C IV and Si IV profiles, and the likely absence of N V and O VI absorption. For a subset of the transitions from subsystems A and C we overplot the line-profile fits derived using the VPFIT software package and mark the components included (dark blue) and not included (light red) in the fit as listed in Table 1. Absorption that is presumed unrelated to SLLS/SDSSJ1204+0221BG (e.g. Ly α features from unrelated redshifts) is presented as a dashed, orange line.

larger values give a damped Ly α profile that contradicts the observed fluxes at $\lambda \approx 4177.5\text{\AA}$ and 4187.5\AA (i.e. $\delta v \approx -100\text{ km s}^{-1}$ and $+750\text{ km s}^{-1}$ in Figure 2). Similarly, the Ly β profile demands effective¹⁰ Doppler parameters $b_{A,C} < 25\text{ km s}^{-1}$. Allowing for these constraints, we derive a value of $N_{\text{HI}}^B = 10^{19.60 \pm 0.15}\text{ cm}^{-2}$ for subsystem B that is independent of its nearly unconstrained Doppler parameter. The error in this N_{HI} estimate includes uncertainty due to the continuum placement and line-blending with subsystems A and C. In the figure, we have overplotted a best-fit solution which assumes $N_{\text{HI}} = 10^{18.6}\text{ cm}^{-2}$ for the subsystems A and C.

¹⁰ The metal-line profiles show these subsystems are the blend of several narrow components but we only consider a single H I cloud for each. Therefore, the b -values reported for the H I gas likely overestimate the values of the individual components.

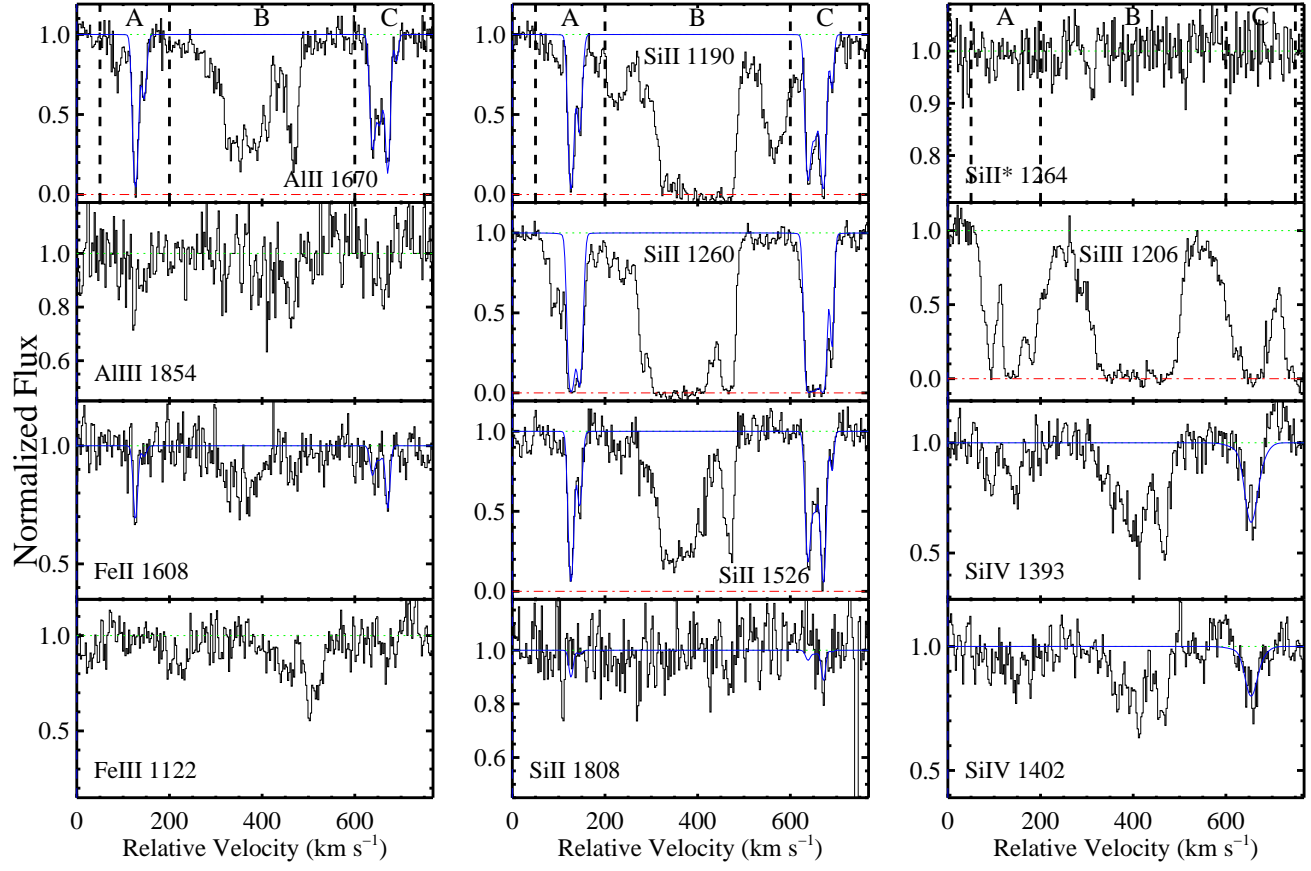


TABLE 1
VOIGT PROFILE SOLUTIONS

Comp	z	$\sigma(z)$ (10^{-5})	v^a (km s^{-1})	b (km s^{-1})	$\sigma(b)$ (km s^{-1})	Ion	$\log N$ (cm^{-2})	$\sigma(N)$
H I								
A	2.43744					H I	18.60	0.40
B	2.44000					H I	19.60	0.15
C	2.44367					H I	18.60	0.40
Metals								
1	2.437010	1.0	+88	12.22	7.77	N II	12.84	0.80
2	2.437150	1.0	+100	60.71	15.80	N II	13.87	0.14
3	2.437451	0.2	+127	4.49	0.31	N I	13.09	0.06
						N II	14.84	0.22
						O I	14.60	0.06
						Al II	12.97	0.13
						Si II	14.07	0.11
						Fe II	13.26	0.08
4	2.437664	0.5	+145	5.82	0.86	N I	12.46	0.27
						N II	13.82	0.05
						O I	13.28	0.12
						Al II	11.92	0.06
						Si II	13.23	0.05
						Fe II	12.40	0.50
5	2.443318	0.6	+639	5.48	0.60	C II*	13.00	0.09
						N I	13.75	0.05
						O I	14.62	0.06
						Al II	12.29	0.07
						Si II	13.65	0.05
						Si IV	12.05	1.40
						Fe II	12.82	0.19
6	2.443497	1.3	+655	9.05	2.83	C II*	12.94	0.13
						N I	13.46	0.11
						O I	14.22	0.16
						Al II	12.26	0.09
						Si II	13.38	0.11
						Si IV	12.76	0.35
						Fe II	12.66	0.31
7	2.443702	0.2	+672	4.35	0.27	C II*	13.35	0.04
						N I	14.33	0.05
						O I	15.35	0.12
						Al II	12.57	0.09
						Si II	14.12	0.08
						Si IV	12.20	1.32
						Fe II	13.16	0.09
8	2.443915	1.0	+691	3.00	2.20	O I	13.74	0.21
						Al II	11.36	0.14
						Si II	12.76	0.09

^aVelocity relative to the redshift of the foreground quasar SDSSJ1204+0221FG, $z_{fg} = 2.4360$.

In Figure 3 we present a sub-set of the metal-line transitions observed along the sightline near the redshift of the foreground quasar. All velocities are relative to the redshift of SDSSJ1204+0221FG, $z_{\text{fg}} = 2.4360$. The various ions observed near this redshift show absorption in roughly three distinct velocity intervals spanning a total interval $\Delta v \approx 650 \text{ km s}^{-1}$. We define these three velocity intervals as ‘subsystems’, A: $+50 \text{ km s}^{-1} < \delta v < +200 \text{ km s}^{-1}$; B: $+200 \text{ km s}^{-1} < \delta v < +600 \text{ km s}^{-1}$; and C: $+600 \text{ km s}^{-1} < \delta v < +750 \text{ km s}^{-1}$. We have measured column densities for the ions observed in these subsystems with two methods: (i) by fitting Voigt-profiles to the data using the VPFIT software package (kindly provided by R. Carswell); and (ii) by integrating the apparent optical depth profile (AODM; Savage & Sembach 1991). The Voigt-profile fitting is most reliably performed on unsaturated transitions of ions which show similar velocity structure. In this case, one can ‘tie’ the redshifts of the components which comprise the velocity profile for all of the ions analyzed and only allow the column densities and Doppler parameters to vary. The VPFIT software package minimizes the χ^2 of the profile fits and reports a best value of the redshift, b -value, and column density for each component introduced by the user.

We were able to employ the Voigt-profile procedure on the majority of low and intermediate ions for subsystems A and C. With the exception of Si IV in subsystem C¹¹, however, we could not recover a consistent solution assuming the same component structure for the low and high-ions. Therefore, we calculate the high-ion column densities using the AODM method integrated across the entire velocity interval of each subsystem. We conclude that the high-ion gas arises in a distinct phase with a unique velocity field. In the ionization modeling that follows (§ 3), one should keep in mind that the subsystems are likely multi-phase absorbers. This means the resulting high-ion to low-ion ratios should be considered upper limits with respect to the nature of the lowest ionization phase. The results of the line-profile fits are overplotted in Figure 3 and tabulated in Table 1.

The velocity profiles of subsystem B are more complicated than subsystems A and C. This complex absorption precludes a well constrained line-profile solution based on individual Voigt profiles. Furthermore, it is apparent from a visual inspection of the Si II and C IV transitions that the ratios of the low-ion to high-ions columns vary significantly from $\delta v = +300$ to $+500 \text{ km s}^{-1}$. Therefore, subsystem B is comprised of gas in at least two different ionization phases. This includes the most highly ionized gas on the sightline (at $\delta v \approx +430 \text{ km s}^{-1}$), where one observes strong C IV and Si IV absorption but very little O I or Si II gas. For subsystem B, therefore, we report total column densities based on the AODM and caution that an analysis of the gas properties must consider multi-phase material.

3. IONIZATION MODELING AND PHYSICAL CONDITIONS

In this section we constrain the ionization state of the gas in the three subsystems identified with the super-LLS identified at $z \approx 2.4360$ toward SDSSJ1204+0221BG, named SLLS/SDSSJ1204+0221BG. One goal is to test the hypothesis that the nearby quasar SDSSJ1204+0221FG is shining on the gas. A test of this hypothesis is to compare the intensity of the ionizing radiation field that reproduces the observed ionic ratios with the predicted flux of the quasar at the impact parameter of the sightline. We constrain the intensity by comparing observed ionic ratios with photoionization models. Another goal is to constrain the chemical abundances of the gas. These measurements reflect the integrated star formation history of the galaxy that hosts (or hosted) the absorber and, in turn, star-formation in this quasar environment. Standard practice is to gauge the contributions of Type II nucleosynthesis relative to Type I abundances from estimates of the α/Fe ratio where α -elements include O, Mg, Si, and S. The data also constrain the N abundance which is expected to trace nucleosynthesis by intermediate mass stars and therefore offers unique constraints on the timescales of star formation (Henry et al. 2000; Henry & Prochaska 2007). This requires an assessment of the ionization state to estimate corrections to the observed ionic ratios.

The analysis focuses on multiple ionization states of individual elements (e.g. N^0/N^+ , $\text{Si}^+/\text{Si}^{+3}$) to avoid uncertainties related to intrinsic abundances. For an optically thick absorber, one expects absorption from ions with ionization potentials (IPs) of one to a few Ryd. Ions with lower ionization potentials should be absent because H I gas is essentially transparent to photons with energies less than 1 Ryd. Photons with energies above a few Ryd will be significantly attenuated by the H I gas and for $h\nu > 4 \text{ Ryd}$ by helium. Our analysis is most sensitive to the shape and intensity of the radiation field at 1 to 4 Ryd, although the nature of the radiation field at higher energies is constrained by observations of N V and O VI transitions: $\text{IP}(\text{N}^{+4}) = 77.4 \text{ eV}$ and $\text{IP}(\text{O}^{+5}) = 113.9 \text{ eV}$.

Finally, we will constrain the electron density n_e of the gas by comparing the relative populations of the $J = 3/2$ and $J = 1/2$ fine-structure levels of C^+ and Si^+ ions (e.g. Prochaska 1999; Silva & Viegas 2002). We will argue the gas is partially ionized and therefore assume collisions by electrons¹² dominate excitation to the $J = 3/2$ upper level. With an estimate of the gas temperature one estimates n_e by measuring the relative populations of the ground and excited states.

In the following sub-sections, we start with the simpler subsystems A and C before considering the more complex subsystem B.

3.1. Subsystem A: $+50 \text{ km s}^{-1} < \delta v < +200 \text{ km s}^{-1}$

Before delving into detailed photoionization models, one can build intuition by making qualitative inspection of the ions detected. Examining subsystem A in Figure 3, one notes strong absorption from a series of low-ions, e.g. O^0 , Si^+ , N^0 , Fe^+ . This is characteristic of Lyman limit systems where the large H I opacity self-shields gas from

¹¹ Even in this case, a reasonable fit required a substantially different Doppler parameter.

¹² The impact parameter of SDSSJ1204+0221BG from SDSSJ1204+0221FG is sufficiently large that indirect UV pumping by SDSSJ1204+0221FG does not contribute to the excitation of these lines.

TABLE 2
IONIC COLUMN DENSITIES

Ion	λ_{rest} (Å)	$\log f$	v_{int}^a (km s ⁻¹)	$\log N_{\text{AODM}}$	$\log N_{\text{VPFIT}}^b$	
A						
C II	1036.3367	−0.9097	[37, 187]	> 14.63	13.18 ± 0.07 14.93 ± 0.18	
C IV				> 14.63		
N I	1548.1950	−0.7194	[57, 227]	13.60 ± 0.03		
N II				13.60 ± 0.03		
N V	1242.8040	−1.1066	[87, 167]	< 13.10	14.62 ± 0.06	
O I				< 13.10		
O VI	1031.9261	−0.8765	[67, 147]	< 13.67		
Al II				< 13.67		
Al III	1854.7164	−0.2684	[67, 187]	< 12.41	13.01 ± 0.12	
Si II				< 12.41		
Si II*	1264.7377	−0.0441	[37, 197]	< 11.93		14.13 ± 0.09
Si III				< 11.93		
Si IV	1206.5000	0.2201	[37, 217]	> 13.66		
Si IV				> 13.66		
Si VI	1393.7550	−0.2774	[57, 187]	12.93 ± 0.03	< 11.93 13.32 ± 0.09	
Fe II	1402.7700	−0.5817	[57, 187]	12.90 ± 0.03		
Fe III				13.03 ± 0.05		
	1122.5260	−1.2684	[67, 167]	< 13.37		
				< 13.37		
B						
C II	1036.3367	−0.9097	[249, 499]	> 15.24	14.09 ± 0.03 14.11 ± 0.03 14.06 ± 0.03 14.00 ± 0.03	
C IV				> 15.24		
N I	1548.1950	−0.7194	[289, 499]	14.09 ± 0.03		
N II				14.11 ± 0.03		
N V	1550.7700	−1.0213	[289, 499]	14.06 ± 0.03	14.00 ± 0.03 14.00 ± 0.03 14.00 ± 0.03 14.00 ± 0.03	
O I	1199.5496	−0.8794	[249, 429]	14.00 ± 0.03		
O VI	1083.9900	−0.9867	[249, 499]	> 15.10		
Al II				> 15.10		
Al III	1242.8040	−1.1066	[289, 499]	< 13.81	15.61 ± 0.03 15.61 ± 0.03 15.61 ± 0.03 15.61 ± 0.03	
Si II				< 13.81		
Si II*	1039.2304	−2.0364	[289, 499]	15.61 ± 0.03		
Si III	1302.1685	−1.3110	[349, 449]	> 15.03		
Si IV	1031.9261	−0.8765	[289, 499]	< 14.58	14.60 ± 0.03 14.60 ± 0.03 14.60 ± 0.03 14.60 ± 0.03	
Al II				< 14.58		
Al III	1670.7874	0.2742	[249, 499]	13.32 ± 0.03		
Si II	1854.7164	−0.2684	[349, 499]	13.32 ± 0.03		
Si II*				12.68 ± 0.08		
Si III	1264.7377	−0.0441	[249, 509]	12.68 ± 0.08	< 12.04	
Si IV				14.60 ± 0.03		
Si VI	1264.7377	−0.0441	[249, 509]	< 12.04		
Fe II	1304.3702	−1.0269	[249, 499]	< 12.04		
Fe III	1526.7066	−0.8962	[249, 499]	< 12.04	13.87 ± 0.04 13.87 ± 0.04 13.87 ± 0.04 13.87 ± 0.04	
Fe IV	1808.0130	−2.6603	[299, 399]	< 14.65		
Fe V	1264.7377	−0.0441	[249, 509]	< 14.65		
Fe VI				< 12.04		
Fe VII	1264.7377	−0.0441	[249, 509]	< 12.04	< 12.04	
Fe VIII	1206.5000	0.2201	[249, 509]	< 12.04		
Fe IX				< 12.04		
Fe X	> 14.02					
Fe XI	1206.5000	0.2201	[249, 509]	> 14.02	13.50 ± 0.03 13.50 ± 0.03 13.50 ± 0.03 13.50 ± 0.03	
Fe XII	1393.7550	−0.2774	[289, 499]	13.50 ± 0.03		
Fe XIII				13.50 ± 0.03		
Fe XIV	1402.7700	−0.5817	[289, 499]	13.50 ± 0.03		
Fe XV	1608.4511	−1.2366	[299, 449]	13.87 ± 0.04	< 12.04	
Fe XVI				13.87 ± 0.04		
Fe XVII	1122.5260	−1.2684	[299, 399]	< 13.35		
Fe XVIII				< 13.35		

^aVelocity interval for the AODM column density measurement. Velocities are relative to the redshift of the foreground quasar SDSSJ1204+0221FG, $z_{fg} = 2.4360$.

^bSum of all fitted components.

TABLE 2
IONIC COLUMN DENSITIES

Ion	λ_{rest} (Å)	$\log f$	v_{int}^a (km s ⁻¹)	$\log N_{\text{AODM}}$	$\log N_{\text{VPFIT}}^b$
C					
C II	1036.3367	−0.9097	[598, 698]	> 14.79	13.61 ± 0.04
C II*				> 14.79	
C IV	1548.1950	−0.7194	[568, 728]	13.66 ± 0.03	
	1550.7700	−1.0213	[568, 728]	13.71 ± 0.03	
N I	1083.9900	−0.9867	[598, 728]	> 14.80	14.47 ± 0.04
N II				> 14.80	
N V	1242.8040	−1.1066	[618, 718]	< 12.58	15.46 ± 0.09
O I				< 12.58	
O VI	1031.9261	−0.8765	[678, 818]	< 13.70	
Al II				< 13.70	
Al III	1854.7164	−0.2684	[648, 718]	< 12.28	12.89 ± 0.05
Si II				< 12.28	
Si II*	1264.7377	−0.0441	[628, 728]	< 11.82	14.31 ± 0.06
Si III				< 11.82	
Si IV	1206.5000	0.2201	[628, 728]	> 13.59	12.93 ± 0.39
Si VI				> 13.59	
Fe II	1122.5260	−1.2684	[678, 778]	< 13.37	
Fe III				< 13.37	

^aVelocity interval for the AODM column density measurement. Velocities are relative to the redshift of the foreground quasar SDSSJ1204+0221FG, $z_{\text{fg}} = 2.4360$.

^bSum of all fitted components.

local or background UV sources. Elements therefore occupy the first ionization state (termed the low-ion) with an ionization potential greater than 1 Ryd. One also identifies strong N II absorption that traces the observed N I profile in subsystem A. The measured ratio of these ionization states is large, $\log[N(\text{N}^+)/N(\text{N}^0)] = +1.8$ dex, revealing the gas is partially ionized. On the other hand, there is only weak Si IV and C IV absorption at these velocities indicating the ionization state of the gas is not extreme. Furthermore, the absence of strong N V and O VI absorption at these velocities limits the flux of photons with energies $h\nu \gtrsim 4$ Ryd and also rules out a collisionally ionized gas with $T \approx 10^5$ K (see Figure 10). Qualitatively, the data suggest a partially ionized gas with $T < 10^5$ K.

There are two main mechanisms that produce a partially ionized gas: collisional ionization and photoionization. Under the assumption of collisional ionization equilibrium (CIE; Sutherland & Dopita 1993), the detection of low-ions like O⁰ and N⁰ requires the electron temperature to be $T_e < 30,000$ K. This constraint is supported by the small b -values measured for the N⁰ gas at $v \approx +130$ km s⁻¹: $b(\text{N}^0) = 4.5 \pm 0.3$ km s⁻¹ (Table 1). If we assume the gas is broadened by purely thermal motions, we can set a 2- σ upper limit to the temperature $T_e < 25,000$ K. We achieve a similar limit by fitting the N gas and Si gas independently at the same redshift and use the difference in Doppler parameters to estimate T . Nevertheless, a CIE model with $T_e \approx 25,000$ K does roughly reproduce the observed ionic ratios of Si⁺/Si³⁺, Al⁺/Al²⁺, and Fe⁺/Fe²⁺ with N⁺/N⁰ discrepant (the model underpredicts this ratio). Therefore, one cannot rule out a model where collisional ionization is the primary mechanism producing the observed ionic ratios, although to invoke this scenario one must introduce a heat source to maintain the gas at this temperature because the cooling time is short ($t_{\text{cool}} \lesssim 10^4$ yr) for any reasonable density. In the following photoionization modelling, we will however assume that photoionization is dominant and thereby set an upper limit to the intensity of the ionizing radiation field. Finally, because the gas is partially ionized one presumes that $T_e > 10,000$ K. In the following and throughout the remainder of the paper we will adopt an electron temperature $T_e = 20,000$ K.

To explore photoionization, we have used the Cloudy software package (Ferland et al. 1998) to calculate the ionization state of plane-parallel slabs with total column density $\log N_{\text{H}} = 18.6$, density $n_{\text{H}} = 0.1$ cm⁻³, and metallicity $[\text{M}/\text{H}] = -0.5$, while varying the ionization parameter $U \equiv \Phi/n_{\text{H}}c$ where Φ is the flux of ionizing photons having $h\nu \geq 1$ Ryd. The results are largely insensitive to this choice of volume density (they are nearly homologous with U), but they do vary with metallicity because this affects the cooling rate of the gas and the electron density. We will demonstrate that the assumed metallicity is consistent with the $[\text{O}/\text{H}]$ value inferred from the observed O⁰/H⁰ ratio. For the calculations, we assume a power-law spectrum $f_\nu \propto \nu^{-1.57}$ which is representative of $z \sim 2$ quasars (Telfer et al.

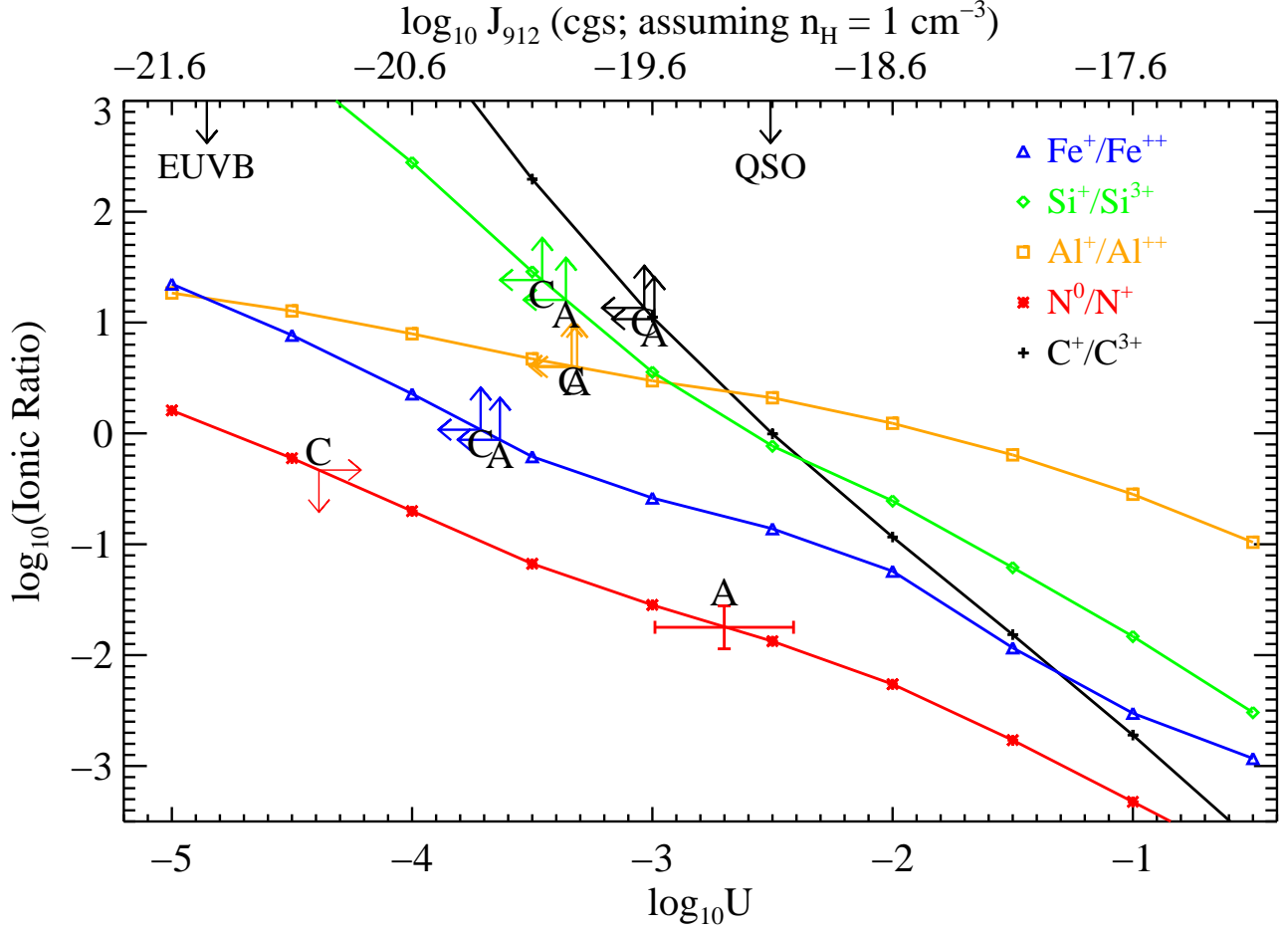


FIG. 4.— The solid curves show predicted ionic ratios as a function of the ionization parameter U for a series of ion pairs. These curves were calculated using the Cloudy software package assuming a plane-parallel slab of constant density material, a $f_\nu \propto \nu^{-1.57}$ power-law spectrum, and solar relative abundances with an absolute metallicity $[M/H] = -0.5$ dex. Overplotted on the curves are observational constraints for subsystems A and C. With the exception of N^0/N^+ in subsystem A, the observations indicate $\log U < -3$ (see the text for a full discussion). Note that the constraints for C and Si are reported as upper limits to U because the high-ion absorption (C^{+3} , Si^{+3}) is likely associated with a different phase. The intensities for the extragalactic UV background (EUVB) and the foreground quasar at a distance of 100 kpc are shown on the top axis.

2002). The results are nearly identical if we instead use the extragalactic UV background (EUVB) field computed by Haardt & Madau (1996) because the radiation fields have very similar slopes at the energies that span the ionization potentials of the observed ions ($h\nu = 1 - 3$ Ryd). When the input U parameter is varied, the algorithm varies the number of gas slabs to maintain a constant N_{HI} value. Because subsystem A is optically thick, the results are sensitive to the assumed N_{HI} value; unfortunately, this quantity is not well constrained by the observations (§ 2). Larger N_{HI} values imply more self-shielding of the inner regions which, in turn, demand a more intense radiation field to explain the observed ionization states. The various ions respond differently to the shielding effects and pose an independent constraint on the N_{HI} value under the assumptions of this photoionization model. For example, we cannot reproduce the observed Fe^+/Fe^{++} , Si^+/Si^{+3} , and N^0/N^+ ratios when $N_{HI} > 10^{19} \text{ cm}^{-2}$; the N^0/N^+ ratios require $\log U = -2$ while the other two ratios set an upper limit $\log U < -3$. Under the assumption of a single-phase photoionization model with $f_\nu \propto \nu^{-1.57}$, the data requires $N_{HI} < 10^{18.75} \text{ cm}^{-2}$ with a preferred value of $N_{HI} \approx 10^{18.6} \text{ cm}^{-2}$. This central value is consistent with the line-profile analysis of $Ly\alpha$ and $Ly\beta$ for subsystem A (Figure 2).

Figure 4 presents the results of the Cloudy calculations for a series of ionic ratios for a wide range of ionization parameters assuming $N_{HI} = 10^{18.6} \text{ cm}^{-2}$. As noted above, we examine multiple ionization states of the same element (e.g. N^0/N^+) to provide constraints that are independent of intrinsic abundances. The observational constraints (Table 3) on the ionic ratios are indicated by vertical error intervals (or lower and upper limits) and the corresponding horizontal error intervals (or lower and upper limits) on $\log U$ are indicated. One notes that even with this lower N_{HI} value, the constraints are not fully consistent with a single U value; in particular the observed N^0/N^+ ratio indicates $\log U \gtrsim -3$ whereas the other ratios imply $\log U < -3$. Although this inconsistency may suggest the low and intermediate ions arise in a multi-phase or non-equilibrium medium, we caution that the systematic uncertainties inherent to photoionization modelling of optically thick absorbers are large (e.g. the assumed spectral shape, cloud

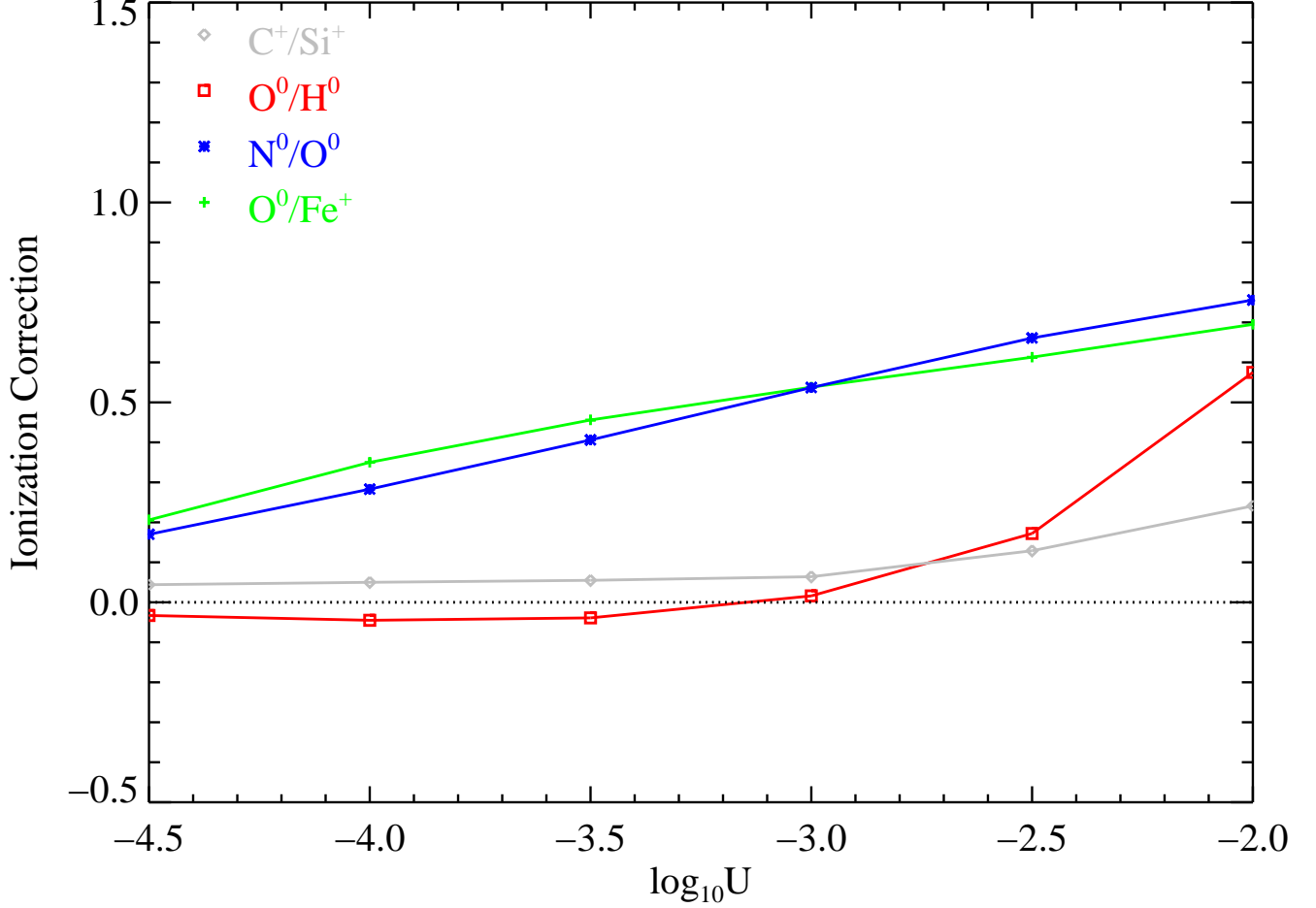


FIG. 5.— Estimated ionization corrections (I.C.) for several ionic ratios as a function of ionization parameter U . These values represent the offset that must be applied to an observed ionic ratio to give the relative elemental abundances, e.g. $\log(N/O) = \log(N^0/H^0) + I.C.(N/O)$. The calculations were performed with the Cloudy software package and assume $N_{HI} = 10^{19} \text{ cm}^{-2}$, a plane-parallel constant density slab with $n_H = 10^{-1} \text{ cm}^{-3}$, a gas metallicity $[M/H] = -0.5$ dex with solar relative abundances, and a power-law ionizing spectrum with $f_\nu \propto \nu^{-1.57}$. Note that the corrections for O^0/H^0 are small for $\log U < -2.5$ dex whereas the N^+/O^0 and O^0/Fe^+ ratios require modest corrections for $\log U > -4.5$ dex.

geometry, and uncertain atomic data). In the following we will adopt an ionization parameter $\log U = -3.0$ dex with an uncertainty of 0.3 dex. This U value is similar to the results derived for other LLS at these redshifts (e.g. Prochaska 1999). It implies an ionization fraction $x \equiv H^+/H = 0.96$ and a total hydrogen column density $N_H \equiv N_{HI}/(1-x) = 10^{20.0} \text{ cm}^{-2} (N_{HI}/10^{18.6} \text{ cm}^{-2})$. Note that the error in $1-x$ is roughly linear with the uncertainty in U for $\log U > -4$ dex.

At low ionization parameters ($\log U < -2.5$; Figure 5), the O^0/H^0 ratio is a good estimator of the oxygen abundance¹³ because the two atoms have very similar ionization potential and also because charge-exchange reactions mediate their ionization fractions. We calculate $[O/H] \equiv \log(O/H) - \log(O/H)_\odot = -0.65 - \log_{10}(N_{HI}/10^{18.6} \text{ cm}^{-2})$ assuming a solar oxygen abundance $\log(O/H)_\odot = -3.34$ dex. The uncertainty in this measurement (and any other chemical abundance measurements of subsystem A) is dominated by the poor constraint on the N_{HI} value. The Ly α and Ly β profiles indicate $N_{HI} < 10^{19} \text{ cm}^{-2}$ which sets a lower limit to the metallicity of 1/10 solar abundance.

Relative abundance ratios (e.g. O/Fe) are less sensitive to the H I column density but are not strictly independent of N_{HI} because it dominates the opacity in our ionization models. Adopting $\log U = -3$ and $\log N_{HI} = 10^{18.6} \text{ cm}^{-2}$, we find the following relative abundance values: $[O/Fe] = +0.6 \pm 0.1$, $[O/C] < +0.75$, and $[N/O] = -0.1 \pm 0.2$ dex (Table 3). The reported errors are dominated by uncertainty in the U parameter. We interpret these chemical abundance measurements in § 4.2.

Independent of photoionization modeling, the data yield a measurement of the electron density from the observed populations of the fine-structure levels of Si^+ and/or C^+ . The $J = 1/2$ ground-state of these ions has a corresponding $J = 3/2$ fine-structure level which can be populated by collisions with ions and atoms, via indirect UV pumping, and also via a magnetic-dipole transition. For a partially ionized gas (demanded by the observed N^+/N^0 ratio),

¹³ Note that the same is true for any CIE model with $T_e < 10^{4.5} \text{ K}$.

TABLE 3
ELEMENTAL ABUNDANCES

Ion	[X/H]	[X/O ⁰]
Subsystem A ^a		
C ⁺	> -1.27	> -0.65
N ⁰	-0.65 ± 0.14	-0.03 ± 0.08
O ⁰	-0.62 ± 0.06	
Al ⁺	-1.02 ± 0.19	-0.40 ± 0.25
Si ⁺	-0.95 ± 0.11	-0.33 ± 0.17
Fe ⁺	-1.26 ± 0.03	-0.64 ± 0.05
Subsystem C ^a		
C ⁺	> -1.10	> -1.32
N ⁰	0.65 ± 0.14	0.43 ± 0.08
O ⁰	0.22 ± 0.06	
Al ⁺	-1.14 ± 0.19	-1.36 ± 0.25
Si ⁺	-0.77 ± 0.11	-0.98 ± 0.17
Fe ⁺	-1.16 ± 0.03	-1.38 ± 0.05

^aAssumes $N_{\text{HI}} = 10^{18.6} \text{ cm}^{-2}$ and $\log U = -3.0 \pm 0.3 \text{ dex}$

collisions with free electrons should dominate excitation to the $J = 3/2$ upper level. Indirect UV pumping could also contribute, but the quasars (foreground and background) are too distant and we assume that there are no important local sources (e.g. OB stars). In any case, contributions from UV pumping would only tighten the following upper limit on n_e . Unfortunately, the transitions from the $J = 3/2$ excited level of C⁺ are blended with the resonant C II transitions of subsystem B. Therefore, only the Si⁺ levels (which have a wider energy separation) are available for analysis. We set an upper limit to the relative populations based on the non-detection of the Si II* 1264 transition, $\log[N(\text{Si}_{J=3/2}^+)/N(\text{Si}_{J=1/2}^+)] < -2.2 \text{ dex}$. For a gas with $T_e \gg 413 \text{ K}$, the level populations for excitation dominated by electron collisions is given by:

$$\frac{N(\text{Si}_{J=1/2}^+)}{N(\text{Si}_{J=3/2}^+)} = \frac{1}{2} + \frac{640T_e^{1/2}}{n_e} \quad (T \gg 413 \text{ K}) \quad . \quad (1)$$

Adopting $T_e = 20,000 \text{ K}$, the observations place an upper limit on the electron density, $n_e < 6 \text{ cm}^{-3}$.

One can use this constraint on the electron density to constrain the hydrogen volume density n_{H} by assuming the ionization fraction from our photoionization model, i.e., $x = 0.96$. We calculate

$$n_{\text{H}} = n_e/x < 6.2 \text{ cm}^{-3} \quad . \quad (2)$$

One can also estimate a lower limit for the characteristic size of the system,

$$\ell \equiv \frac{x}{1-x} \frac{N_{\text{HI}}}{n_e} \quad . \quad (3)$$

We derive $\ell > 5.2(N_{\text{HI}}/10^{18.6} \text{ cm}^{-2}) \text{ pc}$.

3.2. Subsystem C: $+600 \text{ km s}^{-1} < \delta v < +780 \text{ km s}^{-1}$

In comparison with subsystem A, we find similar results for the ionization state of subsystem C. These include strong N II absorption relative to N I which indicates a partially ionized gas. Again, a CIE model with $T_e \approx 20,000 \text{ K}$ yields ionic ratios consistent with the majority of observed ionic ratios, but we will focus on photoionization models of the gas. Like subsystem A, we also find that models with $N_{\text{HI}} < 10^{19} \text{ cm}^{-2}$ are preferred and the observed ionic ratios ($\text{Fe}^+/\text{Fe}^{++}$, N^0/N^+ , $\text{Si}^+/\text{Si}^{+3}$) imply $N_{\text{HI}} \approx 10^{18.6} \text{ cm}^{-2}$ and $\log U \lesssim -3$. Using the same Cloudy model assumed for subsystem A, we derive the chemical abundances listed in Table 3.

In contrast to subsystem A, we measure larger metal column densities and a correspondingly higher oxygen abundance, $[\text{O}/\text{H}] = +0.2 - \log_{10}(N_{\text{HI}}/10^{18.6} \text{ cm}^{-2})$, if the subsystems have comparable N_{HI} values. Even if we have underestimated the H I column density of subsystem C by a factor of 0.5 dex (the maximum value allowed by the observed Ly α profile; Figure 2), the gas metallicity would be roughly solar. This lower limit ($[\text{O}/\text{H}] > -0.25$) matches the highest values observed for damped Ly α systems (Prochaska et al. 2007) and all but a few super-LLS studied to date (P  roux et al. 2006; Prochaska et al. 2006). The data also suggest variations between the oxygen abundances of subsystems A and C (and also B, see below). Abundance variations like these are rarely studied in optically thick absorption line systems because it is difficult to resolve the H I Lyman series (Prochter et al. 2008).

TABLE 4
SUMMARY OF PROPERTIES FOR SLLS/SDSSJ1204+0221BG

Property	A	B	C
$\log(N_{\text{HI}}/\text{cm}^{-2})$	18.6 ± 0.4	19.60 ± 0.15	18.6 ± 0.4
$\log U$	-3.0 ± 0.3	-3.0 ± 0.3	-3.0 ± 0.3
$\log T_e$ (K)	4.3 ± 0.15	4.3 ± 0.15	4.3 ± 0.15
$[\text{O}/\text{H}]^a$	-0.6	-0.6	$+0.2$
$\log(\text{O}^0/\text{Fe}^+) - \log(\text{O}/\text{Fe})_\odot$	$+0.1$	$+0.5$	$+0.8$
$[\text{O}/\text{Fe}]^b$	$+0.6$	$+0.7$	$+1.4$
$\log(\text{N}^0/\text{O}^0) - \log(\text{N}/\text{O})_\odot$	-0.6	-0.7	-0.1
$[\text{N}/\text{O}]^b$	-0.0	-0.5	$+0.4$
$1 - x$	0.04 ± 0.01	0.18 ± 0.05	0.04 ± 0.01
$\log(N_{\text{H}}/\text{cm}^{-2})^c$	20.00	20.34	20.00
n_e (cm^{-3})	< 6.0	< 2.5	$1.7^{+0.3}_{-1}$
n_{H} (cm^{-3})	< 6.2	< 3.1	$1.8^{+0.3}_{-1}$
ℓ (pc) ^c	> 5.2	> 23.3	18.2

^aOxygen metallicity estimated from the observed O^0/H^0 ratio assuming no ionization correction. Because ionization corrections would increase these values, one may consider them lower limits to the oxygen abundances subject to the large uncertainties in $\log N_{\text{HI}}$ for subsystems A and C.

^bAbundance derived from low-ion ratios and the ionization corrections calculated assuming $\log U = -3.0 \pm 0.3$ dex, N_{HI} as listed, $[\text{O}/\text{H}] = -0.5$, and $f_\nu = \nu^{-1.57}$.

^cWe estimate a log uncertainty of 0.8 dex for Subsystems A and C where both N_{HI} and x are uncertain and 0.4 dex for Subsystem B where the N_{HI} value is better constrained. A similar consideration holds for ℓ .

The relative chemical abundances of O/Fe and N/O are also significantly higher in subsystem C than subsystem A: $[\text{O}/\text{Fe}] = +1.3 \pm 0.1$ dex, $[\text{N}/\text{O}] = +0.3 \pm 0.2$ dex. Although these values include ionization corrections (Figure 5), the gas is indisputably α -enhanced and the N/O ratio must be greater than one half solar. This N/O value is unique for optically thick absorbers and the large α -enhancement also exceeds most measurements of O/Fe in extragalactic environments. We interpret these results further in § 4.2.

We derive a constraint on the electron density of subsystem C from observations of fine-structure levels of C^+ and Si^+ . Assuming that excitation of the upper level is dominated by electron collisions, the populations of the excited state to the ground state for C^+ are related to the gas temperature and electron density, e.g.,

$$\frac{N(\text{C}_{J=1/2}^+)}{N(\text{C}_{J=3/2}^+)} = \frac{1}{2} + \frac{37T_4^{1/2}}{n_e} \quad (T \gg 92\text{K}) . \quad (4)$$

As for subsystem A, we assume $T_e = 20,000\text{K}$, and obtain

$$n_e = \frac{106}{2 \frac{N(\text{C}_{J=1/2}^+)}{N(\text{C}_{J=3/2}^+)} - 1} . \quad (5)$$

Although the column density of the $\text{C}_{J=3/2}^+$ excited state is well constrained by the spectra, the resonance C II 1036 and C II 1334 transitions are heavily saturated. A conservative lower limit to $N(\text{C}_{J=1/2}^+)$ is derived by integrating the optical depth profile assuming a normalized flux equal to the 1σ error estimate, $N(\text{C}_{J=1/2}^+) > 10^{14.8} \text{cm}^{-2}$. Combined with our measurement of $N(\text{C}_{J=3/2}^+)$, we set an upper limit to the electron density $n_e < 3.5 \text{cm}^{-3}$. Similar to subsystem A, we also derive an upper limit to n_e from the non-detection of the Si^+ excited level, $n_e < 2.5 \text{cm}^{-3}$ for $T_e = 20,000\text{K}$ (Equation 1). Assuming the same photoionization model ($\log U = -3, x = 0.96$) as for subsystem A, we infer a hydrogen volume density $n_{\text{H}} < 2.6 \text{cm}^{-3}$ and a lower limit to the characteristic size, $\ell > 15.5(N_{\text{HI}}/10^{18.6} \text{cm}^{-2}) \text{pc}$.

Because we have a positive detection for the C II* 1335 transition, we may further constrain the volume density by estimating the total C^+ column density from a proxy ion. A good choice is Si^+ because our Cloudy calculations indicate $\text{Si}^+/\text{Si} \approx \text{C}^+/\text{C}$ for $\log U \approx -3$ dex. This requires, however, that one adopt a value for the intrinsic Si/C ratio. If we assume solar relative abundances $[\text{Si}/\text{C}] = 0$, which is consistent with the C/Si ratio deduced from the ratio of C IV to Si IV assuming the ionization correction of our best fit photoionization model, we estimate $\log N(\text{C}^+) = 15.2$ dex. From equation 4 we estimate $n_e = 1.7 \text{cm}^{-3}$ which nearly matches the upper limit we have derived above. A more conservative estimate is to assume $[\text{Si}/\text{C}] > -1$ and report a lower limit to the electron density, $n_e > 0.2 \text{cm}^{-3}$.

3.3. Subsystem B: $+200 \text{ km s}^{-1} < \delta v < +600 \text{ km s}^{-1}$

As noted in § 2, the velocity profiles of subsystem B are complex and preclude a well-constrained solution using line-profile fitting techniques. Our expectation is that the velocity profiles are comprised of a series of overlapping components each with a line-profile similar to the components observed in subsystems A and C. With higher S/N data, one might be able to discern such structure. For now, we use the AODM to measure ionic column densities for this subsystem. This approach is problematic, however, for constraining the ionization state because the ionic ratios vary across the velocity profiles (e.g. N^+/N^0 is significantly larger at $\delta v = +470 \text{ km s}^{-1}$ than $\delta v = +350 \text{ km s}^{-1}$). Therefore, we cautiously report constraints on the ionization state and chemical abundances. We examine the integrated ionic column densities (and their ratios) which give optical depth weighted averages.

The integrated ionic column density ratios (e.g. N^0/N^+ , Fe^+/Fe^{++}) in subsystem B are consistent with those observed for subsystems A and C. This suggests that the average ionization state of subsystem B is similar to that of subsystems A and C. Empirically, the low observed Fe^+/Fe^{++} and Al^+/Al^{++} ratios imply a modestly ionized gas with $\log U < -2.5$ dex, and the oxygen abundance should follow the O^0/H^0 ratio: $[O/H] = -0.64 \pm 0.15$ dex. This value is lower than the O/H abundance derived for subsystem C and suggests modest abundance variations exist between the subsystems. We also note that the observed O^0/Fe^+ ratio for subsystem B requires at least a modest α -enhancement, $[O/Fe] > +0.4$ dex and that the observed N^0/O^0 ratio implies $[N/O] > -0.7$ dex. These values are similar to the results derived for subsystem A. For the remainder of the paper, we will adopt $\log U = -3.0$ for this subsystem. Because this subsystem has a significantly higher N_{HI} value, this implies a higher neutral fraction ($1 - x = 0.2$) compared to subsystems A and C.

Finally, the non-detection of Si II* 1264 absorption sets an upper limit to the electron density $n_e < 2.5 \text{ cm}^{-3}$ under the assumption that electron collisions dominate the excitation rate and that $T_e = 20,000 \text{ K}$ (Equation 1). If we assume the gas has an ionization fraction near unity, we set a similar upper limit for the hydrogen volume density and a size estimate $\ell > 21 \text{ pc}$.

4. DISCUSSION OF THE OBSERVATIONS

In this section we discuss the observed properties of SLLS/SDSSJ1204+0221BG in terms of the galactic environment around high z quasars. We examine the velocity field of this gas, its chemical abundances, and then test whether SDSSJ1204+0221FG may be shining on the absorbing material. As our discussion focuses on a single system, the degree to which we can generalize these results is questionable. It is nevertheless fruitful to explore various scenarios for interpreting the observations. Table 4 summarizes the physical characteristics of SLLS/SDSSJ1204+0221BG derived in the previous section.

4.1. Kinematic Constraints

The most robust measurements for SLLS/SDSSJ1204+0221BG from our high resolution spectrum of SDSSJ1204+0221BG are on the velocity field of the gas. Both the absolute (i.e. redshift) and relative velocities constrain the origin of the gas and its relation to the foreground quasar SDSSJ1204+0221FG. The redshift of SDSSJ1204+0221FG was measured from our observations of the rest-frame optical [O III] $\lambda 5007$ emission line using the GNIRS spectrometer on the Gemini-S telescope (§ 2, Figure 1). We achieved a velocity precision of $\approx 40 \text{ km s}^{-1}$ giving $z_{fg} = 2.4360 \pm 0.0005$. Figures 2 and 3, which present the velocity profiles of SLLS/SDSSJ1204+0221BG relative to z_{fg} show strong H I and metal-line absorption from $\delta v \approx +70 \text{ km s}^{-1}$ to $+700 \text{ km s}^{-1}$. These absorption profiles have two notable characteristics. First, the gas along the SDSSJ1204+0221BG sightline is asymmetrically distributed relative to z_{fg} , i.e. within a 2000 km s^{-1} window centered on $z = z_{fg}$, there is significant absorption only at $z > z_{fg}$. The nearest ‘cloud’ with $\tau_{Ly\alpha} > 1$ and $\delta v < 0 \text{ km s}^{-1}$ lies off of Figure 2 at $\delta v \approx -1500 \text{ km s}^{-1}$, which corresponds to $\approx 6h^{-1} \text{ Mpc}$ (proper) under the assumption of Hubble expansion. Second, the total velocity width is very large, $\Delta v \approx 650 \text{ km s}^{-1}$. One may compare this value against the velocity widths measured for systems with comparable H I surface density, i.e. the damped Ly α (DLA) and super Lyman limit systems. Regarding the former, the velocity width of SLLS/SDSSJ1204+0221BG exceeds greater than 99% of the Δv values for randomly selected DLAs at $z > 2$ (Prochaska & Wolfe 1997, 2001). Regarding the SLLS population (Péroux et al. 2003), none have as large of a velocity width. The equivalent width of the metal-line transitions (a proxy for velocity width) is also large compared to systems selected on the basis of metal-line absorption (e.g. the Mg II systems; Prochter et al. 2006). In these respects, *the velocity field of the gas near SDSSJ1204+0221FG is extreme.*

Several factors lead us to conclude that the distance between the gas in SLLS/SDSSJ1204+0221BG and SDSSJ1204+0221FG is comparable to the impact parameter. Recall that SLLS/SDSSJ1204+0221BG exhibits a multi-component kinematic structure with unusually large velocity width between the components. If the relative motions of the clouds and the quasar are to be interpreted as Hubble flow, their implied line-of-sight separation would be $\approx 2.8 \text{ Mpc}$ (for $\Delta v \approx 700 \text{ km s}^{-1}$). The chance alignment of several galaxies across this large distance is unlikely however, which we can quantify with clustering arguments. Quasars arise in highly biased regions of the Universe. They are observed to cluster strongly on $\sim 10 h^{-1} \text{ Mpc}$ scales (Croom et al. 2001; Porciani et al. 2004; Croom et al. 2005; Myers et al. 2007a; Shen et al. 2007b) and the correlation function steepens considerably on smaller scales $\sim 100 h^{-1} \text{ kpc}$ (Hennawi 2004; Hennawi et al. 2006b; Myers et al. 2007b, 2008). High redshift quasars also exhibit a large cross-correlation amplitude with star-forming galaxies (Adelberger & Steidel 2005; Coil et al. 2007), and it is possible that galaxies clustered around the quasar are giving rise to the Ly α and metal-line absorption seen in SLLS/SDSSJ1204+0221BG. Another possibility is that the absorption in SLLS/SDSSJ1204+0221BG is not due to a nearby galaxy, but is rather halo gas distributed around the quasar with

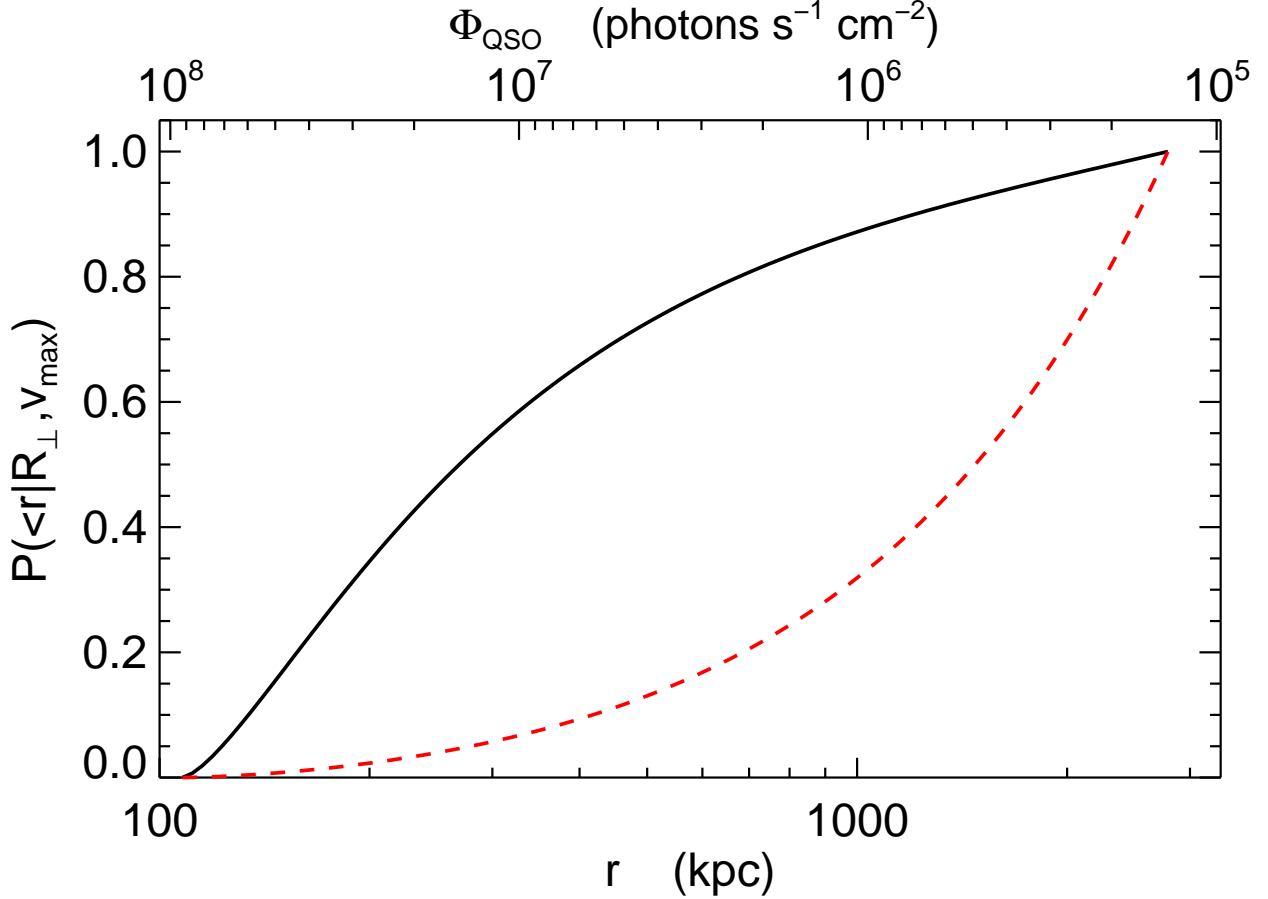


FIG. 6.— Probability distribution of the distance from the foreground quasar. The function $P(< r|R_{\perp}, v_{\max})$ represents the probability that the distance from the foreground quasar is less than r , given a fixed impact parameter R_{\perp} and knowledge that the absorber lies in the velocity interval $\pm v_{\max}$. The impact parameter for SDSSJ1204+0221 is used and a velocity interval of $v_{\max} = 700 \text{ km s}^{-1}$ was assumed. This probability is computed from the quasar absorber correlation function $\xi_{QA} = (r/r_0)^{-\gamma}$ measured by Hennawi & Prochaska (2007), with $\gamma = 2$ and $r_0 = 5.8 h^{-1} \text{ Mpc}$. The solid (black) curve illustrates the probability distribution accounting for clustering with ξ_{QA} . The dashed (red) curve shows the probability if there is no clustering. The upper x-axis shows the ionizing photon flux Φ_{QSO} implied by the SDSS magnitude of SDSSJ1204+0221FG at the given distance.

some density profile. Either scenario results in a clustering pattern around the quasar, which we measured in Hennawi & Prochaska (2007). The probability $P(< r|R_{\perp}, v_{\max})$ that the total distance between the quasar and the absorber is less than r , given a fixed impact parameter R_{\perp} and the knowledge that absorption occurs within a velocity interval $\pm v_{\max}$, is simply an integral over this quasar-absorber correlation function.

Figure 6 shows this cumulative probability for $v_{\max} = 700 \text{ km s}^{-1}$ and the impact parameter of $R_{\perp} = 108 \text{ kpc}$, from which we deduce that the probability for the gas in SLLS/SDSSJ1204+0221BG lying within 500 kpc of SDSSJ1204+0221FG is $\approx 70\%$. Perhaps an even stronger argument that the gas in SLLS/SDSSJ1204+0221BG lies at a distance comparable to the impact parameter is that the physical characteristics (ionization state, H I surface density, chemical abundances) of the subsystems comprising SLLS/SDSSJ1204+0221BG show only modest variations. Whereas, several of these same properties — specifically the metallicity, relative abundance pattern, and the velocity field — are highly anomalous compared to the population of intervening optically thick absorbers. In particular, the only place that such large N/O ratios are observed is in quasar environments. Finally, it is worth emphasizing that the very small sizes deduced for the subsystems of SLLS/SDSSJ1204+0221BG ($d \lesssim 100 \text{ pc}$) imply that their relative separations are also comparable to the impact parameter. The alternative, which would be for the subsystems to be part of a single structure with size $d \lesssim 100 \text{ pc}$, would imply an unphysically large velocity shear across this small distance.

4.2. Clues from Chemical Enrichment

Clues to the origin of SLLS/SDSSJ1204+0221BG are encoded in the enrichment pattern of its gas. In particular, the relative abundances constrain the timescales and intensity of star-formation of the galaxy (or galaxies) that produced the observed metals. Because the gas is partially ionized and we do not observe transitions from all ionization states, we proceed cautiously to interpret the observed ionic ratios. One robust conclusion from our abundance analysis (§ 3; Table 4) is that the gas is highly enriched. The observed O^0/H^0 ratio indicates $[\text{O}/\text{H}] > -1$ across the $\approx 650 \text{ km s}^{-1}$ velocity interval spanning the entire system and we derive an integrated average abundance: $[\text{O}/\text{H}]_{\text{TOT}} > -0.5 \text{ dex}$.

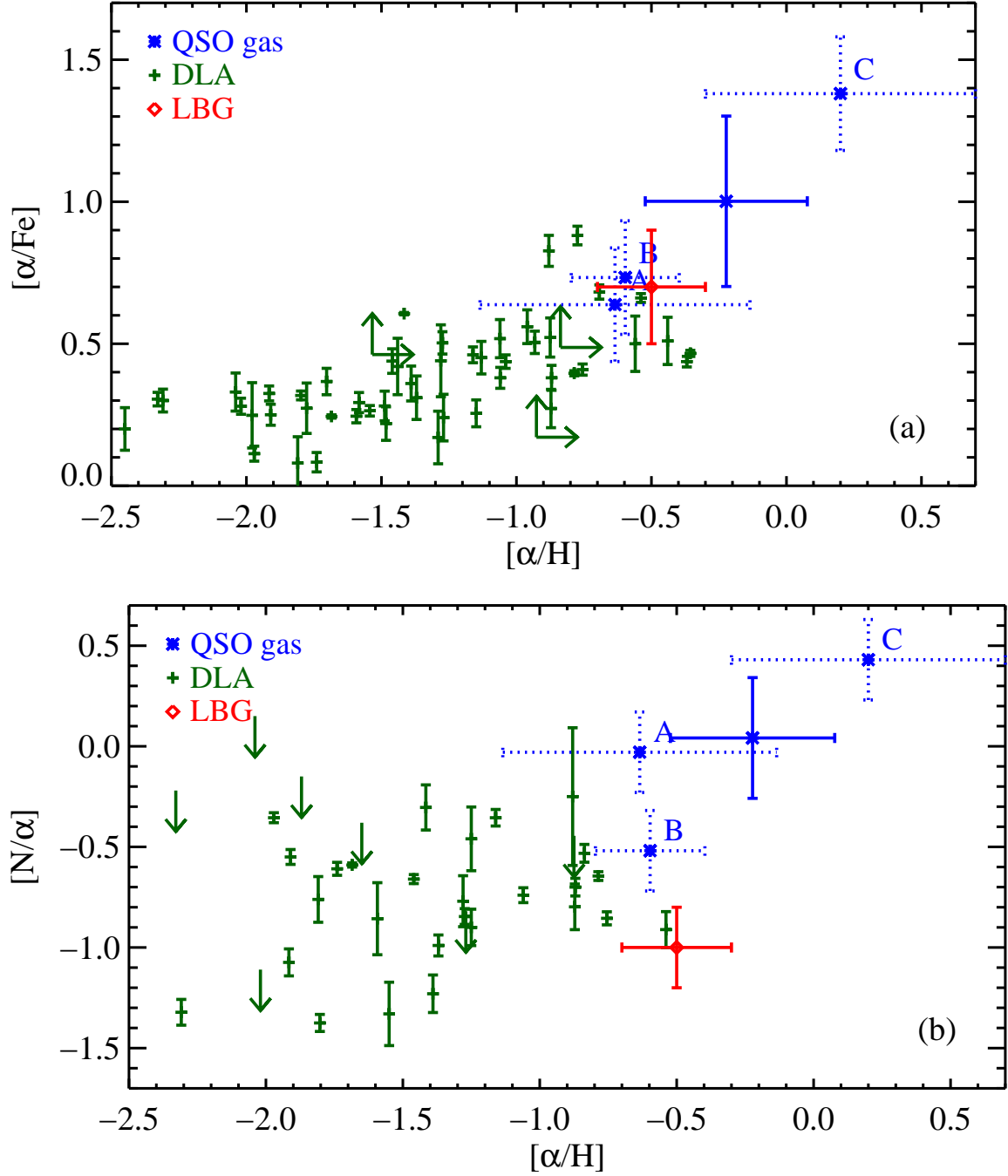


FIG. 7.— Observed gas-phase (a) α/Fe and (b) N/α abundances as a function of alpha abundance $[\alpha/H]$ for galaxies intervening quasar sightlines (DLAs; Prochaska & Wolfe 2001; Prochaska et al. 2007), the three subsystems associated with SDSSJ1204+0221FG (blue dotted), and the N_H -weighted average values (blue solid). We note the gas associated with SDSSJ1204+0221FG has systematically higher metallicity and higher α/Fe , N/O ratios than the majority (or all) DLAs. This indicates gas that was enriched in a ‘starburst’ fashion, i.e. a system with a very high star formation efficiency (Calura et al. 2003).

This metallicity is expressed as a lower limit for several reasons. First, ionization corrections to the observed O^0/H^0 ratios will give larger $[O/H]$ values (Figure 5). Second, the lower limit assumes the nearly maximal N_{HI} values permitted by the data for the three subsystems. If we adopt a modest ionization correction and lower N_{HI} values, the oxygen metallicity for SLLS/SDSSJ1204+0221BG approaches the solar abundance. Finally, a proper derivation of the oxygen metallicity for the SLLS is to take an N_H -weighted average of each subsystem. This is especially important for predominantly ionized gas. Using our fiducial values, we find $\langle [O/H] \rangle = -0.23$ dex assuming no ionization corrections. We emphasize that even a 1/3 solar metallicity ($[O/H] = -0.5$ dex) represents a very high enrichment level. It exceeds the metallicity of nearly all optically thick absorbers at these redshifts: 98% of sightlines randomly intersecting galaxies (DLAs; Prochaska et al. 2003) and 95% of the super-LLS population (Péroux et al. 2007). Such

high enrichment levels are generally observed only in gas within and around star-burst galaxies (Pettini et al. 2002; Simcoe et al. 2006) and in quasar environments (Dietrich et al. 2003; D’Odorico et al. 2004; Arav et al. 2007).

The observations also constrain the relative abundances of O, Fe, and N, e.g. the O/Fe and N/O ratios. These diagnostics are valuable for constraining the star formation history for SLLS/SDSSJ1204+0221BG because each element is associated with a unique nucleosynthetic site and has a unique production timescale. Oxygen is made in massive stars and one predicts minimal delay ($t < 100$ Myr) for its nucleosynthesis and release to the ISM following the onset of star formation. The production of nitrogen and iron, however, is expected to be delayed by several 100 Myr to ≈ 1 Gyr because these elements are made in intermediate mass stars and Type Ia SN respectively. By examining the relative abundances of O, N, and Fe, therefore, one may constrain the duration of the star-formation episode that produced the metals.

Unfortunately, the relative abundance ratios of O, N, and Fe are more sensitive to the ionization state of the gas. The most conservative treatment is to report lower limits to O/Fe and N/O from the observed ionic column density ratios of O^0/Fe^+ and N^0/O^0 . As with O^0/H^0 , corrections to these ionic ratios are positive definite (Figure 5). We measure lower limits to $[O/Fe]$ of +0.1, +0.5, +0.8 dex for subsystems A,B,C respectively and conclude the gas has a super-solar α/Fe ratio. For even a modest ionization correction, the integrated average α/Fe ratio approaches ten times the solar ratio and exceeds the value measured for nearly all intervening absorption line systems. In Figure 7, we present an estimate for these values for the various subsystems and also for the N_H -weighted averages against measurements for a set of high- z galactic observations.

In the local universe, large α/Fe ratios are observed in metal-poor stars (e.g. McWilliam 1997), massive early-type galaxies (Trager et al. 2000), and highly depleted ISM gas (e.g. Savage & Sembach 1996). The first two examples reflect nucleosynthetic enhancements and are attributed to the Type II supernovae of massive stars. The latter example, however, results from the highly refractory nature of Fe relative to O, i.e. one observes enhanced O/Fe gas-phase abundances in the ISM because Fe is preferentially depleted into dust grains. The observed α/Fe enhancement in SLLS/SDSSJ1204+0221BG could be due to one or both of these effects, but our expectation is that differential depletion is not dominant. A high depletion level would be unusual for gas with modest surface and volume densities that is predominantly ionized with a temperature of $T \approx 20,000$ K. It is more likely that the super-solar α/Fe ratios reflect an intrinsic, nucleosynthetic enhancement. Granted the high metallicity of SLLS/SDSSJ1204+0221BG, the α/Fe enhancement suggests a star formation history representative of bright spheroids (e.g. bulges, elliptical galaxies Graves et al. 2007). Chemical evolution modeling suggests these stellar systems underwent a short period of intense star formation where the gas was rapidly enriched by supernovae from massive stars before Type Ia SN could contribute (e.g. Matteucci 1994). We conclude that the metals for SLLS/SDSSJ1204+0221BG were produced in a starburst lasting less than ~ 1 Gyr.

The N/O ratio of the gas offers additional constraints on the star-formation history. Similar to O/Fe, ionization corrections may be important and the conservative approach is to adopt the N^0/O^0 ratio as a lower limit to N/O. We find $[N/O] > -0.7$ dex for subsystems A and B and $[N/O] > -0.2$ dex for subsystem C (Table 4). The observations, specifically the large N^+/N^0 ratio, indicate non-zero ionization corrections. We estimate the correction from photoionization modeling to be +0.25 to +0.5 dex for $\log U = -4$ to -3 dex and conclude that N/O is at least 1/3 the solar ratio in each subsystem and may be super-solar in subsystem C. These values are larger than N/O values observed for quasar absorption line systems (Figure 7, e.g. Henry & Prochaska 2007). Indeed, solar N/O ratios are commonly observed only in quasar environments (Hamann & Ferland 1999; Dietrich et al. 2003; D’Odorico et al. 2004; Arav et al. 2007). This further reflects the high metallicity of SLLS/SDSSJ1204+0221BG because N behaves as a ‘secondary element’ with its yield scaling as the square of the enrichment level $(M/H)^2$. Therefore, one expects near-solar or even super-solar N/O abundances in high metallicity environments. The exception to this expectation is if the system is too young for many intermediate mass stars to have cycled through the AGB phase. The observation of nearly solar N/O in SLLS/SDSSJ1204+0221BG, therefore, implies the gas was enriched over an episode of at least a few 100 Myr (Matteucci & Padovani 1993; Romano et al. 2002).

As noted above, the high metallicity and solar or super-solar N/O and α/Fe ratios for SLLS/SDSSJ1204+0221BG describe a chemical abundance pattern that matches the abundances commonly measured for gas near quasars. This includes the high metallicities inferred from emission lines from the quasar broad line region and the relative abundances derived for narrow associated absorption lines (Dietrich et al. 2003; D’Odorico et al. 2004). We are inclined, therefore, to causally connect the enrichment pattern of SLLS/SDSSJ1204+0221BG with SDSSJ1204+0221FG. A key question that follows is whether the metals were produced by the quasar’s host galaxy or whether they originated in a neighboring galaxy or galaxies. The latter hypothesis would imply that galaxies near quasars have enrichment histories similar to that inferred for the quasar environment, which could be tenable considering that early-type galaxies near the centers of modern clusters have very uniform colors and spectra indicating a common age of formation and star-formation history (e.g. Bower et al. 1992). Alternatively, as we discuss further in the next section, the metals may have been generated during an early episode of star formation in the host galaxy of SDSSJ1204+0221FG, and then transported to large radii $R_\perp \approx 100$ kpc via a large scale outflow in ≈ 100 Myr time. To achieve a high N/O ratio while maintaining a super-solar α/Fe ratio, the data suggest a starburst lasting several 100 Myr but less than ≈ 1 Gyr. It is intriguing that the implied sequence of early, intense star-formation followed by an optically bright quasar phase and possibly a large scale outflow, follows the general prescription for quasar activity proposed by Hopkins and collaborators (Springel et al. 2005a; Cox et al. 2006; Hopkins et al. 2007b).

4.3. Constraints from High-Ion Observations

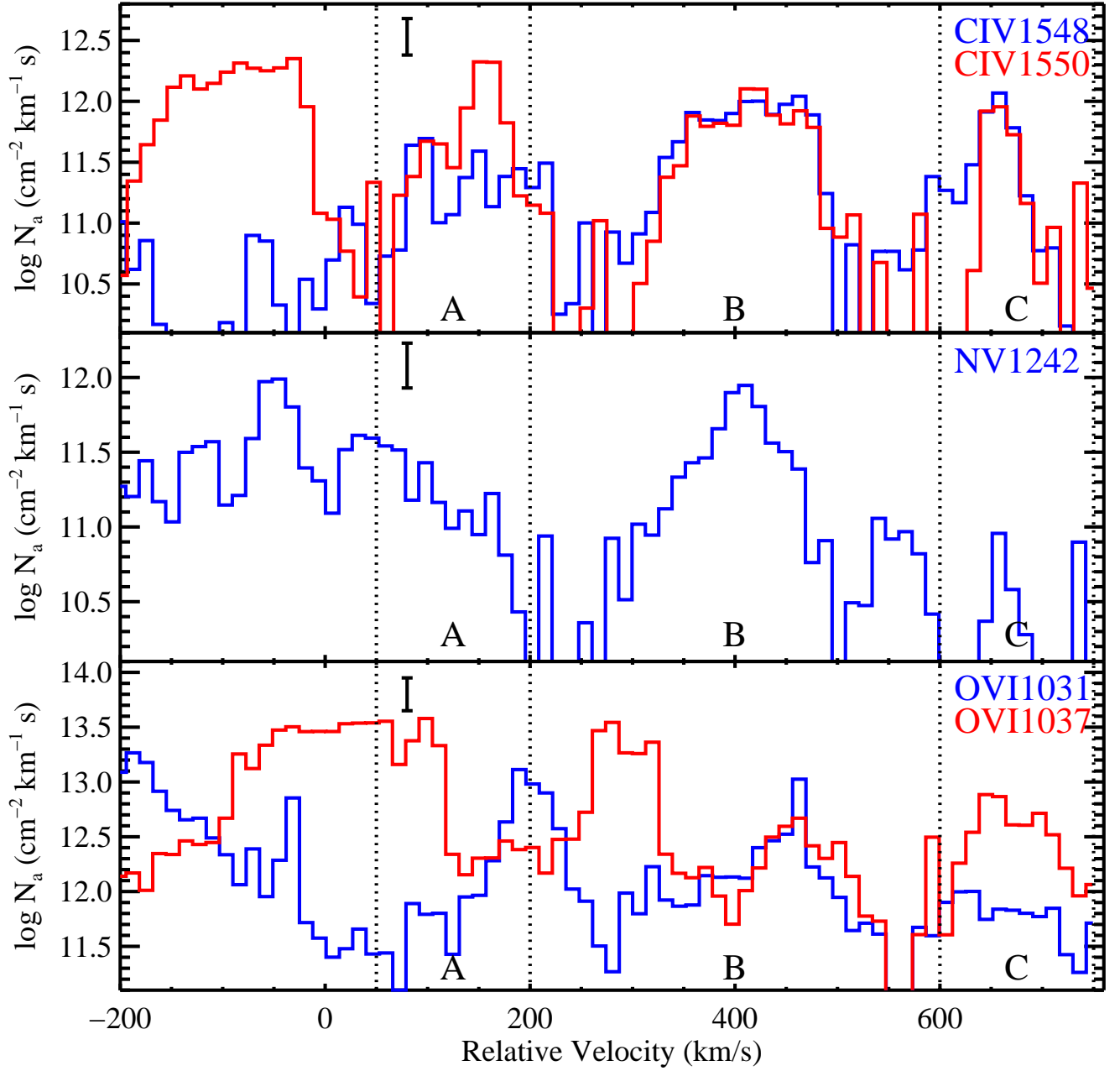


FIG. 8.— Apparent column density N_a profiles for the NV 1242 transition, and the C IV and O VI doublets for velocities relative to $z_{\text{fg}} = 2.4360$. The profiles are significantly contaminated by coincident line-blending which is best revealed by comparing the N_a profiles for the pair of transitions in each doublet. After accounting for this line-blending, we conclude that there is weak (or negligible) N V and O VI absorption in subsystem C and at $\delta v < 0 \text{ km s}^{-1}$. Values and upper limits to the integrated ionic column densities are given in Table 5.

The current paradigm of baryons within galactic halos envisions a hot, diffuse medium that has been heated by shocks during virialization and/or feedback from supernovae within the galaxy. Embedded within this diffuse medium may be cooler, dense clouds that may be photoionized by the local or background UV radiation field. In the Galaxy, this simple picture is supported by the observations of the high velocity clouds (cool, dense clumps, e.g. Wakker & van Woerden 1997; Putman et al. 2002) and the widespread detection of O VI absorption which traces a hotter, diffuse medium (Sembach et al. 2003). This model is also supported by quasar absorption line surveys, i.e. the association of Mg II, C IV, and O VI gas with galactic halos (e.g. Steidel 1993; Chen et al. 2001; Fox et al. 2007). On theoretical grounds, it has been argued that a hot diffuse component pressure confines a population of cold clouds, which are unlikely to be massive enough to be self-gravitating (Mo & Miralda-Escude 1996; Maller & Bullock 2004).

With these scenarios in mind, we are motivated to search for absorption from a diffuse, hot component that could be associated with the halo of SDSSJ1204+0221FG. The sightline to SDSSJ1204+0221BG intersects the presumed galactic halo of SDSSJ1204+0221FG at an impact parameter $R_{\perp} = 108 \text{ kpc}$. As we will see in § 5.1, the virial radius of the dark matter halo expected to host SDSSJ1204+0221FG is $r_{\text{vir}} \simeq 250 \text{ kpc}$, so that our background sightline

TABLE 5
HIGH-ION COLUMN DENSITIES

Ion	SDSSJ1204+0221FG ^a	Subsystem A ^b	Subsystem B ^c	Subsystem C ^d
$\log N(\text{C}^+)$	12.7 ± 0.11	13.4 ± 0.05	14.0 ± 0.05	13.3 ± 0.06
$\log N(\text{N}^{+4})$	< 13.9	< 13.3	< 13.8	< 11.9
$\log N(\text{O}^{+5})$	< 14.9	< 14.4	< 14.8	< 14.0

^aIntegrated AODM column densities for the interval containing SDSSJ1204+0221FG: $-200 \text{ km s}^{-1} < \delta v < +50 \text{ km s}^{-1}$ relative to $z_{fg} = 2.4360$.

^bIntegrated AODM column densities for Subsystem A: $+50 \text{ km s}^{-1} < \delta v < +200 \text{ km s}^{-1}$ relative to $z_{fg} = 2.4360$.

^cIntegrated AODM column densities for Subsystem B: $+200 \text{ km s}^{-1} < \delta v < +600 \text{ km s}^{-1}$ relative to $z_{fg} = 2.4360$.

^dIntegrated AODM column densities for Subsystem C: $+600 \text{ km s}^{-1} < \delta v < +780 \text{ km s}^{-1}$ relative to $z_{fg} = 2.4360$.

easily resolves the virial radius. In § 3, we discussed the detection and analysis of low and intermediate-ion transitions observed in SLLS/SDSSJ1204+0221BG. We also commented on the general absence of strong absorption by high-ions like O^{+5} , C^{+3} , and N^{+4} . These ions trace gas either with a large ionization parameter ($\log U > -2$) or with a high temperature ($T > 10^5 \text{ K}$). Their observed column densities, therefore, constrain the nature of a diffuse and/or hotter phase within the halo of SDSSJ1204+0221FG.

In Figure 8, we present the apparent column densities, $N_a^i \equiv 10^{14.5761} \ln(1/I^i)/(f\lambda)$, of the C IV, N V and O VI profiles (smoothed by 5 pixels) for the velocity interval spanning the quasar redshift and the three subsystems of SLLS/SDSSJ1204+0221BG. The C^{+3} and O^{+5} ions exhibit multiple transitions which allow one to identify line-blending by visual inspection, i.e. regions where the two profiles diverge significantly. The C IV 1548 and 1550 profiles track each other closely for $\delta v > +200 \text{ km s}^{-1}$ indicating a positive detection without blending at these velocities. At $\delta v < +200 \text{ km s}^{-1}$, the profiles diverge because the C IV 1548 profile of component C blends into the C IV 1550 profile of component A (see also Fig 3). Therefore, the C IV 1548 profile sets an upper limit to the column density of C^{+3} at these velocities. At $\delta v \leq 0 \text{ km s}^{-1}$, there is no statistically significant detection of C IV.

The N V and O VI doublets lie within the Ly α forest and therefore are more likely to suffer from line blending. Examining the O VI transitions, the two profiles diverge at nearly all velocities. This indicates that the line-profiles are severely affected by blends, most likely Ly α and Ly β absorption from gas at lower redshift. The only interval where the O VI profiles roughly coincide is at $400 \text{ km s}^{-1} < \delta v < 550 \text{ km s}^{-1}$. One may optimistically interpret the absorption as a positive detection of O^{+5} ions, but the more conservative approach is to report even this absorption as an upper limit. Turning to N V, we present only the N V 1242 transition because the N V 1238 profile is heavily blended with a strong Ly α system at $z = 2.502$. We also expect that the broad absorption at $\delta v < 200 \text{ km s}^{-1}$ is associated with coincident Ly α absorption; meanwhile, the optical depth in subsystem C ($\delta v < 600 \text{ km s}^{-1}$) is not statistically significant. The only plausible N V absorption, therefore, is within subsystem B where one notes the optical depth profile of N V 1242 resembles that of C IV in the interval $300 \text{ km s}^{-1} < \delta v < 500 \text{ km s}^{-1}$. We caution, however, that the O VI profiles do not track N V in this velocity interval. This draws into question a positive detection of N V absorption because the O^{+5} and N^{+4} ions trace gas with similar physical properties and one generally expects coincident N V and O VI absorption. It is possible, therefore, that the apparent N V profile instead tracks an unidentified blend and we report the measured optical depth as an upper limit to $N(\text{N}^{+4})$ in subsystem B.

Table 5 summarizes the column densities of the high-ions in subsystems A, B, and C and in the velocity interval containing $z = z_{fg}$. For C^{+3} and N^{+4} , the column densities are lower than 10^{14} cm^{-2} and fall below 10^{13} cm^{-2} in several regions. For O^{+5} , the upper limits are a factor of ten higher owing to noisier data and a higher frequency of line-blending. All of these values lie below the $\gtrsim 10^{14} \text{ cm}^{-2}$ column densities measured for the low-ions of CNO in SLLS/SDSSJ1204+0221BG (Table 3). This has significant implications for the physical conditions of diffuse gas associated with the galactic halo of SDSSJ1204+0221FG.

A direct conclusion from these observations is that the sightline does not intersect a large column density of optically thin, photoionized material. In the lower panel of Figure 9, we present the predicted column densities of C^{+3} , N^{+4} , and O^{+5} ions for a wide range of physical density assuming an absorber with total hydrogen column density $N_{\text{H}} = 10^{20.5} \text{ cm}^{-2}$ and metallicity $[\text{M}/\text{H}] = -0.5 \text{ dex}$. For these calculations, we assume the gas is illuminated by the SDSSJ1204+0221FG at a distance of $r = R_{\perp}$. Focusing on the parameter space where the gas is optically thin ($n_{\text{H}} < 0.3 \text{ cm}^{-3}$), one predicts column densities exceeding $10^{14.5} \text{ cm}^{-2}$ for all of the ions. Even if we assume a $10\times$ lower metallicity, we can rule out such a phase of gas along the sightline.

The absence of photoionized high-ions like O^{+5} is not particularly surprising, however, because the ambient medium in the outer galactic halo surrounding a high- z quasar almost certainly is at a temperature so high that collisional ionization dominates over photoionization. This material may be observed independently of the gas contributing to SLLS/SDSSJ1204+0221BG. A galaxy with mass $M > 10^{12} M_{\odot}$, for example, has an implied virial temperature in excess of 10^6 K and the dark matter halo expected to host SDSSJ1204+0221FG would have a virial temperature $T_{\text{vir}} \sim 10^7 \text{ K}$ (see § 5.1). In Figure 10 we present predicted column densities for C^{+3} , N^{+4} , and O^{+5} ions assuming

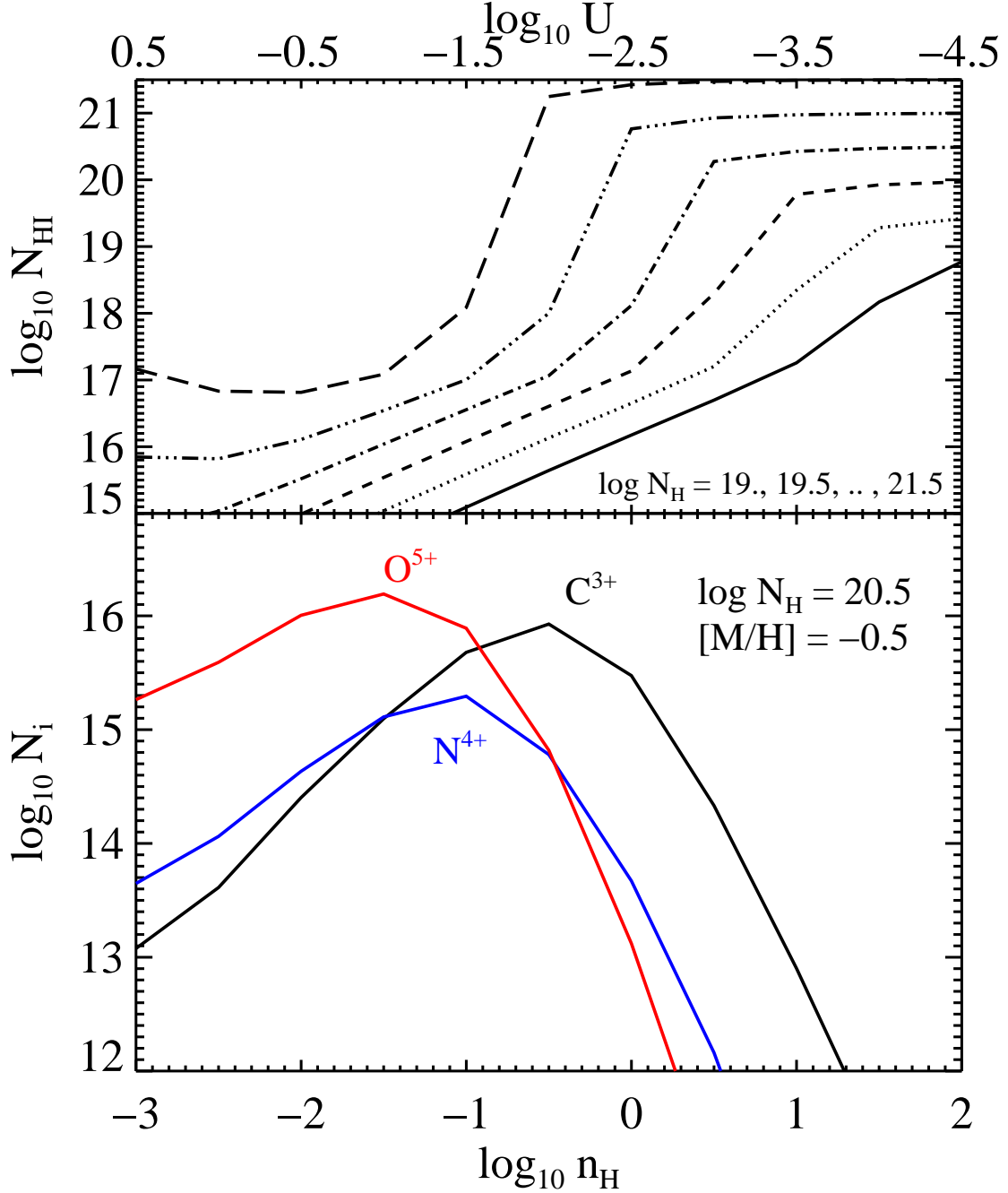


FIG. 9.— Upper panel: Predicted H I column densities for a plane-parallel slab lying at a distance of 100 kpc from SDSSJ1204+0221FG for a range of total H column ($\log N_{\text{H}} = 19, 19.5, \dots, 21$) and as a function of volume density n_{H} . As n_{H} decreases, the effective ionization parameter increases and the gas eventually becomes optically thin (i.e. $N_{\text{HI}} < 10^{17.2} \text{ cm}^{-2}$). Lower panel: Predicted column densities of several metal ions for a plane parallel slab with $N_{\text{H}} = 10^{20.5} \text{ cm}^{-2}$ illuminated by SDSSJ1204+0221FG at a distance of 100 kpc. As the assumed volume density of the gas is lowered, the gas is more photoionized and CNO are pushed into the high-ion states of C^{3+} , N^{4+} , and O^{5+} . The predicted column densities for a metallicity of 1/3 solar are high and easily detectable even in a low-resolution spectrum (e.g. SDSS). These predicted column densities are to be compared against the observed values (Figure 8, Table 5).

collisional ionization equilibrium (CIE; Sutherland & Dopita 1993), $N_{\text{H}} = 10^{21.8} \text{ cm}^{-2}$ and $[\text{M}/\text{H}] = -0.5$ dex. This H column density is the predicted value at $R_{\perp} = 108 \text{ kpc}$ in a $M = 10^{13.3} M_{\odot}$ halo with a Navarro-Frank-White (NFW) profile (concentration $c = 4$) and assuming a gas fraction equal $f_g = 0.17$ equal to the cosmic baryon fraction (Dunkley et al. 2008, see § 5.1). The figure demonstrates that the gas must have $T > 10^6 \text{ K}$ to be consistent with the observed upper limits to $N(\text{O}^{5+})$. The dependence of $N(\text{O}^{5+})$ on T is so strong that even if we assume considerably lower N_{H} and $[\text{M}/\text{H}]$ values for the diffuse component, the gas must have $T > 10^6 \text{ K}$. A cooler phase is only allowed if $\log N_{\text{H}} + [\text{M}/\text{H}] < 17.7$.

The principal conclusion of this section is that a diffuse medium in the halo of

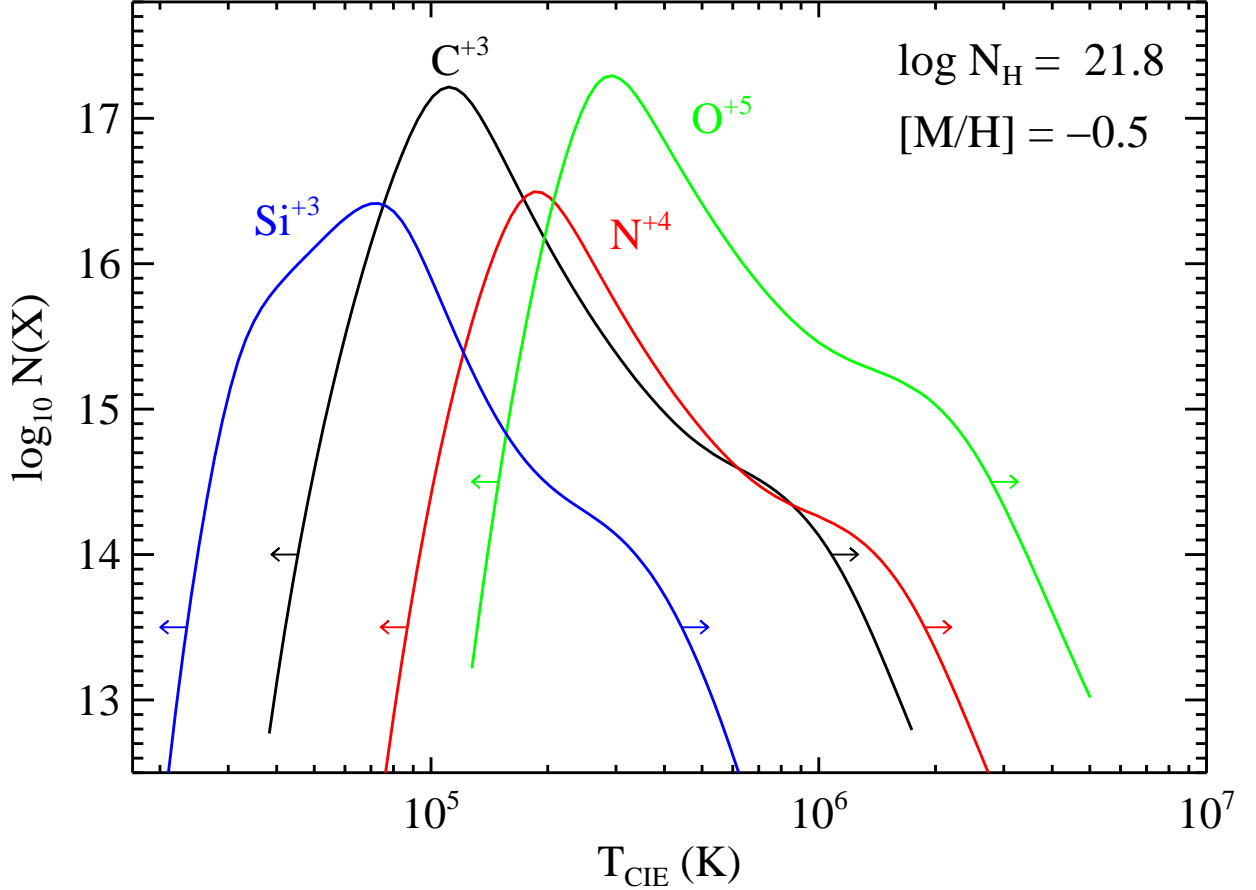


FIG. 10.— Predicted column densities for high-ion states of CNO and Si assuming collisional ionization equilibrium (CIE) for a gas with total H column density $N_{\text{H}} = 10^{21.8} \text{ cm}^{-2}$ and 1/3 solar metallicity. This hydrogen column density corresponds to the estimated baryonic surface density at a 100 kpc impact parameter from a dark matter halo with $M = 10^{13} M_{\odot}$ and an NFW density profile. The arrows on the curves indicate constraints to the temperature based on upper limits to the observed ionic column densities. One notes that the data rule out $3 \times 10^4 \text{ K} < T_{\text{CIE}} < 2 \times 10^6 \text{ K}$.

SDSSJ1204+0221FG, must have a temperature exceeding 10^6 K . This is consistent with the virial temperature $T_{\text{vir}} \sim 10^7 \text{ K}$ for the gas in the $M \gtrsim 10^{13} M_{\odot}$ dark matter halo that is expected to host the f/g quasar (see § 5.1). Note however that the absence of strong high-ion transitions associated with SDSSJ1204+0221FG contrasts with similar observations (using a b/g quasar sightline) of $z \sim 2.3$ star-forming galaxies where strong O VI and N V absorption is detected at similar impact parameters (Simcoe et al. 2006). In addition, the damped Ly α systems (DLAs) also frequently exhibit O VI absorption which reflects a highly ionized, diffuse medium in the halos of these galaxies (Fox et al. 2007). The average $N(\text{O}^{+5})$ for the DLAs exceeds 10^{14} cm^{-2} . The DLA sightlines presumably intersect galactic halos at much smaller impact parameters than $R_{\perp} = 108 \text{ kpc}$. Nevertheless, the high-ion material in DLAs is undoubtedly associated with the galactic halo (Wolfe & Prochaska 2000; Maller et al. 2003; Prochaska et al. 2008a) and may extend to many tens kpc. The fundamental difference is that DLA sightlines will rarely penetrate the galaxies hosting high z quasars and likely trace lower mass halos with significantly lower virial temperatures.

4.4. Is SDSSJ1204+0221FG Shining on SLLS/SDSSJ1204+0221BG?

Of considerable interest to studies of quasars and the buildup of supermassive black holes in the Universe (e.g. Yu & Tremaine 2002; Hopkins et al. 2007c; Shankar et al. 2002) is whether their optical-UV emission is isotropic and or intermittent. Evidence that quasars emit anisotropically or intermittently comes from the null detections of the transverse proximity effect in the Ly α forests of projected quasar pairs (Crotts 1989; Dobrzycki & Bechtold 1991; Fernandez-Soto et al. 1995; Liske & Williger 2001; Schirber et al. 2004; Croft 2004, but see Jakobsen et al. 2003), the anisotropic clustering of optically thick absorbers near quasars (Hennawi & Prochaska 2007; Prochaska et al. 2008b), and the absence of fluorescence detections in optically thick gas proximate to quasars (Hennawi & Prochaska 2008, in prep.; but see Adelberger et al. 2006). Together, these studies provide a statistical case that quasars emit anisotropically or intermittently.

For an individual quasar, one can use a background sightline to observe nearby gas in absorption, and test whether it

is illuminated by studying its ionization state. The general approach is to (1) derive the ionization parameter U of the gas near the quasar using ionic metal line transitions (2) estimate the volume density of the gas, and (3) compare the inferred intensity of the impinging radiation field with that estimated for the nearby quasar. Worseck et al. (2007) and Goncalves et al. (2007) have conducted this test for highly ionized gas near several $z \sim 2$ quasars. The Worseck et al. (2007) study was deemed inconclusive. Goncalves et al. (2007), meanwhile, identified several absorbers proximate to quasars with high ionization parameters and estimated an ionizing radiation field that exceeds the EUVB. Instead, the estimated fluxes roughly match the values calculated for the nearby quasars under the assumption that they emit isotropically. These authors, however, did not place empirical constraints on the gas density, did not consider the effects of collisional ionization, and did not explore the effects of non-solar relative abundances. In these respects, we consider their results to be suggestive but inconclusive.

We can similarly test for illumination of SLLS/SDSSJ1204+0221BG by SDSSJ1204+0221FG. In § 3, we compared the observed ratios of N, Si, Al, Fe, and C atoms and ions against photoionization models assuming a single phase, plane-parallel slab of gas illuminated by a quasar spectrum ($f_\nu \propto \nu^{-1.57}$). For subsystems A+C of

SLLS/SDSSJ1204+0221BG, the majority of the observational constraints imply $\log U < -3.25$. The only exception is the large N^+/N^0 ratio which indicates $\log U \approx -3$ for subsystem A, and $\log U > -4$ for subsystem C. Under the constraints of a single-phase model and a plane-parallel geometry, one cannot identify an equilibrium photoionization model that reproduces all of the observed ionic ratios. By the same token, the observations are inconsistent with any collisional ionization equilibrium model. We do not know if these inconsistencies highlight errors in the atomic data (e.g. dielectronic recombination rates), the oversimplification of a single-phase, plane-parallel geometry, an erroneous shape for the radiation field, and/or the presumption of equilibrium models. We will proceed under the relatively conservative assumption that the ionization parameter $\log U < -3$ and we will comment on implications for significantly smaller values. We also remind the reader that the observed ionic ratios are roughly consistent with a $T \approx 20,000\text{K}$ collisional ionization equilibrium model. Any contribution of collisional ionization processes to the observations would lower the estimated flux of ionizing radiation.

The other key physical constraint is the volume density of the gas n_H . For a predominantly ionized gas, this can be estimated from the electron density n_e . Our analysis of the fine-structure levels of the C^+ and Si^+ ions indicate n_e less than approximately 5 cm^{-3} for each of the subsystems. These upper limits could be improved by obtaining higher S/N observations of the undetected $Si\text{ II}^*$ 1264 transition at $\lambda \approx 4350\text{\AA}$. In any case, we will adopt this conservative limit to the electron density and assume $n_H \approx n_e$ which is appropriate for a predominantly ionized medium.

Adopting $\log U < -3$ and $n_H < 5\text{ cm}^{-3}$, we infer an upper limit to the ionizing photon flux,

$$\Phi_{\text{obs}} = U n_H c < 1.5 \times 10^8 \text{ photons s}^{-1} \text{ cm}^{-2} . \quad (6)$$

We may compare this value with the ionizing flux of SDSSJ1204+0221FG under the assumptions that the gas lies at a distance equal to the impact parameter and that the quasar emits isotropically. Combining the SDSS optical photometry of SDSSJ1204+0221FG with an assumed power-law spectral shape ($f_\nu \propto \nu^{-1.57}$), we derive an AB magnitude $m_{912} = 21.42$ at 1 Ryd. At $z_{\text{fg}} = 2.436$, this gives a specific luminosity $L_{912} = 1.16 \times 10^{30} \text{ erg s}^{-1} \text{ cm}^{-2} \text{ Hz}^{-1}$ and we estimate an ionizing photon flux at $r = R_\perp = 108 \text{ kpc}$ of

$$\Phi_{\text{QSO}} = 9 \times 10^7 \text{ photons s}^{-1} \text{ cm}^{-2} , \quad (7)$$

assuming the quasar emits isotropically. Therefore, the conservative upper limit to Φ_{obs} roughly matches the predicted photon flux from SDSSJ1204+0221FG at the observed impact parameter. In this conservative observational limit, we do not have strong evidence for anisotropic emission.

If we adopt less conservative but more realistic constraints on the ionization parameter and volume density ($\log U < -4$; $n_H < 1\text{ cm}^{-3}$), we set an upper limit to the observed photon flux $\Phi'_{\text{obs}} < 3 \times 10^6 \text{ photons s}^{-1} \text{ cm}^{-2}$. To maintain the null hypothesis that SLLS/SDSSJ1204+0221BG is illuminated, we would require the gas be located at $r > 500 \text{ kpc}$. This large distance is disfavored by other arguments. The extreme velocity field, high metallicity, and quasar-like relative abundances suggest the gas is local to the quasar host galaxy. At $r = 500 \text{ kpc}$ one could associate SLLS/SDSSJ1204+0221BG with a protocluster containing SDSSJ1204+0221FG, but not its galactic halo. Furthermore, the strong clustering of optically thick absorbers around quasars at $z \sim 2.5$ implies a high probability that $r \approx R_\perp$ (Hennawi & Prochaska 2007). In Figure 6, we show the probability of the absorber lying at a distance less than r from the f/g quasar, given the knowledge that it is within a velocity interval $v_{\text{vmax}} = \pm 700 \text{ km s}^{-1}$ and has an impact parameter $R_\perp = 108 \text{ kpc}$. The upper x-axis of the figure shows the corresponding cumulative probability of the ionizing flux ϕ_{QSO} , assuming that SDSSJ1204+0221FG emits isotropically. We calculate a 70% probability that SLLS/SDSSJ1204+0221BG is located within 500 kpc of the quasar.

We independently test whether the transverse direction is illuminated by searching for $\text{Ly}\alpha$ fluorescence from the optically thick gas near the b/g quasar sightline. By coadding a series of longslit exposures of SDSSJ1204+0221 using Gemini/GMOS, amounting to a 7200s total integration, we have not detected any extended emission (Hennawi & Prochaska 2008, in prep.; but see Adelberger et al. 2006) at the f/g quasar redshift near the impact parameter of the b/g quasar sightline. The gas clouds comprising SLLS/SDSSJ1204+0221BG have estimated sizes of $\sim 10 - 100 \text{ pc}$, making them so small that it would be impossible (with current sensitivity) to detect $\text{Ly}\alpha$ emission from the *actual* clouds we see in absorption in SLLS/SDSSJ1204+0221BG. However, the high covering factor of optically thick gas near foreground quasars with $R_\perp \lesssim 100 \text{ kpc}$ characterized statistically by Hennawi et al. (2006a), together with the

detection of three such optically thick subsystems in SLLS/SDSSJ1204+0221BG, argue that the covering factor of optically thick gas is indeed roughly unity at R_\perp near SDSSJ1204+0221FG. If this gas is illuminated it should be emitting detectable Ly α photons. The fluorescent surface brightness of clouds illuminated by SDSSJ1204+0221FG at a distance of $R_\perp = 108$ kpc would be

$SB_{\text{Ly}\alpha} < 4.8 \times 10^{-17} \text{ ergs s}^{-1} \text{ cm}^{-2} \text{ arcsec}^{-2}$. From a preliminary analysis, we conservatively estimate that we could have detected extended emission a factor of ten fainter than this expectation, implying that the distance to the clouds would have to be $r > \sqrt{10} R_\perp$ to render them undetectable if the foreground quasar emits isotropically. Thus, isotropic emission from SDSSJ1204+0221FG is ruled out unless all of the optically thick gas lies beyond $r > 340$ kpc.

4.5. Why Aren't Similar Absorbers Observed along the Line of Sight to Quasars?

Hennawi & Prochaska (2007) have demonstrated that high- z quasars exhibit a high covering fraction to optically thick absorbers at impact parameters $R_\perp \lesssim 200$ kpc, and argued that the incidence of such transverse absorption exceeds the incidence along the line-of-sight to bright high- z quasars. Prochaska et al. (2008b) similarly concluded that there are fewer damped Ly α systems near $z > 2$ quasars than expected from clustering arguments and Wild et al. (2008) have recently reported a similar deficit of strong Mg II absorbers along the line-of-sight compared to the transverse direction. Together these observations argue that quasars emit ionizing radiation anisotropically or intermittently. Hence a paucity of optically thick absorbers are detected along the line-of-sight because this gas, which is by construction illuminated, is photoionized by the quasar. One test of this hypothesis is to search for an enhancement of highly ionized material along the sightline, e.g. Si IV, C IV, N V, O VI. Indeed, Wild et al. (2008) report a higher incidence of C IV absorption along the same sightlines where the lower ionization potential transition, Mg II, is deficient. There is also a high incidence of highly ionized absorbers within several thousand km s^{-1} of the quasar redshift commonly termed narrow associated absorption line systems (NAAL; D'Odorico et al. 2004). We now explore the physical conditions required for SDSSJ1204+0221FG to photoionize/photoevaporate SLLS/SDSSJ1204+0221BG and also the expected properties of SLLS/SDSSJ1204+0221BG if it were illuminated by the quasar, and thus exposed to a more intense radiation field. These calculations are similar to those performed by Chelouche et al. (2007) and we refer the reader to their work for additional analysis.

In Figure 9 we present a series of calculations from the Cloudy software package for constant density gas slabs placed 100 kpc from SDSSJ1204+0221FG along the sightline to Earth. The quasar's specific luminosity was assumed to be a power-law ($L_\nu \propto \nu^{-1.57}$) and was normalized to SDSS photometry: $L_\nu = L_{912}(\nu/\nu_{912})^{-1.57}$ with $L_{912} = 1.16 \times 10^{30} \text{ ergs s}^{-1} \text{ Hz}^{-1}$. In all of the calculations we assume a gas metallicity $[\text{M}/\text{H}] = -0.5$ dex with solar relative abundances. In the upper panel of the Figure, we show the H I column densities for slabs with a series of total H column densities¹⁴ $\log N_H = 19, 19.5, \dots, 21$ as a function of the gas density n_H . For slabs with $N_H = 10^{19} \text{ cm}^{-2}$, the gas has $N_{\text{HI}} < 10^{17.2}$ and is hence optically thin to ionizing photons, provided $n_H < 10 \text{ cm}^{-3}$; while slabs with $N_H = 10^{21} \text{ cm}^{-2}$ are optically thin only if $n_H < 0.1 \text{ cm}^{-3}$.

In § 3, we estimated $N_H \approx 10^{20} \text{ cm}^{-2}$ and $n_H \approx 1 \text{ cm}^{-3}$ for subsystems A and C based on the relative column densities of several ion pairs, our estimate of the H I column density (uncertain by ± 0.4 dex), and an analysis of C II and Si II fine-structure transitions. According to the calculations presented in Figure 9, this gas would have $N_{\text{HI}} \approx 10^{17} \text{ cm}^{-2}$ if it were at 100 kpc from SDSSJ1204+0221FG along our sightline. If the volume density is just a little lower (permitted by the fine-structure analysis), the gas would be optically thin. We conclude that subsystems A and C of SLLS/SDSSJ1204+0221BG would be photoionized by SDSSJ1204+0221FG if it were placed along our sightline. Subsystem B, however, exhibits a larger N_{HI} value and has a larger implied $N_H \approx 10^{20.3} \text{ cm}^{-2}$ value. Assuming $n_H = 1 \text{ cm}^{-3}$, this system would have $N_{\text{HI}} \approx 10^{17.3} \text{ cm}^{-2}$ if illuminated by the SDSSJ1204+0221FG at a distance of 100 kpc. To be optically thin and illuminated at this distance requires $n_H < 1 \text{ cm}^{-3}$. It is important to note that SDSSJ1204+0221FG is relatively faint compared to the brighter quasars studied to establish the low incidence of optically thick absorbers near quasars (e.g. Russell et al. 2006; Prochaska et al. 2008b; Wild et al. 2008). These quasars are a factor of $\sim 5 - 10$ brighter and the resulting ionization parameters are higher by the same factor. Thus clouds with properties similar to SLLS/SDSSJ1204+0221BG could still appear optically thin if illuminated, resulting in no conflict with previous observations. Similarly, it would be very fruitful to characterize the incidence of proximate optically thick absorbers as a function of quasar luminosity.

If an absorber like SLLS/SDSSJ1204+0221BG is photoionized by a nearby quasar, the system may still give rise to several discernible features. If the H I column density exceeds 10^{14} cm^{-2} , it would exhibit a strong Ly α absorption feature. This would be difficult to distinguish from the ambient Ly α forest, however. If this gas has even a modest metallicity, it may show unique metal-line signatures. The lower panel of Figure 9 presents the predicted column densities of several high-ions assuming $N_H = 10^{20.5} \text{ cm}^{-2}$, $[\text{M}/\text{H}] = -0.5$ dex, and that the cloud is at a distance of 100 kpc from SDSSJ1204+0221FG along our sightline. Once the cloud becomes optically thin (at $n_H \lesssim 0.5 \text{ cm}^{-3}$), large column densities of C^{+3} , N^{+4} , and O^{+5} ions are expected. The alkali doublets associated with these ions saturate at column densities of $\approx 10^{14} \text{ cm}^{-2}$ and, therefore, would yield absorption lines that could be detected at even the modest resolution of the SDSS spectroscopic survey. These column densities scale directly with the assumed metallicity and are also sensitive to the N_H value. Combining the high incidence of optically thick gas observed in the transverse direction with the high ionization parameter along the sightline, and using our knowledge of the physical properties of the (unilluminated) absorbing clouds from SLLS/SDSSJ1204+0221BG, we conclude that that a large fraction of

¹⁴ These calculations are nearly self-similar with respect to the ionization parameter U , i.e. we derive similar results if we modify the distance to the slab, the quasar luminosity and n_H provided that U remains constant.

bright quasars should exhibit strong C IV, N V, and O VI absorption at $z \approx z_{\text{em}}$ along their sightlines.

Absorption systems with strong high-ion absorption near quasars with $z_{\text{abs}} \approx z_{\text{em}}$ or small velocity intervals ($\Delta v < 1000 \text{ km s}^{-1}$) have been detected in quasar spectra, and are referred to as narrow associated absorption line (NAAL) systems (e.g. Wampler et al. 1993; Srianand & Petitjean 2000). The most comprehensive survey of these NAALs using high resolution spectra was performed by D’Odorico et al. (2004) who analyzed the UVES key project of $z \approx 2$ quasars. Of the 22 quasars in the sample, D’Odorico et al. (2004) report that 16 exhibit significant C IV absorption within $\pm 5000 \text{ km s}^{-1}$ of z_{em} for a total of 34 C IV systems, 15 of which also exhibit N V absorption. D’Odorico et al. (2004) studied the properties of a subset which allowed for detailed photoionization modeling. The characteristics of this subset are similar in metallicity, density, and relative abundances to SLLS/SDSSJ1204+0221BG (see also § 4.2). Furthermore, the authors used observed limits on the volume density of the gas (from fine-structure analysis) and estimates of partial coverage to infer distances of 10 to 200 kpc from the quasar. We conclude, therefore, that if SLLS/SDSSJ1204+0221BG experienced an ≈ 10 times higher ionization parameter, it would show characteristics common to NAAL systems. Indeed, SDSSJ1204+0221FG is approximately 2.5 mag ($10\times$) fainter than the quasars of the D’Odorico et al. (2004) sample. We speculate that an absorption-line survey of intrinsically faint quasars will show a high incidence of absorbers with properties similar to SLLS/SDSSJ1204+0221BG and a correspondingly lower incidence of NAAL systems. One could perform such a survey with current and future echellette spectrometers on 10m-class telescopes.

5. NEW CLUES ABOUT MASSIVE GALAXY FORMATION

In this section we examine inferences one might draw from our measurements of SLLS/SDSSJ1204+0221BG in the context of galaxy formation models and quasar feedback. With only a single sightline, it is too early to draw firm conclusions on these processes. In part, the following section sets the framework for future discussion. We begin with a review of the expected properties of the dark matter halo for a $z \sim 2.5$ quasar.

5.1. Expected Properties of SDSSJ1204+0221FG’s Dark Halo

Porciani et al. (2004) measured the clustering of quasars in the redshift range $0.8 < z < 2.1$, which allowed them to estimate that quasars are hosted by dark matter halos with mass $M \sim 10^{13} M_{\odot}$. As they found strong evolution of the clustering with redshift, which continues to even higher redshift ($z > 3.0$; see Shen et al. (2007b)), we henceforth assume that SDSSJ1204+0221FG resides in a dark matter halo $M = 10^{13.3} M_{\odot}$, but we caution that this mass is uncertain by a factor of ~ 0.5 dex, due to both measurement error and the intrinsic distribution of quasar host halo masses.

For a dark matter halo of this mass with an NFW profile (Navarro et al. 1997), the virial radius is

$$r_{\text{vir}} = 251 \left(\frac{M}{10^{13.3} M_{\odot}} \right)^{1/3} \text{ kpc}, \quad (8)$$

Thus, if SDSSJ1204+0221FG resides at the center of its host dark matter halo, the SDSSJ1204+0221BG sightline probes it at $\lesssim 50\%$ of the virial radius. If we assume a concentration parameter $c = 4$ (characteristic of high redshift halos), the peak circular velocity of the dark matter halo is

$$v_{\text{circ}} = 604 \left(\frac{M}{10^{13.3} M_{\odot}} \right)^{1/3} \text{ km s}^{-1}, \quad (9)$$

which implies a dynamical time at the impact parameter R_{\perp} of the background sightline of

$$t_{\text{dyn}} \sim R_{\perp}/v_{\text{circ}} = 1.7 \times 10^8 \left(\frac{M}{10^{13.3} M_{\odot}} \right)^{-1/3} \text{ years}. \quad (10)$$

The circular velocity we deduce is comparable to the extreme kinematics observed in the subsystems of SLLS/SDSSJ1204+0221BG. It is thus conceivable that the motions in SLLS/SDSSJ1204+0221BG represent gravitational infall or virial motion of ‘cold gas clouds’ orbiting in the dark matter halo potential, just as galaxies would. To make this more precise we note that the maximum extent spanned by the three components of SLLS/SDSSJ1204+0221BG is $\Delta v \approx 650 \text{ km s}^{-1}$. For a Gaussian distribution, we find that the maximum extent measured from three samples is related to the dispersion by $\Delta v = 1.69\sigma$, so we estimate that the dark matter halo hosting SDSSJ1204+0221FG and SLLS/SDSSJ1204+0221BG has a line-of-sight velocity dispersion $\sigma \simeq 380 \text{ km s}^{-1}$. Tormen (1997) found that the maximum circular velocity of an NFW halo is a factor of ≈ 1.4 times larger than the maximum of the one dimensional velocity dispersion, so our kinematics suggest $v_{\text{circ}} = 540 \text{ km s}^{-1}$. The velocity width of SLLS/SDSSJ1204+0221BG is consistent with the characteristic velocity for the dark matter halos hosting $z \sim 2.5$ quasars (eqn. 9), thus gravitational dynamics in the halo surrounding SDSSJ1204+0221FG could explain the observed kinematics.

One challenge to this scenario is that the velocities of the clouds comprising SLLS/SDSSJ1204+0221BG are systematically offset to positive values relative to SDSSJ1204+0221FG. Such an offset is characteristic of organized motions (e.g. rotation, infall along a filament) rather than a random velocity field and we question whether a highly organized velocity field with large velocity width can occur in the outer halo. It is worth noting, however, that the offset resembles a similar trend observed for optically

thick absorbers (Mg II systems) at $z \sim 1$. For these absorbers, Steidel et al. (2002) and Kacprzak et al. (2007) report a systematic velocity offset between the gas and the systemic velocity of its host galaxy. The origin of this asymmetry is not understood. Another explanation for the observed kinematics is that SLLS/SDSSJ1204+0221BG represents cold material swept up in large scale outflow, which we consider in more detail in § 5.4.

In the standard structure formation picture, gas falling into a massive dark matter halo will be shock heated to near the virial temperature of the dark halo, converting its gravitational kinetic energy into thermal energy. The virial temperature is defined as

$$T_{\text{vir}} = \frac{\mu m_p v_{\text{circ}}}{2k_B} = 1.3 \times 10^7 \left(\frac{M}{10^{13.3} M_\odot} \right)^{2/3} \text{ K}, \quad (11)$$

where μ is the mean atomic weight, which we take as $\mu = 0.59$ for a fully ionized primordial gas. Gas at these high temperatures will be collisionally ionized and should result in negligible H I absorption.

As we detect a large column of enriched and cold photoionized gas at $T \simeq 20,000$ K in the background sightline, it is of interest to calculate the time that it would take gas shock heated to the virial temperature to cool at the distance of our impact parameter. The cooling time of a gas is conventionally taken to be the ratio of its specific thermal energy to the volumetric cooling rate, or $t_{\text{cool}} = [3(n_e + n)kT]/[2n_e n \Lambda]$ where Λ is the cooling function (e.g. Sutherland & Dopita 1993) and n is the total ion density. We can estimate the ion density of the quasar host halo assuming that the total mass (dark matter + gas) distribution follows an NFW density profile $\rho(r)$, with the gas density being a fraction f_g of the total density $\rho_g(r) = f_g \rho(r)$. We have then $n = \rho_g / \mu m_p$, or

$$n(r = 108 \text{ kpc}) \approx 7.5 \times 10^{-3} \left(\frac{f_g}{0.17} \right) \left(\frac{M}{10^{13.3} M_\odot} \right)^{0.73} \text{ cm}^{-3}, \quad (12)$$

where we took $f_g = \Omega_b / \Omega_m = 0.17$ to be the cosmic baryon fraction from Dunkley et al. (2008). We finally find for the cooling time at $r = 108$ kpc, $t_{\text{cool}} \approx 3.2 \times 10^9 (M/10^{13.3} M_\odot)^{-0.22}$ years. Note that at the high virial temperatures $T \sim 10^7$ K characteristic of our dark matter halo, cooling is dominated by thermal bremsstrahlung radiation and hence does not depend strongly on metallicity. According to the current structure formation paradigm, the bulk of the gas interior to the virial radius should have been shock heated to T_{vir} , and the cooling time of this hot phase at $R \simeq 100$ kpc is comparable to the age of the Universe at $z = 2.4360$, $t_H = 2.6 \times 10^9$ years. Thus the impact parameter $R_\perp = 108$ kpc for SDSSJ1204+0221BG probes SDSSJ1204+0221FG at approximately the cooling radius (where $t_{\text{cool}} = t_H$, which is $r_{\text{cool}} = 99$ kpc). Furthermore, because the dynamical time (eqn. 10) is a factor of ~ 20 shorter than the cooling time, the dark matter halo we consider satisfies the condition for stable shock formation (Dekel & Birnboim 2006) and is in the pressure supported “hot halo” regime.

5.2. The Distribution of Cold Gas

From the foregoing discussion, we expect the bulk of the gas near SDSSJ1204+0221FG to have been shock heated to the virial temperature of its hot-halo (see eqn. 11). However, our analysis of SLLS/SDSSJ1204+0221BG indicates a column density $N_{\text{HI}} = 10^{19.65} \text{ cm}^{-2}$, and hence a substantial amount of “cold” gas at $R_\perp \simeq 108$ kpc. Similarly, a high covering factor of high column density ($N_{\text{HI}} > 10^{19} \text{ cm}^{-2}$) cold gas was seen statistically by Hennawi et al. (2006a) and Hennawi & Prochaska (2007). In what follows we combine the Hennawi & Prochaska (2007) measurement of the clustering of cold gas around quasars, with our measurements of the properties of SLLS/SDSSJ1204+0221BG (see Table 4), to estimate the covering factor, density, and volume filling factor of cold gas in the halos surrounding high z massive galaxies.

At a transverse separation R_\perp from a foreground quasar, the covering factor of absorbers can be written (Hennawi & Prochaska 2007)

$$C(R_\perp) = \left\langle \frac{dN}{dD} \right\rangle [1 + \chi_\perp(R_\perp, \Delta D)] \Delta D, \quad (13)$$

where we search over a radial (comoving) distance interval ΔD corresponding to a redshift interval Δz in the background quasar spectrum. Here $\left\langle \frac{dN}{dD} \right\rangle = n_{\text{abs}} A$ is the incidence of absorption line systems per unit comoving distance, which is simply the product of the comoving number density of the clouds which give rise to absorption line systems and their absorption cross section A (in comoving units). The transverse correlation function $\chi_\perp(R, \Delta D)$ accounts for the enhancement due to clustering and can be written as an integral of the 3-d quasar-absorber correlation function, $\xi_{\text{QA}}(r)$, over the search window (see Hennawi & Prochaska 2007, for details). Assuming a power law shape for the quasar-absorber cross-correlation function, Hennawi & Prochaska (2007) measured $r_0 = 9.2_{-1.7}^{+1.5} h^{-1} \text{ Mpc}$ for $\gamma = 1.6$, or $r_0 = 5.8_{-0.6}^{+1.0} h^{-1} \text{ Mpc}$ for $\gamma = 2$. These fits imply covering factors of $C(R_\perp = 108 \text{ kpc}) = 0.29 \pm 0.08$ and $0.35_{-0.07}^{+0.13}$, respectively. For this calculation we chose a projection distance $\Delta D = 19.2 \text{ Mpc}$ along the line of sight, which corresponds to a velocity interval $\pm 700 \text{ km s}^{-1}$, motivated by the 650 km s^{-1} extent of the absorption components in SLLS/SDSSJ1204+0221BG.

For the simplified case of identical clouds of mass M_c , the mass density of cold gas (in proper units) is

$$\rho_{\text{cold}}(r) = \frac{1}{a^3} n_{\text{abs}} [1 + \xi_{\text{QA}}(r)] M_c = \frac{1}{a} \left\langle \frac{dN}{dD} \right\rangle [1 + \xi_{\text{QA}}(r)] N_{\text{H}} \frac{1}{X} \quad (14)$$

where a is the scale factor, M_c is the mass of the clouds, $X = 0.76$ is the hydrogen mass fraction, and $\mu_c = 0.61$ is the mean atomic weight of the cold gas¹⁵. Plugging in numbers using the parameters of SLLS/SDSSJ1204+0221BG we find

$$\rho_{\text{cold}}(r = 108 \text{ kpc}) \approx 3.0 \times 10^{-6} \left[\frac{(108 \text{ kpc}/r_0)^{-\gamma}}{472} \right] \left(\frac{N_{\text{H}}}{10^{20.6} \text{ cm}^{-2}} \right) M_{\odot} \text{ pc}^{-3}. \quad (15)$$

We can compare this to our expectation for the baryon density in an NFW halo at this distance (see eqn. 12), and thus compute the cold gas fraction

$$\frac{\rho_{\text{cold}}}{\rho_g}(r = 108 \text{ kpc}) \approx 0.03 \left(\frac{f_g}{0.17} \right)^{-1} \left[\frac{(108 \text{ kpc}/r_0)^{-\gamma}}{472} \right] \left(\frac{N_{\text{H}}}{10^{20.6} \text{ cm}^{-2}} \right) \left(\frac{M}{10^{13.3} M_{\odot}} \right)^{-0.73}. \quad (16)$$

Unfortunately, this estimate suffers from a large uncertainty. Besides the ~ 0.5 dex in the dark halo mass, the quasar-absorber correlation function has significant errors and an uncertain slope. Also we assumed a single cloud population with a total hydrogen column density $N_{\text{H}} = 10^{20.6} \text{ cm}^{-2}$ equal to the total in SLLS/SDSSJ1204+0221BG. This value may not be representative of the cloud population near quasars as a whole, although the neutral column of SLLS/SDSSJ1204+0221BG $N_{\text{HI}} = 10^{19.65} \text{ cm}^{-2}$ is lower than the average $\langle N_{\text{HI}} \rangle \approx 10^{20.1} \text{ cm}^{-2}$ of the four absorbers with $R \lesssim 200 \text{ kpc}$ in the Hennawi & Prochaska (2007) clustering analysis. Finally, it is important to note that we have assumed a maximal value for the gas fraction, $f_g = \Omega_b/\Omega_m = 0.17$, equal to the universal baryon fraction. While in principle the gas fraction can be this large, it is probably smaller because of gas loss from outflows. In this regard the cold gas fraction in eqn. (15) could easily be a factor ~ 2 higher.

Despite the uncertainties, eqn. (15) illustrates how measurements of the covering factor and column density distribution of optically thick absorbers combined with photoionization modeling, can be used to measure the cold gas density *as a function of radius* from massive dark halos. This new observable¹⁶ thus provides a direct test of ideas which are currently popular in structure formation models, such as the cooling radius, cold-accretion, the formation of pressure supported hot-halos, and multiphase media (see below). Furthermore, although the current estimate crudely assumed that all gas clouds are the same as those in SLLS/SDSSJ1204+0221BG, a larger statistical analysis could use the distribution of cloud column densities measured from high-resolution spectra and photoionization modelling.

Next we use our measurement of the electron density (see § 3 and Table 4) and hence size of the absorbing clouds to determine their volume filling factor. The filling factor can be written

$$C_v(r) = \frac{1}{a^3} n_{\text{abs}} [1 + \xi_{\text{QA}}(r)] V_c = \frac{1}{a} \left\langle \frac{dN}{dD} \right\rangle [1 + \xi_{\text{QA}}(r)] \frac{N_{\text{H}}}{n_{\text{H}}} \quad (17)$$

where we used the fact that the ratio of the cloud volume to cloud area is the absorption path length $V_c/(a^2 A) = \ell = N_{\text{H}}/n_{\text{H}}$. Plugging in numbers we find

$$C_v(r = 108 \text{ kpc}) \approx 2.2 \times 10^{-5} \left[\frac{(108 \text{ kpc}/r_0)^{-\gamma}}{472} \right] \left(\frac{N_{\text{HI}}}{10^{20} \text{ cm}^{-2}} \right) \left(\frac{n_e}{1.7 \text{ cm}^{-3}} \right)^{-1}, \quad (18)$$

where we have used the H I column and electron density measurements for component C (see § 3). The mass of the clouds $M_c \sim \frac{4\pi}{3} n_c \mu_c m_p (\ell/2)^3$, where n_c is the cold gas ion density and R_c is the cloud radius. For a hard sphere the cloud radius is related to the average absorption path by $R_c = \frac{3}{4} \ell$. Again, plugging in numbers for component C, we find

$$M_c = 720 \left(\frac{N_{\text{H}}}{10^{20} \text{ cm}^{-2}} \right)^3 \left(\frac{n_e}{1.7 \text{ cm}^{-3}} \right)^{-2} M_{\odot}, \quad (19)$$

however we caution that this estimate is highly uncertain because of its dependence on large powers of quantities with significant errors.

Our conclusion from eqn. (16) that a few percent of the total baryon supply is in a “cold” gas phase at $T \simeq 20,000 \text{ K}$, implies that SDSSJ1204+0221FG has intercepted a multi-phase medium. This is of particular interest in light of considerable theoretical work which indicates that the hot gas associated with massive galaxies should be thermally unstable and prone to fragmentation instabilities (Field 1965; Fall & Rees 1985; Murray & Lin 1990; Mo & Miralda-Escude 1996; Maller & Bullock 2004, but see Malagoli et al. (1990)). The expected result of these instabilities is a fragmented distribution of cooled material at $T \sim 10^4 \text{ K}$, in pressure equilibrium with a hot gas background (Mo & Miralda-Escude 1996; Maller & Bullock 2004; Dekel & Birnboim 2006). These instabilities have not yet been seen in hydrodynamical simulations of galaxy formation (Katz 1992; Thoul & Weinberg 1995; Springel et al. 2001; Yoshida et al. 2002; Helly et al. 2003), which lack the mass resolution necessary to resolve them (Kaufmann et al. 2006). Some have suggested that the formation of this multiphase medium can dramatically influence galaxy formation, resulting in a maximum galaxy mass in massive halos (Maller & Bullock 2004), or providing an important source of feedback energy (Dekel & Birnboim 2008).

¹⁵ We assume one electron per Helium atom in the cold phase gas.

¹⁶ We note that previous workers have studied the distribution of H I near star-forming galaxies (Adelberger et al. 2003, 2004; Simcoe et al. 2006), but these are significantly less massive galaxies $M_{\text{halo}} \sim 10^{11.5}$ and none estimated a cold gas density.

To this end we compute the pressure $P_c = n_c T_c$ of the cold clouds that we detect in absorption as SLLS/SDSSJ1204+0221BG to be

$$P_c = 7.1 \times 10^4 \left(\frac{n_e}{1.7 \text{ cm}^{-3}} \right) \left(\frac{T}{20,000 \text{ K}} \right) \text{ K cm}^{-3}. \quad (20)$$

This value can be compared to our estimate of the pressure in the NFW halo at $r = 108 \text{ kpc}$ thought to be hosting SDSSJ1204+0221FG, by combining eqns. (11) and (12),

$$P_h \approx 9.8 \times 10^4 \left(\frac{f_g}{0.17} \right) \left(\frac{M}{10^{13.3} M_\odot} \right)^{1.4} \text{ K cm}^{-3}. \quad (21)$$

It is compelling that these pressures are comparable. Our determination of the pressure of the absorbing gas in SLLS/SDSSJ1204+0221BG indicates that the gas clouds could very well be pressure confined by the hot $T \sim 10^7 \text{ K}$ gas which is expected to permeate the dark matter halo of SDSSJ1204+0221FG.

5.3. Could the Absorbing Clouds be in Galaxies Clustered around the Quasar?

We can calculate the number density of the absorbing clouds from eqn. (13) if we have knowledge of the absorption cross section A ,

$$n(r) = n_{\text{abs}} [1 + \xi_{\text{QA}}(r)] = \frac{C(R_\perp)}{A \Delta D} \frac{1 + \xi_{\text{QA}}(r)}{1 + \chi_\perp(R_\perp, \Delta D)}. \quad (22)$$

We use our estimate for the radius of the absorber from component C, $r_{\text{abs}} = 15 \text{ pc}$ (see § 3), to determine $A = \pi r_{\text{abs}}^2$. Combined with $C(R_\perp = 108 \text{ kpc}) = 0.35$ from Hennawi & Prochaska (2007), eqn. (22) gives for the number density

$$n(r = 108 \text{ kpc}) = 3.7 \times 10^7 \text{ Mpc}^{-3} \left(\frac{C}{0.35} \right) \left(\frac{r_{\text{abs}}}{15 \text{ pc}} \right)^{-2} \left(\frac{1 + \xi_{\text{QA}}}{473} \right) \left(\frac{1 + \chi_\perp}{28} \right)^{-1} \quad (23)$$

This extremely high number density of clouds leads us to consider an alternative scenario where the small clouds we observe with characteristic size $r_{\text{abs}} = 15 \text{ pc}$ are organized in larger galactic structures (with characteristic size r_{gal}) which are clustered around the quasar. This scenario would still give rise to the small absorption path length of $r_{\text{abs}} \sim 15 \text{ pc}$, but since the clouds are associated with galaxies the macroscopic absorption cross-section would be $A \pi r_{\text{gal}}^2$, and hence the implied number density of galactic hosts n_{abs} would be significantly smaller than determined from eqn. (23). This scenario could also help explain why the metallicities deduced for SLLS/SDSSJ1204+0221BG are so high in spite of the large impact parameter $R_\perp = 108 \text{ kpc}$ from the quasar. If the absorbers are associated with nearby galaxies, then the characteristic size of these enriched regions would be r_{gal} , obviating the need for the quasar to have transported the metals to large distances, perhaps via a large scale outflow (see § 5.4).

First, we assume the absorbers are as numerous as the faintest most abundant star-forming galaxies which have been studied to date and determine the corresponding size of the enriched regions. Reddy et al. (2007) calculated the luminosity function for a combined sample of brighter spectroscopic LBGs and the fainter photometric LBGs from the Hubble Deep Field North studied by Steidel et al. (1999). The comoving number density of the faintest star-forming galaxies at $z \sim 3$ is $n_{\text{LBG}} = 6.9 \times 10^{-3} \text{ Mpc}^{-3}$ for a flux limit of $M_{\text{AB}}(1700\text{\AA}) < -18.2$, corresponding to $\mathcal{R} < 26.9$ or $L > 0.09 L_*$. Adelberger & Steidel (2005) measured the clustering of LBGs around luminous quasars in the redshift range ($2 \lesssim z \lesssim 3.5$), and found a best fit correlation length of $r_0 = 4.7 h^{-1} \text{ Mpc}$ for a slope of $\gamma = 1.6$, which should be considered an upper limit for the much fainter galaxies we consider, which are likely to cluster less strongly. If we use the Adelberger & Steidel (2005) correlation function to calculate the factor of χ_\perp in eqn. (13), then we find that the size of the absorber galaxies has to be

$$r_{\text{gal}} = 91 \text{ kpc} \left(\frac{C}{0.35} \right)^{1/2} \left(\frac{n_{\text{LBG}}}{6.9 \times 10^{-3} \text{ cm}^{-3}} \right)^{-1/2} \left(\frac{1 + \chi_\perp}{9} \right)^{-1/2}. \quad (24)$$

Since this value for r_{gal} is very similar to R_{perp} there is little point in distinguishing between the star-forming galaxy halo and the quasar halo, or stated in a different way, the average number of LBGs in the cylindrical volume set by R_{perp} and ΔD is, including the effects of clustering, about one ($N_{\text{LBG}} = 0.8$). Thus associating the high-metallicity absorbing clouds with faint LBGs does not help explain the high covering factor of enriched material at large impact parameter.

If the absorption is to be associated with galaxies near the quasar, they must arise from a population much more abundant than $L \sim 0.1 L_*$ galaxies. These dwarf systems will be significantly fainter and smaller. If we arbitrarily choose a value of $r_{\text{abs}} = 20 \text{ kpc}$ for their absorption cross-section radius, then eqn. (13) implies a comoving number density of $n_{\text{dwarf}} = 0.14 \text{ Mpc}^{-3}$. Hence, if galaxies clustered around the quasar have $r_{\text{abs}} = 20 \text{ kpc}$ then they must be twenty times more abundant than the faintest photometric LBGs studied to date. Extrapolating the Reddy et al. (2007) luminosity function fit to achieve this number density implies $L \sim 10^{-3} L_*$, or an apparent magnitude limit of $\mathcal{R} < 31.7$. The challenge to this scenario, however, is achieving a nearly solar metallicity in these extremely faint, high- z dwarf-galaxies. Indeed the damped Ly α systems are thought to arise from a population of faint galaxies and are likely to have an absorption size r_{abs} comparable what we assume, but their metallicities are much lower (see Figure 7) and similarly low metallicities are seen locally in dwarf galaxies.

5.4. Are the Kinematics Tracing an Outflow?

How do we explain the presence of such a large gas mass of highly enriched material with a broad-line-region-like enrichment pattern at such a large distance from the quasar ($r \sim 100$ kpc)? It is tempting to associate the absorbing material with a large scale outflow or galactic wind from SDSSJ1204+0221FG and/or its host galaxy. Indeed, quasars exhibit fast outflows in the form of broad absorption line systems on small scales (within 100pc of the engine) and on large scales as radio jets extending to tens of kpc. Furthermore, high- z quasars are believed to reside in actively star-forming galaxies perhaps with highly elevated star-formation rates. Such galaxies may drive fast outflows that, in principal, could extend to tens or even hundreds of kpc. Therefore, in terms of an outflow, there are two extreme scenarios to consider: (a) a highly collimated outflow such as a radio jet associated with the quasar and (b) a large-scale, expanding ‘bubble’ of cold swept up material driven by star-formation feedback and/or the quasar accretion power. The first “jet” scenario naturally yields an asymmetric velocity field and may accelerate gas to very high speeds. However, it has at least two serious drawbacks. First, the cross-section of a highly collimated outflow is, by definition, small. This is not a viable model for reproducing the high incidence of optically thick absorbers near quasars (Hennawi et al. 2006a; Hennawi & Prochaska 2007), although it might explain the single example presented here. Second, the large relative velocities among the subsystems of SLLS/SDSSJ1204+0221BG contradicts the notion of a collimated flow — in order for an outflow to remain collimated out to ~ 100 kpc is must have a very small velocity shear.

For the case of a large-scale outflow driven by intense star-formation or accretion onto the AGN, there are three issues to consider: (i) is there a viable physical mechanism present to drive a wind to the observed speed?; (ii) will the outflow propagate to a distance exceeding the observed impact parameter, that is $\gtrsim 100$ kpc?; and (iii) will the outflow yield an asymmetric velocity field relative to z_{fg} ? The last point requires an asymmetric outflow which might be achieved by an irregular gas distribution in the halo of SDSSJ1204+0221FG (e.g. variable inertia in different directions) or if the gas has been asymmetrically photoionized by the quasar. The required outflow speed, meanwhile, is a very challenging constraint. Allowing for viewing angle, portions of the outflow would need speeds of greater than 1000 km s^{-1} . This surpasses the speed of outflows generally observed in star-forming galaxies (Pettini et al. 2001; Martin 2005). Finally, theoretical treatments of galactic outflows suggest these will not extend to this large distance in halos with masses characteristics of $z > 2$ quasar host galaxies (Furlanetto & Loeb 2001; Aguirre et al. 2001), but of course this depends on the assumed energetics of the flow.

In what follows we will use the observed properties of SLLS/SDSSJ1204+0221BG to estimate, in an order of magnitude sense, the energetics of the presumed outflow, under the assumption that we have detected cold swept up material. We then consider if an outflow with these energetics could be plausibly produced by a starburst or AGN.

The mass of a shell of material at radius r_w , with column density N_w , and covering solid angle Ω is $M_w = m_p N_H \Omega r_w^2$. If this shell is outflowing at velocity v_w in a wind, the mass outflow rate is $\dot{M}_w \sim M_w v_w / r_w$. For our fiducial values and $\Omega = 2\pi$, we derive $M_w \sim 3 \times 10^{11} M_\odot$ and $\dot{M}_w \sim 3000 M_\odot \text{ yr}^{-1}$. Note that we have taken the outflow velocity to be $v_w = 1000 \text{ km s}^{-1}$ because

SLLS/SDSSJ1204+0221BG shows velocity separations as large as $\simeq 700 \text{ km s}^{-1}$ from the f/g quasar, but this represents only the radial component of the velocity vector. The corresponding energy, power, and momentum deposition rate of the wind, are $E_w \sim 1/2 M_w v_w^2$, $\dot{E}_w \sim 1/2 \dot{M}_w v_w^2$, and $\dot{P}_w \sim \dot{M}_w v_w$, respectively. With our fiducial values, these are $E_w \sim 3 \times 10^{60} \text{ erg}$, $\dot{E}_w \sim 9 \times 10^{44} \text{ erg s}^{-1}$, and $\dot{P}_w \sim 2 \times 10^{37} \text{ g cm s}^{-2}$.

These crude estimates can be compared with the momentum and energy driven winds of a starburst and/or AGN. Following the formalism presented in Murray et al. (2005), the SN deposition rate for a starburst galaxy with star-formation rate \dot{M}_* is

$\dot{P}_{\text{SN}} \sim 2 \times 10^{33} \dot{M}_* / (M_\odot \text{ yr}^{-1}) \text{ g cm s}^{-2}$. A similar deposition rate is inferred from radiation pressure from assuming the gas is optically thick to absorption by dust grains. We conclude that if the absorption in SLLS/SDSSJ1204+0221BG is from material swept up in a large scale wind, the star formation rate required to power the momentum flow is extremely large $\dot{M}_* \sim 10^4 M_\odot \text{ yr}^{-1}$. Furthermore, this estimate should be considered a lower limit because it assumes all momenta deposited into the galaxy are assumed to add coherently which can significantly overestimate the deposition (Socrates et al. 2006).

The rest-frame near ultraviolet luminosity from such a high star-formation rate can be estimated (Kennicutt 1998), and it is $L_{\text{UV}} \sim 10^{47} \text{ erg s}^{-1}$ — this would outshine the quasar bolometric luminosity $L_{\text{QSO}} \simeq 1.4 \times 10^{46} \text{ erg s}^{-1}$ by an order of magnitude, which can easily be ruled out since a starburst spectrum is not observed in SDSSJ1204+0221FG or detected in the SDSS imaging. While the starburst could be significantly extinguished by dust (this is in fact an implicit assumption), the fact that we observe the f/g quasar unextinguished along our line-of-sight implies that we should have been able to see some evidence for a starburst ten times brighter. Finally, we note that radiation pressure from the quasar radiation is also unable to drive the presumed outflow¹⁷, since $\dot{P}_{\text{QSO}} = L_{\text{QSO}}/c \sim 5 \times 10^{35} \text{ g cm s}^{-2}$, which is a factor of forty lower than our estimate.

Next we consider the wind power, again following the formalism in Murray et al. (2005). For SNe, assuming a rate of one per 100 yr per $1 M_\odot \text{ yr}^{-1}$, the SNe energy can only power the outflow for an extremely large star formation rate: $\dot{M}_* \sim 3 \times 10^4 M_\odot \text{ yr}^{-1}$. We conclude that the kinematics of SLLS/SDSSJ1204+0221BG are not driven by SN winds and consider, instead, the energy from the AGN. The absolute B -band magnitude¹⁸ of SDSSJ1204+0221FG is

¹⁷ Here we are imagining that the quasar, viewed from another direction, emits a similar bolometric luminosity but is obscured by dust grains which absorb momentum.

¹⁸ We compute the cross filter K-correction $K_{B_i}(z)$, between apparent magnitude i and absolute magnitude B , which allows us to

$M_B = -24.8$, which corresponds to a bolometric luminosity of $L_{\text{QSO}} = 1.4 \times 10^{46} \text{ erg s}^{-1}$, where we used the McLure & Dunlop (2004) fit to the Elvis et al. (1994) bolometric correction to determine L_{QSO} from M_B . The ratio of the outflow power to the accretion power is then

$$\dot{E}_w/L_{\text{QSO}} \sim 0.06 \left(\frac{\Omega}{2\pi} \right) \left(\frac{N_{\text{H}}}{10^{20.6} \text{ cm}^{-2}} \right) \left(\frac{R_{\perp}}{108 \text{ kpc}} \right) \left(\frac{v_w}{1000 \text{ km s}^{-1}} \right)^3 \text{ erg.} \quad (25)$$

If indeed the AGN is powering an outflow, then $\sim 6\%$ of the accretion power has been coupled to the host via a large scale wind. A similar comparison can be made between the energy of the outflow, which is $E_w \sim 4 \times 10^{60} \text{ erg}$ and the rest-mass energy liberated to grow the supermassive black hole $E_{\text{BH}} = \epsilon_{\text{rad}} M_{\text{BH}} c^2$. Assuming an Eddington ratio of $f_{\text{Edd}} \equiv L_{\text{QSO}}/L_{\text{Edd}} = 0.1$, consistent with recent estimates for a quasar at $z \sim 2.5$ near the luminosity of SDSSJ1204+0221FG (Kollmeier et al. 2006; Shen et al. 2007a), we deduce a black hole mass of $M_{\text{BH}} = 1.1 \times 10^9 \left(\frac{f_{\text{Edd}}}{0.1} \right)^{-1} M_{\odot}$. Thus we can write

$$E_w/E_{\text{BH}} \sim 0.01 \left(\frac{f_{\text{Edd}}}{0.1} \right) \left(\frac{\epsilon_{\text{rad}}}{0.1} \right)^{-1}. \quad (26)$$

To summarize, if the H I and metal line absorption in SLLS/SDSSJ1204+0221BG is from material swept up in a large scale outflow, then the energetics are extreme. Starburst feedback is highly unlikely unless we are willing to consider unprecedented star-formation rates $\dot{M}_* \gtrsim 10^4 M_{\odot} \text{ yr}^{-1}$. Radiation pressure feedback from the quasar cannot drive the outflow even if all of the bolometric luminosity were absorbed by dust grains. Although large, the implied power of the presumed outflow is only a few percent of the bolometric luminosity of the f/g quasar, or similarly, its energy is of order a percent of the radiated rest-mass energy required to grow a $\sim 10^9 M_{\odot}$ black hole. It is intriguing that the we are led to deduce a few percent coupling between the black hole accretion and the host galaxy. This is very similar to the coupling factors used in simulations of quasar feedback. For instance Springel et al. (2005a) must inject a fraction $\eta = 0.05$ of the accreted energy into the host galaxy to reproduce the observed $M_{\text{BH}} - \sigma$ correlation, where η is defined by $E_{\text{feedback}} = \eta \epsilon_{\text{rad}} M_{\text{BH}} c^2$ (see also Granato et al. 2004). However, if such a large amount of energy is being deposited in the host galaxy, radiative losses from the wind could be significant, which we have not considered. Thus, in effect, our estimate of the coupling factor is a lower limit.

Finally, it is worth noting that high speed outflows of cold gas have been identified in a small sample of post-starburst galaxies at $z \sim 0.5$ (Tremonti et al. 2007). In several cases the wind speeds exceed 1000 km s^{-1} and the authors also argue that the energetics may require prior quasar activity. Similarly, the high speeds of narrow associated absorption lines (NAALs) detected in quasars are also suggestive of fast outflows (D’Odorico et al. 2004; Wild et al. 2008). However the mass and energetics of these outflows, detected along the line-of-sight to background sources, cannot be reliably estimated because of the highly uncertain column density of the absorbers and the unknown distance to the absorbing gas.

6. SUMMARY

In this paper, we introduced a novel technique to study the physical state of gas in the halos of luminous quasars, which has the potential to provide powerful constraints on the physical processes governing the formation of massive galaxies. By mining the sky for very rare close associations of quasars (Hennawi 2004; Hennawi et al. 2006b,a), we previously discovered SDSSJ1204+0221, a close projected quasar pair with angular separation $\theta = 13.3''$ corresponding to $R_{\perp} = 108 \text{ kpc}$ at the redshift of the foreground quasar $z_{\text{fg}} = 2.4360 \pm 0.0005$, precisely determined from Gemini/GNIRS near-IR spectroscopy. The spectral and photometric properties of SDSSJ1204+0221FG make it an unremarkable quasar at $z \sim 2.4$. It has an SDSS i -band magnitude of $i = 20.5$, from which we estimate a bolometric luminosity of $L_{\text{QSO}} \simeq 1.4 \times 10^{46} \text{ erg s}^{-1}$, corresponding to a supermassive black hole mass $M_{\text{BH}} \simeq 1.1 \times 10^9 \left(\frac{f_{\text{Edd}}}{0.1} \right)^{-1} M_{\odot}$, if the black hole accretes at one tenth of the Eddington limit. The luminosity of SDSSJ1204+0221FG places it near the ‘knee’ of the $z \sim 2.5$ quasar luminosity function (Croom et al. 2004; Richards et al. 2006), and the clustering of such quasars indicates they inhabit massive dark halos $M \sim 10^{13.3} M_{\odot}$ (Croom et al. 2001; Porciani et al. 2004; Croom et al. 2005), making them the progenitors of massive red-and-dead galaxies observed today. Our impact parameter R_{\perp} easily resolves the expected virial radius $r_{\text{vir}} = 250 \text{ kpc} (M/10^{13.3} M_{\odot})^{1/3}$, and pierces the halo of SDSSJ1204+0221FG at about the cooling radius, where gas shock heated to the virial temperature should take about a Hubble time to cool.

Rather, the only remarkable thing about SDSSJ1204+0221FG is that it forms a close projection with a b/g quasar ($z_{\text{bg}} = 2.53$) which is bright enough ($r = 19.0$) for high resolution spectroscopy. Our Keck HIRES Echelle spectrum of SDSSJ1204+0221BG, the first ever to probe the halo gas of a f/g quasar, resolves the velocity fields of the absorbing gas and allows us to measure precise column densities for H I and the ionic transitions of metals like Si, C, N, O, and Fe. These measurements allow us to place constraints on the physical state of the gas near the f/g quasar, such as its kinematics, temperature, ionization structure, chemical enrichment patterns, volume density, the size of the absorbers, the intensity of the impingent radiation field, as well as test for the presence of hot collisionally ionized gas. We first summarize the results for our single sightline, and then discuss their implications for massive galaxy formation and the quasar phenomenon.

determine M_B from the SDSS i -band photometry.

6.1. Model Independent Constraints

In our Keck/HIRES spectrum of SDSSJ1204+0221BG, we identify a super Lyman limit system (SLLS) with a redshift $z = 2.44$. A Voigt profile fit to the Ly α and Ly β profiles imply a total H I column density $N_{\text{HI}} = 10^{19.65 \pm 0.15} \text{ cm}^{-2}$. The H I absorption occurs redward of z_{fg} , spanning from $\delta v = +50 \text{ km s}^{-1}$ to $+780 \text{ km s}^{-1}$. There is no H I absorption detected ($N_{\text{HI}} < 10^{13.5} \text{ cm}^{-2}$) in the velocity interval $\delta v = -1500 \text{ km s}^{-1}$ to 0 km s^{-1} . We identify a series of metal lines coincident in velocity with the H I absorption (distributed in three primary components) that includes transitions from a range of ionization states of C, O, Fe, Si, Al, and N. We observe an integrated O⁰/H⁰ ratio of $\log[N(\text{O}^0)/N(\text{H}^0)] = -3.9 \text{ dex}$ which indicates a highly enriched gas. Ignoring ionization corrections to this ratio, which should be negligible, the average gas metallicity is $[\text{O}/\text{H}] = -0.5 \text{ dex}$. Both the extreme kinematics and high metallicity of this system are highly uncommon for intervening SLLSs.

The Doppler parameters of the low and intermediate ions are small ($b \lesssim 5 \text{ km s}^{-1}$) indicating a gas temperature $T \simeq 20,000 \text{ K}$. At all velocities we observe an ionic ratio $\text{N}^+/\text{N}^0 > 1$ which implies the gas is predominantly ionized. We observe weak, (if any) C IV, N V, and O VI absorption indicating a modest (or negligible) quantity of metal-enriched gas with $T \approx 10^5$ to 10^6 K in the halo surrounding SDSSJ1204+0221FG.

6.2. Model Dependent Constraints

Under the assumption that the gas is photoionized by a hard radiation field (e.g. the nearby quasar or the EUVB), we estimate an ionization parameter $\log U = -3.0 \pm 0.3$ for the gas. This implies an ionization fraction $x = 0.96$ for the two lower column density components, and $x = 0.2$ for the component with the largest column. The total implied hydrogen column density of the system is $N_{\text{H}} = 10^{20.6} \text{ cm}^{-2}$. Applying ionization corrections to the observed N⁰/O⁰ ratio, we infer solar to super-solar N/O abundances. At high z , such large N/O values are only found in gas associated with quasar environments. At $\delta v \approx +700 \text{ km s}^{-1}$, we detect absorption from the excited fine-structure level of C⁺, C II* 1335. Under the assumptions that electron collisions dominate the C⁺ excitation and that $N(\text{C}^+) = N(\text{Si}^+) + \log(\text{C}/\text{Si})_{\odot}$, we estimate an electron density $n_{\text{e}} = 0.2$ to 10 cm^{-3} . By comparing this volume density to the ionization corrected column density, we determine characteristic sizes $\ell \sim 10$ to 100 pc for the absorbing ‘clouds’.

The properties of the SLLS toward SDSSJ1204+0221BG – $z \approx z_{\text{fg}}$, extreme kinematics, high metallicity, and a solar N/O ratio – argue that this gas is located within the halo of SDSSJ1204+0221FG. There is an additional statistical argument: the strong clustering of optically thick absorbers around $z \sim 2$ quasars (Hennawi & Prochaska 2007) implies the SLLS is likely to lie at a distance near the observed transverse distance (see Figure 6). We summarize in the next subsection several interpretations drawn from associating SLLS/SDSSJ1204+0221BG with the galactic halo of SDSSJ1204+0221FG.

We tested the hypothesis that the SLLS/SDSSJ1204+0221BG is illuminated by ionizing radiation from f/g quasar by comparing the radiation field intensity inferred from analysis of the SLLS against the value expected from SDSSJ1204+0221FG. Adopting the most conservative parameters for the SLLS ($\log U = -3$ and $n_{\text{H}} = 5 \text{ cm}^{-3}$), illumination of the SLLS cannot be ruled out if it is located at $r = R_{\perp} = 108 \text{ kpc}$ from SDSSJ1204+0221FG. Adopting more realistic values ($\log U = -4$ and $n_{\text{H}} < 1 \text{ cm}^{-3}$), we conclude that SLLS/SDSSJ1204+0221BG is not illuminated by SDSSJ1204+0221FG, unless the SLLS is located at an unlikely distance of greater than 500 kpc . We further demonstrated that if a system like SLLS/SDSSJ1204+0221BG were located along the sightline to a bright quasar at $r < 100 \text{ kpc}$, and hence illuminated, then it would exhibit properties characteristic of the narrow associated absorption line (NAAL) systems. This would include strong absorption by high-ion transitions of O VI, N V, and C IV, optically thin H I absorption, and solar chemical abundances. The absence of strong high-ion absorption in this SLLS further suggests it is not illuminated by SDSSJ1204+0221FG and it also indicates that there is not a large reservoir of warm ($T \approx 10^5$ to 10^6 K) gas in the halo surrounding the quasar. We suggest that there may still be a diffuse shock heated medium but that it has a high temperature ($T > 10^6 \text{ K}$), characteristic of the virial temperature of the massive dark matter halo $M \gtrsim 10^{13} M_{\odot}$ expected to be hosting the f/g quasar. If it exists, this material undetectable in absorption with the transitions accessible with our b/g quasar spectrum.

6.3. Interpretation and Outlook

The covering factor of cold $T \sim 10^4 \text{ K}$, neutral, optically thick gas is nearly unity for transverse sightlines to $z \sim 2$ quasars with $R_{\perp} \lesssim 100 \text{ kpc}$ (Hennawi et al. 2006a), although this high column density absorbing gas is rarely observed along the line-of-sight to individual quasars (Russell et al. 2006; Prochaska et al. 2008b). The explanation for this anisotropic absorption is that the transverse direction is much less likely to be illuminated by the f/g quasar ionizing flux, either because of obscuration or intermittent emission (Hennawi et al. 2006a; Hennawi & Prochaska 2007; Prochaska et al. 2008b). Besides this anisotropic absorption pattern, several independent lines of evidence corroborate this picture for the case of SDSSJ1204+0221. First, we modeled the ionization state of SLLS/SDSSJ1204+0221BG which indicates that the gas is unlikely illuminated by SDSSJ1204+0221FG (see § 4.4). Second, we failed to detect high-ion transitions like N V or O VI that should have been seen if the gas were highly ionized by a hard radiation field (see § 4.3). Third, we showed that if gas clouds similar to those in SLLS/SDSSJ1204+0221BG were at a similar distance along the line-of-sight (and hence illuminated), they would explain the population of much more highly ionized associated NAALs, commonly detected in quasar spectra (see § 4.5). Fourth, fluorescent Ly α emission is not observed near R_{\perp} in SDSSJ1204+0221 (Hennawi & Prochaska 2008); whereas the clouds responsible for the high covering factor of optically thick gas (Hennawi et al. 2006a) near quasars (three such clouds were detected in SLLS/SDSSJ1204+0221BG), would be emitting detectable Ly α photons if illuminated (Hennawi & Prochaska 2008).

The upshot of this anisotropic illumination picture is that the b/g quasar sightline probes the physical state of gas near SDSSJ1204+0221FG which is *shadowed and hence unaltered by the intense ionizing radiation emitted by the f/g quasar*.

By combining the statistical covering factor measured by Hennawi & Prochaska (2007) with the total N_{H} column determined for SLLS/SDSSJ1204+0221BG, we argued in § 5.2 that the amount of cold gas at $r \sim 100$ kpc is significant, amounting to $\sim 3\%(\frac{f_g}{\Omega_b/\Omega_m})^{-1}$ of the total expected gas density of the f/g quasar’s dark matter halo, if the gas fraction f_g is equal to the cosmic baryon fraction Ω_b/Ω_m . Similarly, if one assumes the material is distributed in a thin shell of radius R_{\perp} which subtends $\Omega = 2\pi$, the implied gas mass is $M \sim 3 \times 10^{11} M_{\odot}$. Although we have deduced much about the physical state of this cold gas (see Table 4), its origin is still unclear. The biggest clue could lie in its extreme enrichment patterns. The nearly solar metallicity of SLLS/SDSSJ1204+0221BG and its roughly solar N/O relative abundance make it anomalous relative to the population of intervening SLLS and DLAs (see Figure 7). Indeed at $z \sim 2.5$ such high metallicities have only been observed on kpc scales in starburst galaxies (Pettini et al. 2001; Steidel et al. 2003) and solar N/O has only been observed in the broad-line regions of quasars (Dietrich et al. 2003; Arav et al. 2007) or in the NAALs (D’Odorico et al. 2004).

How do we explain the presence of such a large cold gas mass of highly enriched material with a broad-line-region-like enrichment pattern at such a large distance from the quasar $r \sim 100$ kpc? It is tempting (and fashionable) to associate the absorbing material with a large scale outflow or galactic wind. If we are observing dense material swept up by an outflow then the energetics are extreme $\dot{E}_w \sim 10^{45} \text{ erg s}^{-1}$. A starburst cannot drive this wind unless we are willing to consider unprecedented star-formation rates $\dot{M}_* \gtrsim 10^4 M_{\odot} \text{ yr}^{-1}$. Radiation pressure feedback from the quasar cannot drive an outflow with this power even if its bolometric luminosity were completely absorbed by dust grains (along a different direction than our line-of-sight). However, the power of the flow is only a few percent of SDSSJ1204+0221FG’s estimated bolometric luminosity, or similarly, its energy is of order a percent of the radiated rest-mass energy required to grow a $\sim 10^9 M_{\odot}$ black hole. So the feedback hypothesis suggests a coupling between black hole accretion and outflow which is comparable to the value used by simulators to reproduce the supermassive black hole $M_{\text{BH}} - \sigma$ correlation (e.g. Springel et al. 2005a). Furthermore, radiative losses from such an energetic flow could be significant, so our estimate of the coupling factor must be considered a lower limit. If we are in fact observing feedback in SLLS/SDSSJ1204+0221BG, then the kinematics, radial extent, and high metallicity of the emergent outflow bear intriguing similarities to the giant Ly α nebulae observed in high- z radio galaxies. However, it is difficult to explain why such an energetic outflow would result in so little material at intermediate temperature $T \sim 10^{4.5} - 10^6 \text{ K}$, which we would have easily detected (but did not, see § 4.3).

But we may not be observing an outflow at all. The observed kinematics in SLLS/SDSSJ1204+0221BG, although extreme relative to the intervening SLLS population, are consistent with the expected gravitational motions if the f/g quasar is indeed hosted by a massive dark matter halo $M \gtrsim 10^{13} M_{\odot}$, as indicated by the strong clustering of $z \sim 2.5$ quasars (Croom et al. 2001; Porciani et al. 2004; Croom et al. 2005). In this alternative scenario, the absorption is being caused by cold clouds, with sizes $r_{\text{abs}} = 10 - 100$ pc, unit covering factor and implied volume filling factor $C_v \sim 10^{-5} - 10^{-4}$, which are either infalling or virialized in the deep potential well of the massive dark matter halo. We estimated the pressure of these clouds to be $P \sim 10^5 \text{ K cm}^{-3}$, which intriguingly matches the pressure of the $T_{\text{vir}} \sim 10^7 \text{ K}$ shock-heated gas expected to permeate the massive dark matter halo hosting the f/g quasar. This pressure equilibrium is reminiscent of a large class of galaxy formation models that postulate cold $T \sim 10^4 \text{ K}$ clouds pressure confined by a hot shock heated virialized medium (Mo & Miralda-Escude 1996; Maller & Bullock 2004; Dekel & Birnboim 2006), and these scenarios might explain the lack of significant intermediate temperature $T \sim 10^{5-6} \text{ K}$ gas near the f/g quasar. However, if we are indeed detecting pressure confined cold clouds undergoing gravitational motions, why should these clouds have such a high metallicity? This question is all the more puzzling considering that the expected cooling time of the tenuous virialized hot gas would be comparable to the Hubble time at $r \sim 100$ kpc. While it may be more plausible to associate the cold gas and metals with star-forming galaxies clustered around the quasar, they would need to be extremely abundant $n \sim 0.1 \text{ Mpc}^{-3}$ to produce the near unit covering factor of cold gas and metals. These faint $L \sim 10^{-3} L_*$ dwarf galaxies would need to enrich spheres of $r_{\text{abs}} \sim 20$ kpc to solar metallicity, which seems implausible in light of the low metallicities observed in most DLAs (see Figure 7) and the similarly low values seen locally in dwarf galaxies.

With just a single sightline, we cannot distinguish between a quasar powered outflow or cold clouds undergoing gravitational motions. However, similar observations of a statistical sample of projected quasar pairs stand to teach us a tremendous amount about the physics of massive galaxy formation. This is nicely illustrated by the preliminary comparison of the absorption line properties of $z \sim 2.2$ quasars to $z \sim 2.3$ star-forming galaxies presented in Fig 11. The primary motivation for this comparison is that, across the two populations, we are afforded a mass baseline of more than an order of magnitude. The clustering of star-forming galaxies at $z \sim 2$ indicates that they inhabit dark matter halos with $M \lesssim 10^{12} M_{\odot}$, making them the likely progenitors of $\sim L_*$ galaxies that inhabit the “blue-cloud” of the color magnitude diagram today (Conroy et al. 2007); whereas, the stronger clustering of quasars at $z \sim 2$ implies larger halo masses $M \gtrsim 10^{13} M_{\odot}$ (Croom et al. 2001; Porciani et al. 2004; Croom et al. 2005), making them progenitors of massive red-and-dead galaxies on the red sequence. Hence in comparing quasars to star-forming galaxies at $z \sim 2$, *we are effectively comparing the progenitors of quenched galaxies to those of un-quenched galaxies*.

The lower panel of Figure 11 plots the H I column density of absorbers at the f/g quasar (or galaxy) redshift versus the impact parameter to the b/g quasar sightline. The (red) circles are the thirteen f/g quasars ($\langle z_{\text{fg}} \rangle = 2.2$) with a background quasar within $R_{\perp} < 350$ kpc uncovered by Hennawi et al. (2006a), and (blue) squares are seven f/g

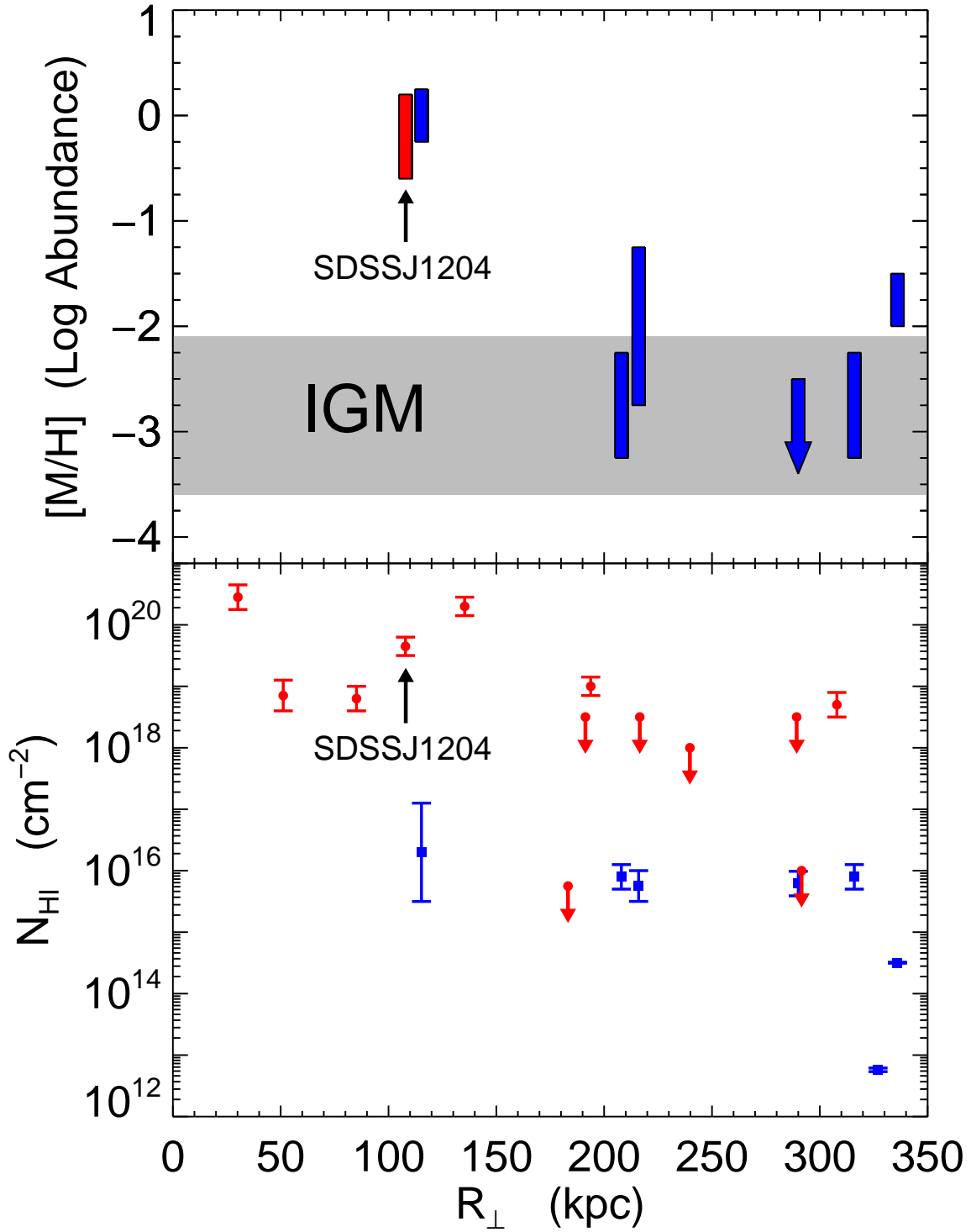


FIG. 11.— Comparison of absorption line properties of $z \sim 2.5$ f/g quasars to $z \sim 2.5$ star forming galaxies. The lower panel plots the H I column density versus impact parameter for absorbers, detected in a b/g quasar spectrum, coincident with the f/g quasar (or galaxy) redshift. The (red) circles are thirteen projected quasar pairs uncovered in Hennawi et al. (2006a) with $R_{\perp} < 350$ kpc, and (blue) squares are seven f/g $z \sim 2.5$ star-forming galaxies studied in absorption against a bright b/g quasar by Simcoe et al. (2006). Downward pointing arrows are upper limits on N_{HI} for the f/g quasars, which reflects our inability to measure reliable column densities below $N_{\text{HI}} \lesssim 18.5$ from the moderate resolution ($\text{FWHM} \sim 125 \text{ km s}^{-1}$) b/g spectra used in Hennawi et al. (2006a). Because the Simcoe et al. (2006) study used a high resolution b/g spectrum they do not suffer from this limitation. The gray shaded region indicates the range of abundances observed in the low density IGM.

star-forming galaxies ($\langle z_{\text{fg}} \rangle = 2.3$) studied in absorption against a bright b/g quasar by Simcoe et al. (2006). The vertical rectangles in the upper panel illustrate the range of metallicities encountered in the individual components of each system at each impact parameter. The only f/g quasar metallicity measured thus far is for SDSSJ1204+0221 (this work), whereas Simcoe et al. (2006) measured metallicities near six f/g galaxies.

Two notable features of Fig 11 warrant further discussion. First, at $R_{\perp} \simeq 100$ kpc, one galaxy and one quasar metallicity have been measured, and both indicate abundances near solar. Simcoe et al. (2006) attributed the high metallicity of their smallest impact parameter system (MD103) to galaxy formation feedback, and we similarly cited the high metallicity of SDSSJ1204+0221 as the most compelling argument for an outflow powered by the quasar. By mapping out the run of abundance with impact parameter in this plot, one could characterize the size of the enriched regions around protogalaxies with a significant mass lever-arm. If feedback is responsible for the metals at large impact parameters, measuring the abundance-impact parameter relation would constrain the energetics and transport processes characterizing the relevant feedback mechanism. Furthermore, this measurement would be fundamental to any discussion of the enrichment history of the IGM and the ICM.

The second noteworthy feature of Figure 11 is that on small scales the f/g quasars appear to have N_{HI} column densities significantly larger than the f/g galaxies. This comparison is complicated by the fact that the dark matter halos that host the quasars are expected to be larger and more massive than those hosting the galaxies. For reference, Conroy et al. (2007) estimated that the average halo mass of $z \sim 2$ star-forming galaxies to be $M = 10^{12} M_{\odot}$, which implies a virial radius $r_{\text{vir}} = 89$ kpc; whereas, at $z \sim 2.4$ we are using $M = 10^{13.3} M_{\odot}$ implying $r_{\text{vir}} = 250$ kpc (Porciani et al. 2004). At an impact parameter of $R_{\perp} = 100$ kpc, the ratio of the total hydrogen column densities of these dark matter halos is $N_{\text{H}}^{\text{QSO}}/N_{\text{H}}^{\text{gal}} = 5$, whereas the quasars in Fig 11 have H I column densities a factor $\gtrsim 100$ times larger than the galaxies for $R_{\perp} \lesssim 200$ kpc. Although we caution that the statistics in the lower panel of Figure 11 are still very poor, it is nevertheless interesting to speculate about the implications of this tentative result. Why would the quasars have a much larger reservoir of cold gas at $R_{\perp} \sim 100$ kpc, of order a few percent of the total expected gas density (see § 5.2), than star-forming galaxies? Can this difference be attributed to a distinct feedback mechanism operating in quasars that does not occur in star-forming galaxies? If instead the absorbers at $R_{\perp} \sim 100$ kpc arise from cold gas accretion rather than outflows, then the larger relative density of cold gas around quasars is particularly puzzling. Cosmological hydrodynamical simulations predict the opposite trend with dark halo mass: cold accretion accounts for a smaller fraction of the total accreted gas in higher mass halos where shocks become stable throughout the halo and the cold filamentary mode of accretion disappears (Kereš et al. 2005; Dekel & Birnboim 2006; Ocvirk et al. 2008). Whether the cold gas around quasars is ejected by feedback or accreted in gravitational collapse, what is the ultimate fate of this material? Does it eventually fall back onto the quasar host galaxy or do the gas and metals blend into the IGM. Do we expect to observe a similar cold halo of gas around nearby massive elliptical galaxies, since their progenitors are $z \sim 2$ quasars like SDSSJ1204+0221FG?

Although preliminary, the putative trends in Figure 11 provoke fundamental questions about feedback, quenching and the physics of massive galaxy formation. Yet this discussion represents just two measurements (metallicity and N_{HI}) gleaned from our analysis of the spectrum of SDSSJ1204+0221BG. Other properties of the gas such as its kinematics, temperature, ionization structure, relative abundance patterns, the presence or absence of a hot collisionally ionized phase, and the volume density and size of the clouds, have a similar potential to constrain the physics of massive galaxy formation if they can be mapped out for statistical samples. Such a statistical analysis is well within reach. To date, our pair confirmation program (Hennawi 2004; Hennawi et al. 2006b,a) has confirmed about 90 pairs of quasars with impact parameter $R < 300$ kpc and $z_{\text{fg}} > 1.6$, and about a comparable number still remain to be discovered in the existing SDSS photometric data. Of the known pairs, only about five are bright enough $r \lesssim 19$ for high resolution (FWHM ~ 10 km s $^{-1}$) echelle spectroscopy like the HIRES spectrum used to study SLLS/SDSSJ1204+0221BG. However, higher throughput but lower resolution echellette spectrographs, such as the Echellette Spectrograph and Imager (ESI, Sheinis et al. 2002) on Keck II, the Magellan Echellette (MagE) on the Magellan Clay Telescope, or the planned X-Shooter spectrograph (D’Odorico et al. 2006) for the VLT, can deliver spectra with FWHM $\sim 30 - 50$ km s $^{-1}$ and the required signal to noise ratio (~ 10 per resolution element), in 1-2 hours for $r \lesssim 21.5$, which would make *all* of the quasar pairs known observable. Although these instruments have lower spectral resolution, they roughly resolve the H I Lyman series affording precise estimates of N_{HI} . Furthermore, such data would yield metallicity and relative abundance estimates to a precision of 0.3 dex, and would allow for the construction of photoionization models with an accuracy comparable to that achieved in this work.

The most important aspect of the approach taken to understanding galaxy formation in this study and Simcoe et al. (2006) (see also Adelberger et al. 2003), is that they provide the first observational constraints on the physical state of the *gas* on scales \gtrsim kpc in high- z protogalaxies. Although the ideas behind quenching and feedback were introduced to explain the observed properties of local galaxy stellar populations, such as the bimodality in the color magnitude diagram (Strateva et al. 2001; Baldry et al. 2004; Bell et al. 2004; Blanton et al. 2005; Faber et al. 2007) and the sharp cutoff in the luminosity function (Benson et al. 2003), these are fundamentally gas dynamics problems. Many of the relevant hydrodynamical and physical processes can be (or are nearly) resolved by simulation grids with current technology. Conversely, predicting how this gas physics manifests itself in the stellar populations of local or high- z galaxies requires that the uncertain “sub-grid” physics of star formation be inserted by hand, or with the aid of semi-analytical recipes. Thus, observational constraints on the gas provide especially fruitful comparisons to theory. If the techniques presented here for a single object can be expanded to statistical samples, that will constitute a significant step on the road toward understanding massive galaxy formation.

We acknowledge helpful discussions with T.J. Cox, P. Hopkins, P. Madau, B. Mathews, E. Ramirez-Ruiz, R. Simcoe, and A. Wolfe. We are grateful to R. Simcoe for kindly providing the galaxy data in Figure 11 in electronic form. For part of this work JFH was supported by NASA through Hubble Fellowship grant # 01172.01-A awarded by the Space Telescope Science Institute, which is operated by the Association of Universities for Research in Astronomy, Inc., for NASA, under contract NAS 5-26555. JXP acknowledges funding through an NSF CAREER grant (AST-0548180) and NSF grant (AST-0709235). JFH is currently supported by the National Science Foundation through the Astronomy and Astrophysics Postdoctoral Fellowship program (AST-0702879).

The conclusions of this work are partly based on observations obtained at the Gemini Observatory through Gemini Program ID GS-2006A-Q-3. Gemini Observatory is operated by the Association of Universities for Research in Astronomy (AURA) under a cooperative agreement with the NSF on behalf of the Gemini partnership: the National Science Foundation (United States), the Science and Technology Facilities Council (United Kingdom), the National Research Council (Canada), CONICYT (Chile), the Australian Research Council (Australia), CNPq (Brazil) and CONICET (Argentina).

The conclusions of this work are based on data collected from observatories at the summit of Mauna Kea. The authors wish to recognize and acknowledge the very significant cultural role and reverence that the summit of Mauna Kea has always had within the indigenous Hawaiian community. We are most fortunate to have the opportunity to conduct observations from this mountain.

REFERENCES

- Adelberger, K. L., & Steidel, C. C. 2005, *ApJ*, 627, L1
 Adelberger, K. L., Steidel, C. C., Kollmeier, J. A., & Reddy, N. A. 2006, *ApJ*, 637, 74
 Adelberger, K. L., Steidel, C. C., Shapley, A. E., Hunt, M. P., Erb, D. K., Reddy, N. A., & Pettini, M. 2004, *ApJ*, 607, 226
 Adelberger, K. L., Steidel, C. C., Shapley, A. E., & Pettini, M. 2003, *ApJ*, 584, 45
 Aguirre, A., Hernquist, L., Schaye, J., Weinberg, D. H., Katz, N., & Gardner, J. 2001, *ApJ*, 560, 599
 Arav, N., Gabel, J. R., Korista, K. T., Kaastra, J. S., Kriss, G. A., Behar, E., Costantini, E., Gaskell, C. M., Laor, A., Kodituwakku, C. N., Proga, D., Sako, M., Scott, J. E., & Steenbrugge, K. C. 2007, *ApJ*, 658, 829
 Bajtlik, S., Duncan, R. C., & Ostriker, J. P. 1988, *ApJ*, 327, 570
 Baldry, I. K., Glazebrook, K., Brinkmann, J., Ivezić, Z., Lupton, R. H., Nichol, R. C., & Szalay, A. S. 2004, *ApJ*, 600, 681
 Begelman, M. C., & Cioffi, D. F. 1989, *ApJ*, 345, L21
 Bell, E. F., Wolf, C., Meisenheimer, K., Rix, H.-W., Borch, A., Dye, S., Kleinheinrich, M., Wisotzki, L., & McIntosh, D. H. 2004, *ApJ*, 608, 752
 Benson, A. J., Bower, R. G., Frenk, C. S., Lacey, C. G., Baugh, C. M., & Cole, S. 2003, *ApJ*, 599, 38
 Bernstein, R., Burles, S. M., & Prochaska, J. 2008, In prep
 Blanton, M. R., Eisenstein, D., Hogg, D. W., Schlegel, D. J., & Brinkmann, J. 2005, *ApJ*, 629, 143
 Boroson, T. 2005, *AJ*, 130, 381
 Bowen, D. V., Hennawi, J. F., Ménard, B., Chelouche, D., Inada, N., Oguri, M., Richards, G. T., Strauss, M. A., Vanden Berk, D. E., & York, D. G. 2006, *ApJ*, 645, L105
 Bower, R. G., Lucey, J. R., & Ellis, R. S. 1992, *MNRAS*, 254, 601
 Calura, F., Matteucci, F., & Vladilo, G. 2003, *MNRAS*, 340, 59
 Cao, X. 2005, *ApJ*, 631, L101
 Chelouche, D., Ménard, B., Bowen, D. V., & Gnat, O. 2007, *ArXiv e-prints*, 706
 Chen, H.-W., Lanzetta, K. M., & Webb, J. K. 2001, *ApJ*, 556, 158
 Coil, A. L., Hennawi, J. F., Newman, J. A., Cooper, M. C., & Davis, M. 2007, *ApJ*, 654, 115
 Conroy, C., Shapley, A. E., Tinker, J. L., Santos, M. R., & Lemson, G. 2007, *ArXiv e-prints*, 711
 Cox, T. J., Di Matteo, T., Hernquist, L., Hopkins, P. F., Robertson, B., & Springel, V. 2006, *ApJ*, 643, 692
 Croft, R. A. C. 2004, *ApJ*, 610, 642
 Croom, S. M., Boyle, B. J., Shanks, T., Smith, R. J., Miller, L., Outram, P. J., Loaring, N. S., Hoyle, F., & da Ângela, J. 2005, *MNRAS*, 356, 415
 Croom, S. M., Shanks, T., Boyle, B. J., Smith, R. J., Miller, L., Loaring, N. S., & Hoyle, F. 2001, *MNRAS*, 325, 483
 Croom, S. M., Smith, R. J., Boyle, B. J., Shanks, T., Miller, L., Outram, P. J., & Loaring, N. S. 2004, *MNRAS*, 349, 1397
 Crotts, A. P. S. 1989, *ApJ*, 336, 550
 de Kool, M., Arav, N., Becker, R. H., Gregg, M. D., White, R. L., Laurent-Muehleisen, S. A., Price, T., & Korista, K. T. 2001, *ApJ*, 548, 609
 Dekel, A., & Birnboim, Y. 2006, *MNRAS*, 368, 2
 —. 2008, *MNRAS*, 383, 119
 Dietrich, M., Hamann, F., Shields, J. C., Constantin, A., Heidt, J., Jäger, K., Vestergaard, M., & Wagner, S. J. 2003, *ApJ*, 589, 722
 Dobrzycki, A., & Bechtold, J. 1991, *ApJ*, 377, L69
 D’Oroico, S., Dekker, H., Mazzoleni, R., Vernet, J., Guinouard, I., Groot, P., Hammer, F., Rasmussen, P. K., Kaper, L., Navarro, R., Pallavicini, R., Peroux, C., & Zerbi, F. M. 2006, in Presented at the Society of Photo-Optical Instrumentation Engineers (SPIE) Conference, Vol. 6269, Ground-based and Airborne Instrumentation for Astronomy. Edited by McLean, Ian S.; Iye, Masanori. Proceedings of the SPIE, Volume 6269, pp. 626933 (2006).
 D’Oroico, V., Cristiani, S., Romano, D., Granato, G. L., & Danese, L. 2004, *MNRAS*, 351, 976
 Dunkley, J., Komatsu, E., Nolte, M. R., Spergel, D. N., Larson, D., Hinshaw, G., Page, L., Bennett, C. L., Gold, B., Jarosik, N., Weiland, J. L., Halpern, M., Hill, R. S., Kogut, A., Limon, M., Meyer, S. S., Tucker, G. S., Wollack, E., & Wright, E. L. 2008, *ArXiv e-prints*, 803
 Elias, J. H., Joyce, R. R., Liang, M., Muller, G. P., Hileman, E. A., & George, J. R. 2006, in Presented at the Society of Photo-Optical Instrumentation Engineers (SPIE) Conference, Vol. 6269, Ground-based and Airborne Instrumentation for Astronomy. Edited by McLean, Ian S.; Iye, Masanori. Proceedings of the SPIE, Volume 6269, pp. 62694C (2006).
 Elvis, M. 2000, *ApJ*, 545, 63
 Elvis, M., Risaliti, G., & Zamorani, G. 2002, *ApJ*, 565, L75
 Elvis, M., Wilkes, B. J., McDowell, J. C., Green, R. F., Bechtold, J., Willner, S. P., Oey, M. S., Polonski, E., & Cutri, R. 1994, *ApJS*, 95, 1
 Faber, S. M., Willmer, C. N. A., Wolf, C., Koo, D. C., Weiner, B. J., Newman, J. A., Im, M., Coil, A. L., Conroy, C., Cooper, M. C., Davis, M., Finkbeiner, D. P., Gerke, B. F., Gebhardt, K., Groth, E. J., Guhathakurta, P., Harker, J., Kaiser, N., Kassin, S., Kleinheinrich, M., Konidaris, N. P., Kron, R. G., Lin, L., Luppino, G., Madgwick, D. S., Meisenheimer, K., Noeske, K. G., Phillips, A. C., Sarajedini, V. L., Schiavon, R. P., Simard, L., Szalay, A. S., Vogt, N. P., & Yan, R. 2007, *ApJ*, 665, 265
 Fabian, A. C., & Iwasawa, K. 1999, *MNRAS*, 303, L34
 Fall, S. M., & Rees, M. J. 1985, *ApJ*, 298, 18
 Ferland, G. J., Korista, K. T., Verner, D. A., Ferguson, J. W., Kingdon, J. B., & Verner, E. M. 1998, *PASP*, 110, 761
 Fernandez-Soto, A., Barcons, X., Carballo, R., & Webb, J. K. 1995, *MNRAS*, 277, 235
 Ferrarese, L., & Merritt, D. 2000, *ApJ*, 539, L9
 Field, G. B. 1965, *ApJ*, 142, 531
 Fox, A. J., Bergeron, J., & Petitjean, P. 2008, *MNRAS*, 388, 1557
 Fox, A. J., Petitjean, P., Ledoux, C., & Srianand, R. 2007, *A&A*, 465, 171
 Furlanetto, S. R., & Loeb, A. 2001, *ApJ*, 556, 619
 Gaskell, C. M. 1982, *ApJ*, 263, 79

- Gebhardt, K., Bender, R., Bower, G., Dressler, A., Faber, S. M., Filippenko, A. V., Green, R., Grillmair, C., Ho, L. C., Kormendy, J., Lauer, T. R., Magorrian, J., Pinkney, J., Richstone, D., & Tremaine, S. 2000, *ApJ*, 539, L13
- Goncalves, T. S., Steidel, C. C., & Pettini, M. 2007, *ArXiv e-prints*, 711
- Granato, G. L., De Zotti, G., Silva, L., Bressan, A., & Danese, L. 2004, *ApJ*, 600, 580
- Graves, G. J., Faber, S. M., Schiavon, R. P., & Yan, R. 2007, *ApJ*, 671, 243
- Grevesse, N., Asplund, M., & Sauval, A. J. 2007, *Space Science Reviews*, 130, 105
- Gunn, J. E., & Peterson, B. A. 1965, *ApJ*, 142, 1633
- Haardt, F., & Madau, P. 1996, *ApJ*, 461, 20
- Hamann, F., & Ferland, G. 1999, *ARA&A*, 37, 487
- Helly, J. C., Cole, S., Frenk, C. S., Baugh, C. M., Benson, A., Lacey, C., & Pearce, F. R. 2003, *MNRAS*, 338, 913
- Hennawi, J. F. 2004, Ph.D. Thesis
- Hennawi, J. F., & Prochaska, J. X. 2007, *ApJ*, 655, 735
- . 2008, *ArXiv Astrophysics e-prints*
- Hennawi, J. F., Prochaska, J. X., Burles, S., Strauss, M. A., Richards, G. T., Schlegel, D. J., Fan, X., Schneider, D. P., Zakamska, N. L., Oguri, M., Gunn, J. E., Lupton, R. H., & Brinkmann, J. 2006a, *ApJ*, 651, 61
- Hennawi, J. F., Strauss, M. A., Oguri, M., Inada, N., Richards, G. T., Pindor, B., Schneider, D. P., Becker, R. H., Gregg, M. D., Hall, P. B., Johnston, D. E., Fan, X., Burles, S., Schlegel, D. J., Gunn, J. E., Lupton, R. H., Bahcall, N. A., Brunner, R. J., & Brinkmann, J. 2006b, *AJ*, 131, 1
- Henry, R. B. C., Edmunds, M. G., & Köppen, J. 2000, *ApJ*, 541, 660
- Henry, R. B. C., & Prochaska, J. X. 2007, *PASP*, 119, 962
- Hopkins, P. F., Bundy, K., Hernquist, L., & Ellis, R. S. 2007a, *ApJ*, 659, 976
- Hopkins, P. F., Cox, T. J., Kereš, D., & Hernquist, L. 2008, *ApJS*, 175, 390
- Hopkins, P. F., Hernquist, L., Cox, T. J., & Keres, D. 2007b, *ArXiv e-prints*, 706
- Hopkins, P. F., Richards, G. T., & Hernquist, L. 2007c, *ApJ*, 654, 731
- Humphrey, A., Villar-Martín, M., Vernet, J., Fosbury, R., di Serego Alighieri, S., & Binette, L. 2008, *MNRAS*, 383, 11
- Kacprzak, G. G., Churchill, C. W., Steidel, C. C., Ceverino, D., Klypin, A. A., & Murphy, M. T. 2007, *ArXiv e-prints*, 710
- Katz, N. 1992, *ApJ*, 391, 502
- Kauffmann, G., & Haehnelt, M. 2000, *MNRAS*, 311, 576
- Kaufmann, T., Mayer, L., Wadsley, J., Stadel, J., & Moore, B. 2006, *MNRAS*, 370, 1612
- Kawata, D., & Gibson, B. K. 2005, *MNRAS*, 358, L16
- Kennicutt, Jr., R. C. 1998, *ARA&A*, 36, 189
- Kereš, D., Katz, N., Weinberg, D. H., & Davé, R. 2005, *MNRAS*, 363, 2
- Kollmeier, J. A., Onken, C. A., Kochanek, C. S., Gould, A., Weinberg, D. H., Dietrich, M., Cool, R., Dey, A., Eisenstein, D. J., Jannuzi, B. T., Le Floc'h, E., & Stern, D. 2006, *ApJ*, 648, 128
- Kormendy, J., & Richstone, D. 1995, *ARA&A*, 33, 581
- Liske, J., & Williger, G. M. 2001, *MNRAS*, 328, 653
- Lu, Y., & Mo, H. J. 2007, *MNRAS*, 377, 617
- Magorrian, J., Tremaine, S., Richstone, D., Bender, R., Bower, G., Dressler, A., Faber, S. M., Gebhardt, K., Green, R., Grillmair, C., Kormendy, J., & Lauer, T. 1998, *AJ*, 115, 2285
- Malagoli, A., Rosner, R., & Fryxell, B. 1990, *MNRAS*, 247, 367
- Maller, A. H., & Bullock, J. S. 2004, *MNRAS*, 355, 694
- Maller, A. H., Prochaska, J. X., Somerville, R. S., & Primack, J. R. 2003, *MNRAS*, 343, 268
- Martin, C. L. 2005, *ApJ*, 621, 227
- Matteucci, F. 1994, *A&A*, 288, 57
- Matteucci, F., & Padovani, P. 1993, *ApJ*, 419, 485
- McCarthy, P. J. 1993, *ARA&A*, 31, 639
- McLure, R. J., & Dunlop, J. S. 2004, *MNRAS*, 352, 1390
- McWilliam, A. 1997, *ARA&A*, 35, 503
- Menci, N., Fontana, A., Giallongo, E., Grazian, A., & Salimbeni, S. 2006, *ApJ*, 647, 753
- Miley, G. 1980, *ARA&A*, 18, 165
- Miley, G., & De Breuck, C. 2008, *A&A Rev.*, 1
- Mo, H. J., & Miralda-Escude, J. 1996, *ApJ*, 469, 589
- Murray, N., Quataert, E., & Thompson, T. A. 2005, *ApJ*, 618, 569
- Murray, S. D., & Lin, D. N. C. 1990, *ApJ*, 363, 50
- Myers, A. D., Brunner, R. J., Nichol, R. C., Richards, G. T., Schneider, D. P., & Bahcall, N. A. 2007a, *ApJ*, 658, 85
- Myers, A. D., Brunner, R. J., Richards, G. T., Nichol, R. C., Schneider, D. P., & Bahcall, N. A. 2007b, *ApJ*, 658, 99
- Myers, A. D., Richards, G. T., Brunner, R. J., Schneider, D. P., Strand, N. E., Hall, P. B., Blomquist, J. A., & York, D. G. 2008, *ApJ*, 678, 635
- Navarro, J. F., Frenk, C. S., & White, S. D. M. 1997, *ApJ*, 490, 493
- Nesvadba, N. P. H., Lehnert, M. D., Eisenhauer, F., Gilbert, A., Tecza, M., & Abuter, R. 2006, *ApJ*, 650, 693
- Ocvirk, P., Pichon, C., & Teyssier, R. 2008, *ArXiv e-prints*, 803
- Osterbrock, D. E., & Ferland, G. J. 2006, *Astrophysics of gaseous nebulae and active galactic nuclei* (Astrophysics of gaseous nebulae and active galactic nuclei, 2nd. ed. by D.E. Osterbrock and G.J. Ferland. Sausalito, CA: University Science Books, 2006)
- Péroux, C., Dessauges-Zavadsky, M., D'Odorico, S., Kim, T.-S., & McMahon, R. G. 2003, *MNRAS*, 345, 480
- . 2007, *MNRAS*, 382, 177
- Péroux, C., Dessauges-Zavadsky, M., Kim, T., McMahon, R. G., & D'Odorico, S. 2002, *Ap&SS*, 281, 543
- Péroux, C., Kulkarni, V. P., Meiring, J., Ferlet, R., Khare, P., Lauroesch, J. T., Vladilo, G., & York, D. G. 2006, *A&A*, 450, 53
- Pettini, M., Rix, S. A., Steidel, C. C., Adelberger, K. L., Hunt, M. P., & Shapley, A. E. 2002, *ApJ*, 569, 742
- Pettini, M., Shapley, A. E., Steidel, C. C., Cuby, J.-G., Dickinson, M., Moorwood, A. F. M., Adelberger, K. L., & Giallisco, M. 2001, *ApJ*, 554, 981
- Porciani, C., Magliocchetti, M., & Norberg, P. 2004, *MNRAS*, 355, 1010
- Prochaska, J. X. 1999, *ApJ*, 511, L71
- Prochaska, J. X., Chen, H.-W., Wolfe, A. M., Dessauges-Zavadsky, M., & Bloom, J. S. 2008a, *ApJ*, 672, 59
- Prochaska, J. X., Gawiser, E., Wolfe, A. M., Castro, S., & Djorgovski, S. G. 2003, *ApJ*, 595, L9
- Prochaska, J. X., Hennawi, J. F., & Herbert-Fort, S. 2008b, *ApJ*, 675, 1002
- Prochaska, J. X., O'Meara, J. M., Herbert-Fort, S., Burles, S., Prochter, G. E., & Bernstein, R. A. 2006, *ApJ*, 648, L97
- Prochaska, J. X., & Wolfe, A. M. 1997, *ApJ*, 487, 73
- . 2001, *ApJ*, 560, L33
- Prochaska, J. X., Wolfe, A. M., Howk, J. C., Gawiser, E., Burles, S. M., & Cooke, J. 2007, *ApJS*, 171, 29
- Prochter, G., Prochaska, J., Burles, S., & Bernstein, R. A. 2008, *In prep*
- Prochter, G. E., Prochaska, J. X., & Burles, S. M. 2006, *ApJ*, 639, 766
- Putman, M. E., de Heij, V., Staveley-Smith, L., Braun, R., Freeman, K. C., Gibson, B. K., Burton, W. B., Barnes, D. G., Banks, G. D., Bhathal, R., de Blok, W. J. G., Boyce, P. J., Disney, M. J., Drinkwater, M. J., Ekers, R. D., Henning, P. A., Jerjen, H., Kilborn, V. A., Knezek, P. M., Koribalski, B., Malin, D. F., Marquarding, M., Minchin, R. F., Mould, J. R., Oosterloo, T., Price, R. M., Ryder, S. D., Sadler, E. M., Stewart, I., Stootman, F., Webster, R. L., & Wright, A. E. 2002, *AJ*, 123, 873
- Reddy, N. A., Steidel, C. C., Pettini, M., Adelberger, K. L., Shapley, A. E., Erb, D. K., & Dickinson, M. 2007, *ArXiv e-prints*, 706
- Rees, M. J., & Ostriker, J. P. 1977, *MNRAS*, 179, 541
- Reuland, M., van Breugel, W., de Vries, W., Dopita, M. A., Dey, A., Miley, G., Röttgering, H., Venemans, B., Stanford, S. A., Lacy, M., Spinrad, H., Dawson, S., Stern, D., & Bunker, A. 2007, *AJ*, 133, 2607
- Richards, G. T., Strauss, M. A., Fan, X., Hall, P. B., Jester, S., Schneider, D. P., Vanden Berk, D. E., Stoughton, C., Anderson, S. F., Brunner, R. J., Gray, J., Gunn, J. E., Ivezić, Ž., Kirkland, M. K., Knapp, G. R., Loveday, J., Meiksin, A., Pope, A., Szalay, A. S., Thakar, A. R., Yanny, B., York, D. G., Barentine, J. C., Brewington, H. J., Brinkmann, J., Fukugita, M., Harvanek, M., Kent, S. M., Kleinman, S. J., Krzesiński, J., Long, D. C., Lupton, R. H., Nash, T., Neilsen, Jr., E. H., Nitta, A., Schlegel, D. J., & Snedden, S. A. 2006, *AJ*, 131, 2766
- Richards, G. T., Vanden Berk, D. E., Reichard, T. A., Hall, P. B., Schneider, D. P., SubbaRao, M., Thakar, A. R., & York, D. G. 2002, *AJ*, 124, 1

- Rix, S. A., Pettini, M., Steidel, C. C., Reddy, N. A., Adelberger, K. L., Erb, D. K., & Shapley, A. E. 2007, *ApJ*, 670, 15
- Romano, D., Silva, L., Matteucci, F., & Danese, L. 2002, *MNRAS*, 334, 444
- Russell, D. M., Ellison, S. L., & Benn, C. R. 2006, *MNRAS*, 367, 412
- Savage, B. D., & Sembach, K. R. 1991, *ApJ*, 379, 245
- . 1996, *ARA&A*, 34, 279
- Scannapieco, E., & Oh, S. P. 2004, *ApJ*, 608, 62
- Scannapieco, E., Silk, J., & Bouwens, R. 2005, *ApJ*, 635, L13
- Schirber, M., Miralda-Escudé, J., & McDonald, P. 2004, *ApJ*, 610, 105
- Scott, J., Bechtold, J., Dobrzycki, A., & Kulkarni, V. P. 2000, *ApJS*, 130, 67
- Sembach, K. R., Wakker, B. P., Savage, B. D., Richter, P., Meade, M., Shull, J. M., Jenkins, E. B., Sonneborn, G., & Moos, H. W. 2003, *ApJS*, 146, 165
- Shankar, F., Weinberg, D. H., & Miralda-Escudé, J. 2002, *ArXiv e-prints*, 578, 33
- Sheinis, A. I., Bolte, M., Epps, H. W., Kibrick, R. I., Miller, J. S., Radovan, M. V., Bigelow, B. C., & Sutin, B. M. 2002, *PASP*, 114, 851
- Shen, Y., Greene, J. E., Strauss, M. A., Richards, G. T., & Schneider, D. P. 2007a, *ArXiv e-prints*, 709
- Shen, Y., Strauss, M. A., Oguri, M., Hennawi, J. F., Fan, X., Richards, G. T., Hall, P. B., Schneider, D. P., Szalay, A. S., Thakar, A. R., Vanden Berk, D. E., F., A. S., & Bahcall, N. A. 2007b, *AJ*, accepted
- Sijacki, D., Springel, V., di Matteo, T., & Hernquist, L. 2007, *MNRAS*, 380, 877
- Silk, J., & Rees, M. J. 1998, *A&A*, 331, L1
- Silva, A. I., & Viegas, S. M. 2002, *MNRAS*, 329, 135
- Simcoe, R. A., Sargent, W. L. W., Rauch, M., & Becker, G. 2006, *ApJ*, 637, 648
- Socrates, A., Davis, S. W., & Ramirez-Ruiz, E. 2006, *ArXiv Astrophysics e-prints*
- Springel, V., Di Matteo, T., & Hernquist, L. 2005a, *ApJ*, 620, L79
- . 2005b, *ApJ*, 620, L79
- Springel, V., Yoshida, N., & White, S. D. M. 2001, *New Astronomy*, 6, 79
- Srianand, R., & Petitjean, P. 2000, *A&A*, 357, 414
- Steidel, C. C. 1993, in *Astrophysics and Space Science Library*, Vol. 188, *The Environment and Evolution of Galaxies*, ed. J. M. Shull & H. A. Thronson, 263–+
- Steidel, C. C., Adelberger, K. L., Gialvalisco, M., Dickinson, M., & Pettini, M. 1999, *ApJ*, 519, 1
- Steidel, C. C., Adelberger, K. L., Shapley, A. E., Pettini, M., Dickinson, M., & Gialvalisco, M. 2003, *ApJ*, 592, 728
- Steidel, C. C., Kollmeier, J. A., Shapley, A. E., Churchill, C. W., Dickinson, M., & Pettini, M. 2002, *ApJ*, 570, 526
- Strateva, I., Ivezić, Ž., Knapp, G. R., Narayanan, V. K., Strauss, M. A., Gunn, J. E., Lupton, R. H., Schlegel, D., Bahcall, N. A., Brinkmann, J., Brunner, R. J., Budavári, T., Csabai, I., Castander, F. J., Doi, M., Fukugita, M., Györy, Z., Hamabe, M., Hennessy, G., Ichikawa, T., Kunszt, P. Z., Lamb, D. Q., McKay, T. A., Okamura, S., Racusin, J., Sekiguchi, M., Schneider, D. P., Shimasaku, K., & York, D. 2001, *AJ*, 122, 1861
- Sutherland, R. S., & Dopita, M. A. 1993, *ApJS*, 88, 253
- Telfer, R. C., Zheng, W., Kriss, G. A., & Davidsen, A. F. 2002, *ApJ*, 565, 773
- Thoul, A. A., & Weinberg, D. H. 1995, *ApJ*, 442, 480
- Tormen, G. 1997, *MNRAS*, 290, 411
- Trager, S. C., Faber, S. M., Worthey, G., & González, J. J. 2000, *AJ*, 119, 1645
- Tremonti, C. A., Moustakas, J., & Diamond-Stanic, A. M. 2007, *ApJ*, 663, L77
- Tripp, T. M., Sembach, K. R., Bowen, D. V., Savage, B. D., Jenkins, E. B., Lehner, N., & Richter, P. 2007, *ArXiv e-prints*, 706
- Tytler, D., & Fan, X.-M. 1992, *ApJS*, 79, 1
- Tytler, D., Gled, M., Melis, C., Chapman, A., Kirkman, D., Lubin, D., Paschos, P., Jena, T., & Crotts, A. P. S. 2007, *ArXiv e-prints*, 711
- Ueda, Y., Akiyama, M., Ohta, K., & Miyaji, T. 2003, *ApJ*, 598, 886
- Vanden Berk, D. E., Richards, G. T., Bauer, A., Strauss, M. A., Schneider, D. P., Heckman, T. M., York, D. G., Hall, P. B., Fan, X., Knapp, G. R., Anderson, S. F., Annis, J., Bahcall, N. A., Bernardi, M., Briggs, J. W., Brinkmann, J., Brunner, R., Burles, S., Carey, L., Castander, F. J., Connolly, A. J., Crocker, J. H., Csabai, I., Doi, M., Finkbeiner, D., Friedman, S., Frieman, J. A., Fukugita, M., Gunn, J. E., Hennessy, G. S., Ivezić, Ž., Kent, S., Kunszt, P. Z., Lamb, D. Q., Leger, R. F., Vernet, J., Fosbury, R. A. E., Villar-Martín, M., Cohen, M. H., Cimatti, A., di Serego Alighieri, S., & Goodrich, R. W. 2001, *A&A*, 366, 7
- Villar-Martín, M., Sánchez, S. F., Humphrey, A., Dijkstra, M., di Serego Alighieri, S., De Breuck, C., & González Delgado, R. 2007, *MNRAS*, 378, 416
- Vogt, S. S., Allen, S. L., Bigelow, B. C., Bresee, L., Brown, B., Cantrall, T., Conrad, A., Couture, M., Delaney, C., Epps, H. W., Hilyard, D., Hilyard, D. F., Horn, E., Jern, N., Kanto, D., Keane, M. J., Kibrick, R. I., Lewis, J. W., Osborne, J., Pardeilhan, G. H., Pfister, T., Ricketts, T., Robinson, L. B., Stover, R. J., Tucker, D., Ward, J., & Wei, M. Z. 1994, in *Proc. SPIE Instrumentation in Astronomy VIII*, David L. Crawford; Eric R. Craine; Eds., Volume 2198, p. 362, 362–+
- Wakker, B. P., & van Woerden, H. 1997, *ARA&A*, 35, 217
- Wampler, E. J., Bergeron, J., & Petitjean, P. 1993, *A&A*, 273, 15
- Wild, V., Kauffmann, G., White, S., York, D., Lehnert, M., Heckman, T., Hall, P. B., Khare, P., Lundgren, B., Schneider, D. P., & Vanden Berk, D. 2008, *ArXiv e-prints*, 802
- Wolfe, A. M., & Prochaska, J. X. 2000, *ApJ*, 545, 591
- Worseck, G., Fechner, C., Wisotzki, L., & Dall’Aglio, A. 2007, *A&A*, 473, 805
- Wyithe, S., & Loeb, A. 2003, *ArXiv Astrophysics e-prints*
- York, D. G., Adelman, J., Anderson, Jr., J. E., Anderson, S. F., Annis, J., Bahcall, N. A., Bakken, J. A., Barkhouser, R., Bastian, S., Berman, E., Boroski, W. N., Bracker, S., Briegel, C., Briggs, J. W., Brinkmann, J., Brunner, R., Burles, S., Carey, L., Carr, M. A., Castander, F. J., Chen, B., Colestock, P. L., Connolly, A. J., Crocker, J. H., Csabai, I., Czarapata, P. C., Davis, J. E., Doi, M., Dombeck, T., Eisenstein, D., Ellman, N., Elms, B. R., Evans, M. L., Fan, X., Federwitz, G. R., Fiscelli, L., Friedman, S., Frieman, J. A., Fukugita, M., Gillespie, B., Gunn, J. E., Gurbani, V. K., de Haas, E., Haldeman, M., Harris, F. H., Hayes, J., Heckman, T. M., Hennessy, G. S., Hindsley, R. B., Holm, S., Holmgren, D. J., Huang, C.-h., Hull, C., Husby, D., Ichikawa, S.-I., Ichikawa, T., Ivezić, Ž., Kent, S., Kim, R. S. J., Kinney, E., Klaene, M., Kleinman, A. N., Kleinman, S., Knapp, G. R., Korienek, J., Kron, R. G., Kunszt, P. Z., Lamb, D. Q., Lee, B., Leger, R. F., Limmongkol, S., Lindenmeyer, C., Long, D. C., Loomis, C., Loveday, J., Lucinio, R., Lupton, R. H., MacKinnon, B., Mannery, E. J., Mantsch, P. M., Margon, B., McGehee, P., McKay, T. A., Meiksin, A., Merelli, A., Monet, D. G., Munn, J. A., Narayanan, V. K., Nash, T., Neilsen, E., Neswold, R., Newberg, H. J., Nichol, R. C., Nicinski, T., Nonino, M., Okada, N., Okamura, S., Ostriker, J. P., Owen, R., Pauls, A. G., Peoples, J., Peterson, R. L., Petravick, D., Pier, J. R., Pope, A., Pordes, R., Prosapio, A., Rechenmacher, R., Quinn, T. R., Richards, G. T., Richmond, M. W., Rivetta, C. H., Rockosi, C. M., Ruthmansdorfer, K., Sandford, D., Schlegel, D. J., Schneider, D. P., Sekiguchi, M., Sergey, G., Shimasaku, K., Siegmund, W. A., Smee, S., Smith, J. A., Snedden, S., Stone, R., Stoughton, C., Strauss, M. A., Stubbs, C., SubbaRao, M., Szalay, A. S., Szapudi, I., Szokoly, G. P., Thakar, A. R., Tremonti, C., Tucker, D. L., Uomoto, A., Vanden Berk, D., Vogeley, M. S., Waddell, P., Wang, S.-i., Watanabe, M., Weinberg, D. H., Yanny, B., & Yasuda, N. 2000, *AJ*, 120, 1579
- Yoshida, N., Stoehr, F., Springel, V., & White, S. D. M. 2002, *MNRAS*, 335, 762
- Yu, Q., & Tremaine, S. 2002, *MNRAS*, 335, 965